Direct Measurement of Turbulent Fluxes on a Pleasure Boat over Lake Kasumigaura

WANG JINGYUAN
201821231

January 2020

A Master's Thesis Submitted to
The Graduate School of Life and Environmental Sciences,
the University of Tsukuba
in Partial Fulfillment of the Requirements
for the Degree of Master of Environmental Sciences

Abstract

Latent heat flux and sensible heat flux (*LE* and *H*) are two important components in the process of energy exchange between the surface and the atmosphere. Many studies focus on turbulent fluxes on air-sea and air-land interaction, but fewer studies focus on air-lake interaction. For direct measurements, an aircraft and a large ship have been used as a platform, but not a small ship. In this study, the possibility of a ship-based determination of turbulent fluxes over Lake Kasumigaura was investigated. The spatial distribution of fluxes was also discussed.

The data collected by field measurement was presented and the observation system on a pleasure boat was described. Then turbulent fluxes were calculated by the eddy correlation method and were compared with those of the bulk methods.

Results show that wind speeds measured from the ship are larger than those obtained by interpolating station data when the ship is kept heading into the wind. But wind speeds measured from the ship are smaller than the latter when the wind blows from behind the ship. The comparison of the two methods reports that a good agreement is found between *LE* and *H* of the bulk methods and those of the eddy correlation method.

Wind direction has influences on wind speeds collected by field measurement. However, wind direction shows no direct correlation with turbulent fluxes by the two methods. The comparison of the two methods indicates that the observation system on a small ship is applicable to measure turbulent fluxes. In general, the influence of wind speed on the spatial distribution of turbulent fluxes appears to be larger than the difference of vertical concentrations under relatively strong wind speed conditions. While the influence of the difference of vertical concentrations is more important under relatively weak wind speed conditions.

In field measurements, the unstable power supply from the ship is suspected to have an influence on some of the data measurements. To calculate accurate turbulent fluxes, the observing system needs to be improved.

Key words: the eddy correlation, bulk method, turbulent, ship measurement

Contents

List of Tables

List of Figures

1. Introduction

1.1. General Background

Lakes serve as vital water resources and popular tourist destinations. The process of energy exchange over lakes plays an important role in regional climate change and has a large influence on the regional hydrologic regimes (Rouse et al., 2008). Latent heat flux and sensible heat flux (*LE* and *H*) are two important components in the process of energy exchange between the lake surface and the atmosphere. Many studies have focused on turbulent fluxes on air-sea interaction (Cook et al., 2015; Takahashi et al., 2000), but fewer on air-lake interaction. Therefore it is necessary to estimate *LE* and *H* over lakes.

The bulk method has been widely used in measuring turbulent fluxes for its convenience to use routine mean value of meteorological data. However, the eddy correlation method is the most reliable method for turbulent fluxes measurements (Fujitani, 1981).

1.2. Previous studies: fluxes based on aircraft and large ship

For direct measurement, the aircraft and the large ship have been used to measure *H*, *LE* and CO_2 fluxes and have been applied to wind measurements. Axford (1968) used an inertial platform to measure the small scale variations in the vertical gust and horizontal wind shear. It was said that the inertial platform system will become a quick and accurate method of measuring wind measurements with a data recording system installed on the airplane. However, it has some limitations when measuring turbulent fluxes by the aircraft. In the study of Lenschow et al. (1989), the aircraft was used to measure mean horizontal wind speed and high-frequency fluctuations of three components of air speeds, which are used to calculate fluxes of heat. It reported that the process of estimating air velocity has inherent limitations. The accuracy depends on aircraft flight characteristics and response time.

A ship is the only feasible platform for open-ocean flux measurements under a wide range of conditions (Mitsuta et al., 1973). For the large ship, Fujitani (1985) described a stable platform system on a large ship that was designed to measure turbulent fluxes by the eddy correlation method, and it was found that this system is applicable to measurements even under rough sea surface conditions. A similar observation system was applied in the study of Tsukamoto et al., (1990). Turbulent fluxes were determined by the eddy correlation method based on direct measurements over the open sea area south of Japan in their study and ship motion correction for wind speeds, which was believed difficult, seemed to work well. CO_2 fluxes over the equatorial Indian Ocean were measured by a flux observation system fixed on a large ship (Kondo et al., 2007). The system was fixed on the foremast of the ship to minimize the dynamical and thermal effects of the ship's body. White noise is shown in the CO_2 density fluctuation at the high frequency but has no influence on the CO_2 fluxes.

1.3. Previous studies: turbulent fluxes over Lake Kasumigaura

For Lake Kasumigaura, turbulent fluxes of momentum, *LE* and *H* were obtained by the eddy correlation measurements at the observation mast (Mitsuta et al., 1970). In their study, the observation mast was built on the shore about 4 m from the coastline because of technical difficulties and the bank behind the mast was suspected to affect the observation of the mean vertical motion. Evaporation distribution was estimated using the bulk method by observatories data (Sugita et al., 2014; Kondo et al., 1994). Evaporation distribution was also evaluated by satellite data and meteorological data from observatories around Lake Kasumigaura (Ikura, 2010; Sugita, 2019). Ogawa (2018) discussed *LE* and *H* spatial distribution over Lake Kasumigaua by observatories data. These studies showed that the spatial distribution of the evaporation flux is mainly influenced by wind speed and wind direction, and the higher fluxes have been found in the southeastern area and the lake center area. The study of Sugita (2019) indicated that fluxes near the shoreline were quite different from those offshore. The spatial distribution of turbulent fluxes over Lake Kasumigaura has not been measured by direct measurement, except for Harada (2015). In his study, *H* and *LE* were calculated by the bulk method and data was collected by the observation system installed on a small ship. However, it was only measured on two winter days. What is more, the spatial distribution of turbulent fluxes over Lake Kasumigaura has not been calculated by the eddy method.

1.4. Purpose of this study

The purpose of this study is to investigate into possibility of a ship-based determination of turbulent fluxes over Lake Kasumigaura is investigated. What is more, the spatial distribution characteristics of turbulent fluxes are also discussed.

2. Study Area

Lake Kasumigaura, located in the southeastern part of Ibaraki prefecture (Fig. 1), is the second-largest lake in Japan. The lake is a shallow lake, with a mean water depth of 4 m and a maximum water depth of 7 m. A total of 56 rivers inflow into the lake, with 1.7 billion m^3/year. The average precipitation into the lake is 0.3 billion m^3/year (http://www.pref.ibaraki.jp/soshiki/seikatsukankyo/kasumigauraesc/18_foreignlanguage/documents/01_outline%20of%20lake%20kasumigaura.pdf).

The catchment area is 2157 km^2 and the river basin population is about 960,000 as of the end of FY 2002. As a valuable water resource, the lake provides over 60 tons of water a second, of which about 83% goes to agriculture, 13% to industry and 4% to domestic water supply (http://www.worldlakes.org/lakedetails.asp?lakeid=8394).

Lake Kasumigaura is composed by Nishiura, Kitaura and Sotona Sakaura. The study area is Nishiura, the largest component of Lake Kasumigaura, with a surface area of 172 km^2.

3. Theory

In this study, H and LE were calculated by the eddy correlation method and then were compared with those of the bulk methods. Fluxes by the two different methods were both calculated from 15 min data (details of data are introduced in Section 4.1).

3.1. The eddy correlation method

The eddy correlation method is the only direct method for measurement of heat and trace gas (Kondo et al., 2007)

$$LE = \rho_a L_e \overline{w'q'} \tag{1}$$

$$H = \rho_a C_p \overline{w'T'} \tag{2}$$

Where L_e: latent heat for vaporization, ρ_a: atmospheric density, w: vertical velocity of wind, q: specific humidity, C_p: specific heat of air at constant pressure, T: air temperature, x' : the deviation from the mean, and $\overline{x_1 x_2}$: covariance of x_1 and x_2. In this study, w, q and T are 10 HZ data. In this study, T is measured by a sonic anemometer (see Section 4).

3.2. Bulk method

Bulk method is convenient to calculate fluxes by using routine meteorological data.

$$H = C_p \rho_a C_h U_{10} \left(T_s - T_a\right) \tag{3}$$

$$LE = L_e C_e \rho_a U_{10} \left(q_s - q\right) \tag{4}$$

Where C_h: bulk coefficient for H, C_e : bulk coefficient for Latent heat flux, U_{10}: wind speed at 10 m height, q_s: saturation specific humidity, T_a: air temperature and T_s: water surface temperature. T_s, T_a, q_s, and q are the average value of 15 min and T_a is measured by hygro-thermometer (see Section 4).

For the two methods, C_p is 1004.7 J/kg/k (Tsukamoto et al., 2001). ρ_a, q, q_s and L_e are calculated by equations as follows.

$$\rho_a = \frac{1.293(P - 0.378e) \times 273.15}{(273.15 + T) \times 1013.25} \tag{5}$$

$$q = \frac{0.622e}{P} \tag{6}$$

$$q_s = \frac{0.622e_s}{P} \tag{7}$$

$$L_e = 2.50025 \times 10^6 - 2.365 \times 10^3 T \tag{8}$$

Where P: atmospheric pressure, e: vapor pressure, and e_s: saturation vapor pressure. These equations are mentioned in Sugita et al. (2009).

For the bulk methods, e is calculated from relative humidity (R_h) and air temperature. e_s is calculated from T_s with assuming saturation condition in the water surface. According to Sugawara et al. (1994),

$$e = \frac{Rh}{100} \times 6.11 \times 10^{\frac{7.5T}{237.3+T}} \tag{9}$$

$$e_s = 6.11 \times 10^{\frac{7.5T_S}{237.3+T_S}} \tag{10}$$

On the other hand, for the eddy correlation method, e is calculated by equation bellow (Sugita et al., 2009).

$$e = \frac{\rho_{\mathrm{H_2O}}(T+273.15)}{216.7} \tag{11}$$

4. Measurements

4.1. Ship measurement

Data were directly collected by an observation system on a moving pleasure boat. The boat is from Lacus Marina company, with 5.5 m high and 15.0 m long (see Fig. 2). The typical cruising speed is 9 km/h. The sensors were installed on the top of the foremast at 7.5 m height above the water surface. There are two ship courses (Fig. 3), whose continuous track was recorded by a GPS receiver of the ship observation system, except for Run 6. Ship course of Run 6 was recorded by a GPS device (Colorado, Garmin company) because the GPS receiver failed to collect data. One ship course is from Tsuchiura to Itako, about one hour, and the other one is from Tsuchiura to Tamatsukuri, about 30 minutes.

The observation system mainly included an accelerometer, a sonic anemometer thermometer, and a gas analyzer. The accelerometer is to measure ship motions (details are shown in Section 5.1). The sonic anemometer is to measure three components of wind speed and air temperature. The gas analyzer is to get the concertation of CO_2 and H_2O. Data is recorded by rugged data loggers (CR1000 and CR10X). The observation system installed on ship is shown in Fig. 4. Instruments and measurement items are shown in Table 1.

The observation period was made from 2018.06 to 2019.06, but only part of them was used to calculate turbulent fluxes in this study because of missing data due to instruments problem. From Tsuchiura to Itako is a run, and from Itako to Tsuchiura is another run. Each run is divided into several segments with each duration of 15 minutes and fluxes are calculated from 15 min segment. Table 2 shows each segment of seven runs.

4.2. Koshin

The data from observatories were used in this study to correct data observed from ship measurements (see Section 5.2). The external view of Koshin Observatory is shown in Fig. 5. Observation items used in this study are air temperature T_a (℃), water temperature T_w (℃), water surface temperature T_s (℃), and upward and downward long wave radiation $R_l\uparrow, R_l\downarrow$ (W/m^2). Observation items and instruments are shown in the Table 2. Data of 2018/6/16, 2018/6/17, 2018/6/24 and 2018/9/23 on the days of the ship measurements were used.

4.3. Observatories around Lake Kasumigaura

There are many other observatories around Lake Kasumigaura besides Koshin observatory. Water temperature T_w (℃) used in this study is from Koshin, Asooki, Hirayama, Kakeumaoki, and Kamayaoki observatories. Wind speed and wind direction are from Koshin, Asooki, Koshin, Dejima, Itako, Hasaki, Odaka, Tsuchiura, Hokota, Wanigawa, Kakeumaoki, Kamayaoki, Tamatsukuri, and Azumamura observatories. The locations of those stations are shown in Fig. 1. The items and instruments used in this study are shown in Table 4 and Table 5. Data on the same days introduced in the last section were used.

5. Analysis

5.1. Calculation of wind speeds

Three components of wind speed were measured by a sonic anemometer fixed to the ship's body, which means the observed wind speed is relative to the ship coordinate. Therefore, wind speed needs to be transferred to the earth coordinate and wind speed induced by ship motions needs to be removed.

Besides ship motion correction, coordinate rotation correction is also a necessary step in micro-meteorological studies of surface-air exchange before the observed fluxes can be meaningfully interpreted (Lee et al., 2005). After the rotation, x is the main horizontal wind direction, y is perpendicular to the x-direction, and z is perpendicular to the x-y plane. This system will be called the wind-based coordinate system.

5.1.1. Ship motion correction

Ship motion (Fig. 6) was mainly measured three components of ship speed V_x, V_y, V_z

(m/s) and three attitude angles (pitching θ, yawing ψ and rolling angles ϕ). The positive rolling motion is lifting the left side of the ship and the positive pitching motion is lifting the head of the ship. Then the positive yawing motion is moving the head of the ship to the right. They were calculated from accelerations and angular rates which were measured by an accelerometer.

According to Takahashi et al. (2005), wind speed after ship motion correction is given by equation as follows:

$$U_{wind} = TU + V_{s1} + \Omega \times T(R - r) \tag{12}$$

Where U_{wind} (u_1, v_1, w_1) is the wind speed vector relative to the earth coordinate after ship motion correction, T is transformation matrix from the ship coordinate to the earth coordinate, U (u_0, v_0, w_0) is the observed wind speed vector by ship, V_{s1} is ship speed vector, Ω is the angular velocity vector of the ship coordinate around the reference coordinate, R is the position vector of the anemometer with respect to the ship coordinate and r is the ship motion sensor from the center of gravity. In this study, anemometer is nearly installed the same position with accelerometer (ship motion sensor), which means $R = r$, thus the third term of equation (12) is always zero. U_{wind}, T and V_{s1} were all calculated at every instance.

First, the observed wind speeds were converted from ship coordinate to the earth coordinate by T. Then ship speeds were removed from the observed wind speeds.

Fig.7 is shown time traces of three accelerations and three angular rates of Run 1. Vertical acceleration mainly measured gravitational acceleration. The mean values of two horizon accelerations and three angular rates are not zero during Run 1. It is caused by inherent drifts in the inertial platform, the offset of electrical circuits and/or gyroscope drift (Fujitani, 1985; Axford, 1968). Before calculating ship speeds, gravitational acceleration and the drifts of accelerations and angular rates have to be removed. To remove the gravitational acceleration and the drifts, the mean value is always removed from raw data.

According to Fujitani (1985), to determine the optimum averaging time, the mean square deviations of mean values from the average of the entire observational period with different averaging time were calculated. In this study, the mean square deviations were calculated by equation (13):

$$y = \frac{\sum_{i=1}^{n/t_1}\left(\frac{1}{t_1}\int_{(i-1)t_1}^{it_1} x dt_1 - \frac{1}{t}\int_0^t x dt\right)^2 t_1}{n} \tag{13}$$

Where y: mean square deviations, t_1: different averaging time, t: the run time, $\frac{1}{t_1}\int_{(i-1)t_1}^{it_1} x dt_1$: mean values with the averaging time t_1, $\frac{1}{t}\int_0^t x dt$: average of the run, x: raw data of three accelerations, n: number of data of a run, i = 1, 2, 3……n/t_1 and n/t_1: number of data with the averaging time t_1.

For all seven runs, mean square deviations were calculated for three accelerations and three angular rates by equation (13) with different t_1, and plotted against t_1 (Fig. 8-Fig. 13). Less than 60% of the maximum of the mean square deviations was seen as constant and the mean square deviations were almost constant or slightly decreased when the averaging time was longer than one minute. Therefore one minute was chosen as the optimum averaging time. Then mean values with one minute were removed from raw data of accelerations and angular rates by equation (14)

$$x = x_1 - x_{ave} \tag{14}$$

Where x_1 is the raw data of accelerations of each run, x_{ave} is the average value of every 60 s and x is accelerations after correction. Fig. 14 is time traces of three accelerations and three angular rates of Run 1 after correction.

5.1.1.1. Ship speeds

Three components of ship speeds were calculated from three components of accelerations by the integration equation. According to Fujitani (1985), the integration function is given by:

$$x(t+\Delta t) = x(\mathrm{t}) + \frac{\Delta t}{2} \cdot \dot{x}(t) + \frac{\Delta t}{2} \cdot \dot{x}(t+\Delta t) \tag{15}$$

Where $x(\mathrm{t})$ and $\dot{x}(t)$ are time series and their first derivatives, respectively.

Equation (15) was applied for three accelerations to estimate ship speeds and the integrator of three components runs for the whole run time.

$$V_{s1} = V_{s0} + x(t+\Delta t) \tag{16}$$

Where V_{s0} (V_{s0x}, V_{s0y}, V_{s0z}) is the initial ship speed vector and in this study, the initial speed V_{s0x}, recorded by the GPS device, is 9 m/s. V_{s0y} and V_{s0z} are assumed as 0 m/s. Fig. 15 is an example of ship speeds of Run 1.

5.1.1.2. Transformation matrix

Attitude angles were calculated in the same way as ship speeds. Three attitude angles (θ, ψ, ϕ) were integrated from three angular rates by equation (15). Then equation (17) was applied to three attitude angles to calculate transformation matrix.

Transformation matrix was given by Fujitani (1985)

$$T = \begin{bmatrix} \cos\psi\cos\theta & -\sin\psi\cos\phi + \cos\psi\sin\theta\sin\phi & \sin\psi\sin\phi + \cos\psi\sin\theta\cos\phi \\ \sin\psi\cos\theta & \cos\psi\cos\phi + \sin\psi\sin\theta\sin\phi & -\cos\psi\sin\phi + \sin\psi\sin\theta\cos\phi \\ -\sin\theta & \cos\theta\sin\phi & \cos\theta\cos\phi \end{bmatrix} \tag{17}$$

Where θ, ψ, ϕ are pitching, yawing and rolling angles, respectively. An example of Transformation matrix of Run 1 is seen in Fig. 16. Fig. 17 is an example of wind speeds of Run 1 observed and after ship motion correction.

5.1.2. Rotation correction

Twice rotations were done in this study to change wind speed from the earth coordinate to the wind-based coordinate. The first step is to make sure the mean lateral wind speed $\bar{v} = 0$, then the second step is to force the mean vertical wind speed $\bar{w} = 0$. According to Tsukamoto (2001),

$$\theta_1 = \tan^{-1}\left(\frac{\overline{v_0}}{\overline{u_0}}\right) \tag{18}$$

$$U_1 = u_0 \cos\theta_1 + v_0 \sin\theta_1 \tag{19}$$

$$v = -u_0 \sin\theta_1 + v_0 \cos\theta_1 \tag{20}$$

$$\varphi = \tan^{-1}\left(\frac{\overline{w_0}}{\overline{U_1}}\right) \tag{21}$$

$$u = U_1 \cos\varphi + w_0 \sin\varphi \tag{22}$$

$$w = -U_1 \sin\varphi + w_0 \cos\varphi \tag{23}$$

Where u_0, v_0, w_0 are the observed instantaneous longitudinal, lateral and vertical wind speeds, respectively. $\overline{u_0}$, $\overline{v_0}$, $\overline{w_0}$ are of 15 min average of those, and u, v, w are the instantaneous longitudinal, lateral and vertical wind speeds after rotation correction. Fig. 18 is an example of wind speed after ship motion correction and rotation correction of Run 1.

5.1.3. Wind speeds

As mentioned above, it is difficult to calculate the true wind speed as the ship motion is difficult to remove from the wind speed measured by the ship observation system. Therefore, to confirm whether the ship motion correction worked well, corrected wind speeds (u) measured by ship were compared with those from the interpolation of the observatories' data.

Each observatory measures wind speeds and wind direction at a different height. First, U_x and U_y at each station were calculated from wind speed and wind direction, then they were adjusted to 7.5 m by a profile equation, the same height as the ship observation system.

$$U_{7.5} = \frac{ln(\frac{7.5}{z_0})}{ln\left(\frac{z}{z_0}\right)} \tag{24}$$

Details were introduced in Ikura (2010).

$U_{x7.5}$ and $U_{y7.5}$ were spatially interpolated (Lake Kasumigaura was divided into 20×20 grids), and values of them along the ship courses were extracted. Finally, the mean value of wind speed $U_{7.5}$ and wind direction were calculated from $U_{x7.5}$ and $U_{y7.5}$ of each grid, then they were compared with u.

5.2. Data Correction

5.2.1. Calibration of equipment

The sensors, IRT, LI7500 and hygro-thermometer, were calibrated before used in field measurements. T_s from IRT, T_a and R_h from hygro-thermometer were corrected by equations shown in Fig. 19 to Fig. 21.

5.2.2. Trend removal

The data may have trend because of sensor problem and the ship moving. The trend of data was checked before calculating fluxes. Fig. 12 is an example of raw data of Run 1 (q_a, T_a). It was found that T_a of Run 5 had an obvious trend, and it was corrected by equation shown in Fig. 23.

5.2.3. Correction for T_s

T_s measured by IRT installed on the ship was found the presence of outliers. Therefore, it was corrected by using data from observatories around Lake Kasumigaura.

T_s of Koshin Observatory was calculated from $R_l \uparrow$ then was compared with it from IRT. Because the IRT at Koshin Observatory tends to produce higher temperature when the sunshine is strong (Fig. 24). The data of 2018/6/15 was chosen, because of the similar weather condition with the day of Run 1-Run 7. T_s, the same day with Run 1-Run 7, was calculated from $R_l \uparrow$ and was corrected by equation shown in Fig. 24. Then, T_s at the other observatories was estimated as follows.

$$\Delta T = T_{s1} - T_{w1} \tag{25}$$

$$T_{s2} = T_{w2} + \Delta \mathrm{T} \tag{26}$$

Where T_{s1} and T_{w1} are water surface temperature and water temperature from Koshin Observatory at the same time, T_{s2} and T_{w2} are water surface temperature and water temperature at the same time of other observatories. Difference of T_s and T_w from Koshin Observatory at the same time was calculated. Then the difference was applied to the other observatories to estimate the unknown T_s. Finally the values of T_s at each observatory were spatially interpolated. From the interpolation map, T_s along the ship track was determined. The comparison of T_s measured by ship and T_s from interpolation of stations was shown in

Fig. 25.

5.2.4. Height adjustment for bulk method and correction for bulk coefficient

According to Wei et al. (2016),

$$C_{hn} = \frac{c_1}{U_{7.5}} \times exp[-\{ln(U_{7.5}) - c_2\}^3] + c_3 + c_4 U_{7.5} \tag{27}$$

$$C_{en} = \frac{d_1}{U_{7.5}} \times exp[-\{ln(U_{7.5}) - d_2\}^3] + d_3 + d_4 U_{7.5} \tag{28}$$

Where $\mathrm{C_{hn}}$ and C_{en} are bulk coefficients under neutral conditions. $c_1 = 2.121021886 \times 10^{-3}, c_2 = 0.2751502697, c_3 = 9.120266534 \times 10^{-4}$, $c_4 = 1.6479059 \times 10^{-5}$, and $d_1 = 9.078622125 \times 10^{-4}, d_2 = 0.2173819734, d_3 = 1.137911624 \times 10^{-3}$, $d_4 = -1.538412447 \times 10^{-5}$.

Then LE_n and H_n assumed under neutral conditions are calculated by equation (3) and (4), using C_{hn} and C_{en}. As the bulk methods are usually applied with data at 10 m, wind speed *U*, air temperature and specific humidity measured by ship were adjusted to 10 m by profile equations bellow.

$$\overline{U_{10}} = \overline{U_{7.5}} + \frac{u_*}{k} \ln\left(\frac{10}{7.5}\right) \tag{29}$$

$$\overline{T_{a10}} = \overline{T_{a7.5}} - \frac{\overline{w't'}}{ku_*} \ln\left(\frac{10}{7.5}\right) \tag{30}$$

$$\overline{q_{10}} = \overline{q_{7.5}} - \frac{\overline{w'q'}}{ku_*} \ln\left(\frac{10}{7.5}\right) \tag{31}$$

Where $\overline{U_{10}}$, $\overline{T_{a10}}$, $\overline{q_{10}}$: wind speed, air temperature and specific humidity at 10 m, $\overline{U_{7.5}}$, $\overline{T_{a7.5}}$, $\overline{q_{7.5}}$: wind speed, air temperature and specific humidity measured by ship at 7.5 m, u_*: friction speed and $k = 0.4$, Karman constant.

$$\overline{w't'} = \frac{H_n}{C_p \rho_a} \tag{32}$$

$$\overline{w'q'} = \frac{LE_n}{L_e \rho_a} \tag{33}$$

u_* is calculated by equations (34)-(36).

$$Z_0 = \exp(3.397 - 4.063U_{7.5} + 0.4906{U_{7.5}}^2 - 0.023705{U_{7.5}}^3 + 0.0004093{U_{7.5}}^4) \tag{34}$$

$$Cdn = \frac{k^2}{[ln(Z/Z_0)]^2} \tag{35}$$

$$U_* = \sqrt{Cdn} \times \overline{U_{7.5}} \tag{36}$$

Where Z_0 is the roughness length for wind speed, Z is the measurement height 7.5 m, Cd_n is the drag coefficient under neutral conditions.

Considering unstable conditions during the observations, bulk coefficients were corrected and were given by:

$$Ch = \frac{k^2}{[ln(Z/Z_0) - \Psi_M][ln(Z/Z_{0h}) - \Psi_H]} \tag{37}$$

$$Ce = \frac{k^2}{[ln(Z/Z_0) - \Psi_M][ln(Z/Z_{0v}) - \Psi_v]} \tag{38}$$

$$Cd = \frac{k^2}{[ln(Z/Z_0) - \Psi_M]^2} \tag{39}$$

Where Ψ_M, Ψ_H, Ψ_v are the stability correction function of *Z*/*L*. Z_{0h}, Z_{0v} are the roughness length of air temperature and specific humidity. *L*, the Obukhov length, is calculated by equation (40).

$$L = \frac{-T_{a10} U_*^3}{kg\left(\overline{w^{'}t^{'}} + 0.61 T_{a10} \overline{w^{'}q^{'}}\right)} \tag{40}$$

As $\xi = \frac{10}{L}$<0 in all runs, which means unstable conditions during field observations, Ψ_H and Ψ_v are calculated from equation (41) and (42)

$$\Psi_M = 2ln\frac{1+x}{2} + ln\frac{1+x^2}{2} - 2tan^{-1}x + \frac{\pi}{2} \tag{41}$$

$$\Psi_H = \Psi_V = 2ln\frac{1+x^2}{2} \tag{42}$$

Where $x = (1 - 16 \times \xi)^{\frac{1}{4}}$.

Z_{0h} and Z_{0v} are calculated by equation (43)-(46).

$$\mathrm{Re} = \frac{Z_0 U_*}{\upsilon} \tag{43}$$

$$\upsilon = (1.33239 + 0.00902 \times T_{a10}) \times 10^{-5} \tag{44}$$

$$Y = Z_0/Z_{0h} = \exp(4.880 + 1.2678x + 0.07863x^2 + 9.0557 \times 10^{-5}x^3 - 0.0002912x^4) \tag{45}$$

$$Z_{0h} = Z_{0v} = Z_0/Y \tag{46}$$

Where $x = ln(Re)$, Re: Reynolds number, v: kinematic viscosity. Then LE and H are calculated by equation (3) and (4), using Ch and Ce. Repeat calculations described above, until the value of LE and H are nearly constant.

5.2.5. Correction for T_a from anemometer

T_a from anemometer are higher than true air temperature because of instrument observation principal, therefore it was corrected by using T_a from hygro-thermometer (Fig. 26). Then q_a was also corrected by q_a from hygro-thermometer (Fig. 27). Fig. 28 is an example of time series of q_a and T_a after correction.

5.2.6. Correction for H from the eddy correlation method

$$H = H_s - 0.061LE \tag{47}$$

The air temperature T used in eddy correlation method is measured by the sonic anemometer. It is a virtual temperature, including variation of water vapor. Thus the correction for H from the eddy correlation method is corrected by equation (47) (Tsukamoto, 2001).

5.3. Data quality control

5.3.1. Steady state test

Typical non-stationarity is driven by the change of meteorological variables through the time of the day, change of weather patterns, significant meso-scale variability, or changes of the measuring point relative to the measuring events such as the phase of a gravity wave (Foken et al., 2005). This test was to check the stationarity of the flow. Each 15 minutes data was divided into 3 intervals.

$$RQ\overline{x'w'} = \left|\frac{\overline{x'w'}(5min) - \overline{x'w'}(15min)}{\overline{x'w'}(15min)}\right| \times 100 \tag{48}$$

Where x is u, v, q, c (CO_2 concentration), t (air temperature). $\overline{x'w'}$ $(5\ min)$: average of three 5 min intervals, $\overline{x'w'}$ $(15\ min)$: average of 15 min duration. Table 6 is a table of quality flags for stationarity. According to value of RQ, stationarity of each 15 min data is divided into class1 to class 9, from steady to not steady. Result was shown in Table 7 and it indicated that the stationarity of Run 6 and Run 7 are not so good.

5.3.2. Spectral analysis

Spectral analysis is a widely used method to identify whether the data are reliable in flux observation (Wei, 2013). It gives a general condition of measurement data. Each 15 min data of H_2O, CO_2, T_a, w, wt, wq and wc were applied by fast Fourier Transform method and the results were shown in Fig. 29. The blue line is the raw result of spectral analysis and the orange line is the result after applying moving average according to the method mentioned in Matsuyama et al. (2005). The period of moving average is 5.

6. Results and discussion

6.1. Data quality

RQ was calculated by equation (15) and stationarity of each 15 min segment of each run was classified according to Table 6. The stationarity of data between class 6 to class 9 is not so good for calculating turbulent fluxes. Class 1 and class 2 are high quality data. Thus, results indicate that stationary of Run 6 and Run 7 are not so good (Table 7).

On the other hand, spectral analysis was applied to the corrected data. Fig. 29 is an example of Run 1. It reports that the slopes are closed to $-5/3$, which means satisfying the requirement of fluxes. The blue line is the raw result and the orange line is the result after applying moving average.

Fig. 30 is a case of vertical wind speed measured by using a stable platform system on a ship over the tropical marine (Fujitani, 1985). The spectra of observed wind speeds appears a peak induced by the ship motions at around 0.1 HZ, while the corrected ones show no distinct peak. In this study, different from oceans, the spectral peak is not shown in the spectra of observed wind speeds (Fig. 31). In the study of Fujitani (1985), it is explained that the spectral peak is caused by ship motions responding to ocean swells. The significant wave period of Lake Kasumigaura is less than 3 s (Miyao, 2010), which means no swells in Lake Kasumigaura. Thus, it is reasonable that no peak shows in the spectra of observed wind speeds over Lake Kasumigaura.

6.2. Wind speeds and wind directions

Wind speeds were interpolated by using stations' data (Section 5.1.3), then were compared with wind speeds measured from the ship. Fig. 32 is an example of wind speeds interpolation of Run 1.

The comparison of wind speeds shows scatters from the 1:1 line (see Fig. 33), but still reports that the values of wind speeds measured from the ship have a good agreement with those from the interpolation of stations' data. Thus, the present ship motion correction seems to work well.

The wind direction of Run 1 and Run 2 is southeast and Run 3 to Run 6 is northeast. Run 7 is west. The results of the comparisons of wind speeds are mainly divided into two situations by the relation between wind direction and ship moving direction. One is that the wind blows from behind the ship, such as Run 2, Run 4 and Run 6 (Fig. 34-Fig. 36). In this condition, wind speeds measured from the ship are smaller than those from observatories. The other one is that the ship is kept heading into the wind, such as Run 1, Run 3, Run 5 and Run 7 (Fig. 34-Fig. 37). While in this condition, wind speeds measured from the ship are larger than observatories data. It indicates that the relation of wind direction and ship motion direction has an influence on wind speeds when using the ship observation system.

6.3. The comparisons of H and LE by the two methods

LE and H were calculated from each 15 min segment by the eddy correlation method and the bulk method and were compared with each other. The comparison of LE by the two methods shows that LE of Run 1, Run 4 and part of Run 2 by the eddy correlation method is larger than bulk method, while LE of Run 3, Run 5, Run 7 and part of Run 2 by the eddy correlation method is smaller than the bulk method (Fig. 38). On the other hand, the comparison of H by the two methods shows that H by the bulk method is a little larger than it by the eddy correlation method in general (Fig. 39). The eddy fluxes calculated are compared with the bulk variables to see the correlation between results from the two methods (Fig. 40 and Fig. 41). In the two figures, C_e and C_h are shown as dotted lines. The mean value of C_e and C_h are 1.1×10^{-3}. The value is compatible with other studies obtained from water (Takahashi, 2005: $C_e = 1.2 \times 10^{-3}$; Fujitani, 1981: $C_e = 1.03 \times 10^{-3}$, $C_h = 1.2 \times 10^{-3}$). Thus the comparison of the two methods reports a good agreement between LE and H by the bulk method and those by the eddy correlation method.

The scatters from the 1:1 line show no clear pattern and no clear correlation with the relationship of wind directions and ship moving directions. However, it is hard to say that wind directions have no influence on fluxes when using the ship observation system. The scatters are also compared with stationary of data and results are shown in Fig. 42 and Fig. 43. Different colors are different classes of each segment. The scatters from 1:1 line show no clear relationship with stationarity of data, neither.

The agreement of turbulent fluxes by the two methods indicates that the observation system on a small ship is applicable to measure turbulent fluxes. However, in field measurements, the observation system needs to be improved. For example, data of some runs is failed to collect because of the unstable power supply from the ship. It is suspected to have an influence on the accuracy of measured data as mentioned before, which may has an influence on the accuracy of the eddy correlation method. As for the influence of wind direction and ship moving direction, further calculations and studies need to be applied, such as error analysis.

6.4. The spatial distribution of H and LE

The mean values of each run of net radiation (R_n) and heat fluxes into the lake body (G) are shown in Table 10.

G is calculated by equations as follows.

$$G = R_n - H - LE \tag{49}$$

$$R_n = R_s \downarrow - R_s \uparrow + R_l \downarrow - R_l \uparrow \tag{50}$$

Where R_n: net radiation, R_s: short wave radiation, R_l: long wave radiation, ↑: upward, and ↓: downward. $R_s \downarrow$ and $R_l \downarrow$ are measured by 4-component radiometer. $R_s \uparrow$ and $R_l \uparrow$ are calculated by equations bellows.

$$R_s \uparrow = \alpha_s R_s \downarrow \tag{51}$$

$$R_l \uparrow = \varepsilon_s \sigma T_s^4 - (1 - \varepsilon_s)\, R_l \downarrow \tag{52}$$

Where α_s: albedo, ε_s: emissivity, σ: Stefan Bolzmann constant (= 5.6704×10^{-8} $Wm^{-2}\,K^{-4}$). In this study, ε_s of water surface is 1. Albedo is calculated by using Koshin Observatory's data.

In these runs, the lake body was heated, which means energy was stored in the water body, except for Run 2. The difference of Run 2 is possibly caused by the weak net radiation and large *LE* and *H* due to relatively strong wind speed.

To see the spatial distribution of fluxes, q, q_s, T_a, T_s, U, R_n, H and LE by the two methods have to be adjusted to the same time at first, as these items change over time.

Time correction is applied to these items by equation (53) (Harada, 2015),

$$\alpha = \beta \times \frac{B}{A} \tag{53}$$

where β: directly measured value by ship, A: Koshin Observatory value at X_1 o'clock, B: Koshin observatory value at the same time as β. In this study, we adjust the time to the middle of each run time, which means, the time of A is the middle of each run time.

Fig. 44 - Fig. 57 are examples of the spatial distribution of q, q_s, (q_s-q), or T_a, T_s, (T_s-T_a), U, R_n, H and LE by the two methods. It is difficult to compare variation of these items in the same figure as they have a different magnitude. Thus, in these figures, *Y* axis is convert to nondimensionalization axis by equation (54)

$$Y = \frac{X - \overline{X}}{S_x} \tag{54}$$

Where X is these items expect LE and H, $\overline{X}$ is average the value of them, and S_x is the standard deviation of X.

The results of spatial distribution are divided into two cases according to different wind speed (Table 5). One is a windy condition with a mean value of wind speed 5-8 m/s (Run 1, Run 2 and Run 7), the other one is relatively weak wind condition with a mean value of wind speed 1-5 m/s (Run 3, Run 4, Run 5 and Run 6).

The characteristics of the spatial distribution of *LE* and *H* can be identified by comparing them with variables in the bulk equations (Equations (3) and (4)). It shows the spatial distribution of them, in the lake scale, was mainly determined by the vertical concentration differences (q_s-q), (T_s-T_a) or U. For Run 1, the spatial distribution of (q_s-q), (T_s-T_a) are roughly consistent with U (Fig. 44 and Fig. 45). *LE* and *H* also have the similar spatial distribution. For Run 2 (Fig. 46 and Fig. 47), the influence of wind speeds on the spatial distribution is clearly larger than (q_s-q) and (T_s-T_a). For Run 5 (Fig. 52 and Fig. 53), the influence of (q_s-q) and (T_s-T_a) appears to be slightly larger than wind speed. While for Run 3, Run 4 and Run 6, the influence of wind speed and vertical concentration seems equally important. By comparing with Run 2 (6.87 m/s) and Run 5 (1.87 m/s), the wind speed has a larger effect on the turbulent fluxes under relatively strong windy conditions, while the vertical concentration differences were the main impact factor under the relatively weak wind speed conditions. What is more, the vertical concentration differences were determined by q or T_a (Run 1, Run 7), T_s or q_s (Run 3, Run 4, Run 5, Run 6) and both q, q_a or T_s, T_a (Run 2).

In these runs, the value of T_s decreased from Tsuchiura to Itako, expect for Run 3. The distinctive value of T_s collected from Run 5 and Run 6, are observed in Tsuchiura-iri where the water depth is less than 1 m. It agrees with the study of Sugita (2019), which reports that distinctive values can be observed near coastal lines. It is explained that under the windy conditions, closeness to the coastal lines affects the variation of T_s, causing a nonhomogeneous distribution.

7. Conclusions

In this study, ship-based observations of *LE* and *H* over Lake Kasumigaura were presented. Turbulent fluxes were calculated by the eddy correlation method and compared with those from the bulk method. The spatial distribution of fluxes was also discussed.

The comparisons of wind directions with wind speed indicated that wind speed measurements from the moving ship worked well. Wind direction has an influence on wind speeds collected by the ship observation system. Specifically, it reports the larger wind speed when the ship is kept heading into the wind and the smaller wind speed when the wind blows from behind the ship.

The comparison of two methods indicates that the observation system on a small ship is applicable to measure turbulent fluxes. The relation of wind direction and ship moving direction has influences on wind speeds measured from the ship. However, the influence of this relation on turbulent fluxes has not been clarified. Further studies need to be applied to figure it out. As future work, field measurement should be designed under conditions when the ship is kept heading into the wind and the conditions when the wind blows from behind the ship.

About the characteristics of the spatial distribution of turbulent fluxes, the influence of wind speeds on the distribution spatial of *LE* and *H* appears larger under relatively strong wind speed conditions. When wind speeds are weak, the influence of the difference of vertical concentrations is more important.

In field measurements, the unstable power supply from the ship is suspected to have an influence on data measurements. To calculate accurate turbulent fluxes, the observing system needs to be improved. The accuracy of wind speed also needs to be improved.

Acknowledgements

I would like to gratitude my supervisor Prof. Michiaki Sugita for his strong support through my whole master studies. He has provided me with a lot of help and support for my field measurements. His patience and kindness help me improve rapidly. Thanks also to Prof.Yamanaka, Prof. Tsujimura and Prof. Asanua for their excellent suggestion and encouragement for my research. I also give my best thanks and respect to Prof. Fumiyoshi Kondo, from Japan Coast Guard Academy, for his valuable suggestion of my study. The inertial measurement system (IMU-440CA-200) is a loaner from Prof. Kondo for which we are also grateful.

I also thank my colleagues of hydrological science, University of Tsukuba, Ms. Tang Yidi. She helps me finish my experiments. Special thanks to Mr. Zang Chao, a member of Sugita lab, for his help in my field measurements each time. I cannot finish my thesis without his help. Also thanks to the other members of Sugita lab, especially Mr. Ishikawa. He is so nice to give me a lot of encouragement.

I am very grateful to the staff of the company Lacus Marina. They provide a lot of help to my field measurement. I cannot believe I can finish my field measurement without their help. The observatories' data were provided by the Kasumigaura River Office of the Kanto Regional Development Bureau, Ministry of Land, Infrastructure, Transport, and Tourism of Japan. I also appreciate them.

At last, thanks also to all my other friends who give me support in my master life, especially Mrs. Wei. I cannot finish my master thesis without her strong support. At the same time, I would like to thank my parents for their support and encouragement. .

References

Afoxd DN. 1968. On the accuracy of wind measurements using an inertial platform in an aircraft, and an example of a measurement of the vertical mesostructure of atmosphere. Journal of Applied Meteorology, Vol. 7, pp.645-666.

Foken T, G'ockede M, Mauder M, Mahrt L, Amiro B and Munger W. 2005. Post-field data quality control, in X. Lee, W. Massman and B. Law (eds), Handbook of Micrometeorology, Atmospheric and Oceanographic Sciences Library, Springer Netherlands, pp. 181–208.

Fujitani T. 1985. Method of turbulent flux measurement on a ship by using a stable platform system. Papers in Meteorology and Geophysics, Vol. 36, pp.157-170.

Sugawara H and Kondo J. 1994. Errors in calculation of saturation vapor pressure, Journal of Japan Society of Hydrology and Water Resources, Vol. 7, pp.440-443.

Kondo F and Tsukamoto O. 2006. Air-sea CO_2 flux by the eddy covariance technique in the equatorial Indian Ocean, Journal of Oceanography, Vol. 63, pp. 449-456.

Kondo J. 1994. Mizukankyo-NO-Kishougaku. Asakura Publ. Co. Ltd., Tokyo: Japan; 348 (in Japanese).

Lee JM, Lee CJ, ShikKim Y, GiChoi G and MoonLew J. 2016. Determination of global ice loads on the ship using the measured full-scale motion data, International Journal of Naval Architecture and Ocean Engineering, Vol. 8, pp. 301-311.

Lee X, Finnigan, J and Paw U, K. 2005, Coordinate systems and flux bias error, in X. Lee, W. Massman and B. Law (eds), Handbook of Micrometeorology, Vol. 29, Atmospheric and Oceanographic Sciences Library, Springer Netherlands, pp. 33–66.

Lenschow, DH and Spyer-Duran. P. 1989. Measurement techniques: air motion sensing, Research Aviation Facility Bulletin No. 23

Mitsuta Y, Hanafusa T, Maitani T and Fujitani T. 1970. Turbulent fluxes over the Lake Kasumigaura, Special contributions, Geophysical Institute, Kyoto University, No. 10, pp. 75-84.

Sugita M, Ikura H, Miyano A, Yamamoto K and Wei ZW. 2014. Evaporation from Lake Kasumigaura: annual totals and variability in time and space, Hydrological Research Letters, 8, 103-107.

Sugita M. 2019. Spatial variability of the surface energy balance of Lake Kasumigaura and implications for flux measurements, Hydrological Sciences Journal, pp. 1-14

Peter AC and Ian AR. 2015. Aircraft-based observations of air-sea turbulent fluxes around the British Isles, Quarterly Journal of the Royal Meteorological Society,141, 139-152.

Rouse WR, Blanken PD, Duguay CR, Oswald CJ and Schertzer WM. 2008. Climate-lake interactions. In: Woo M.K. (ed.), Cold region atmospheric and hydrologic studies: The Mackenzie GEWEX experience, Ⅴol. 2:Hydrologic processes, Springer-Verlag, New York, pp. 139–160.

Takahashi S, Nabekura M, Tsukamoto O, Iwata T, Takemi T and Ishida H. 2000. Sea surface heat flux evaluation by on-board technique over tropical western Pacific, Sea and Air, Vol. 76, No. 2

Takahashi S, Kondo F, Tsukamoto O, Ito Y, Hirayama S and Ishida H. 2005. On-board automated the eddy flux measurement system over open ocean, SOLA, Vol. 1, 37-40.

Takeda A. 1981. Effects of water wave motions on spectral characteristics of wind fluctuations in the marine atmospheric surface layer, Journal of the Meteorological Society of Japan, Vol. 59, No. 4.

Wei Z. 2013. Estimation of surface fluxes using bulk transfer methods over lake surface: an example of Lake Kasumigaura. MS thesis, Graduate School of Life and Environmental Sciences, the University of Tsukuba, pp. 15－56.

Wei Z, Miyano A and Sugita M. (2016): Drag and Bulk Transfer Coefficients Over Water Surfaces in Light Winds, Boundary-Layer Meteorol, 10, 1－25.

伊倉宏弥 (2010): 衛星データを用いた霞ヶ浦湖面における蒸発量分布の推定. 筑波大学大学院生命 環境科学研究科修士論文, pp.130.

小川信平 (2018): 霞ヶ浦西浦における熱収支と熱分布特性の解明。筑波大学大学院生生命環境科学研究科地球科学専攻修士学位論文, pp. 1-160.

原田瑞穂 (2015): 二酸化炭素・温度・比湿測定に基づく大気－湖沼間のフラックス分布の推定－霞 ヶ浦土浦入りを対象として－. 筑波大学大学院生命環境科学研究科卒業論文, pp. 1-80

杉田倫明・田中正・筑波大学水文科学研究室 (2009): 水文科学, 共立出版, pp. 21－93.

塚本 修・文字 信貴 (2001): 地表面フラックス測定法, 気象研究ノート, 199, pp. 21.

宮野愛子 (2010): バルク式を用いた湖面におけるフラックスの算出. 筑波大学大学院生命環境科学 研究科修士論文, pp. 18

Table 1 Data measured by ship observation system

Items	Equipment	Sampling time	Average time
3 components wind speed and air temperature	Sonic anemometer (Gill Instruments Ltd., R3A and 1590-PK-020/W)	0.1 s	0.1s
Water surface temperature	Infrared radiation thermometer (Minorta, 505)	5 s	1min
Air temperature and specific humidity	Hygo-thermometer with a radiation shield (natural ventilation)	5 s	1min
Downward short wave radiation and downward long wave radiation	4-component radiometer (Kipp & Zonen B.V., CNR-1)	5 s	1min
Three accelerations and three angular rates	Inertial measurement system (Crossbow Technology., IMU-440CA-200)	0.1 s	Instantaneous
H_2O and CO_2 concentration	Gas analyzer (LI-COR, Inc., LI-7500)	0.1 s	Instantaneous

Table 2 General condition of data measurement

Run		YYYY.MM.DD	Time (JST)	Start-Destination	Weather condition	T_a (℃)	Radiation (W/m^2)	Wind speed (m/s)
1	1-1	2018.06.16	10:03-10:17	Tsuchuura-Itako	cloudy	14.0	291±84	6.20
	1-2		10:10-10:24			14.1		7.24
	1-3		10:18-10:32			14.3		8.54
	1-4		10:20-10:34			14.3		8.60
	1-5		10:33-10:47			14.5		8.10
2	2-1	2018.06.16	15:20-15:34	Itako-Tsuchiura	cloudy	15.3	144±49	8.43
	2-2		15:30-15:44			15.3		7.02
	2-3		15:35-15:49			15.3		7.08
	2-4		15:45-15:59			15.3		6.18
	2-5		15:50-16:04			15.3		5.63
3	3-1	2018.06.17	10:07-10:21	Tsuchuura-Itako	cloudy	16.7	562±186	5.34
	3-2		10:15-10:29			16.8		4.88
	3-3		10:20-10:34			16.9		4.56
	3-4		10:30-10:44			17.1		4.68
	3-5		10:35-10:49			17.2		5.10
4	4-1	2018.06.17	15:30-15:44	Itako-Tsuchiura	cloudy	18.8	237±34	4.34
	4-2		15:40-15:54			18.9		4.26
	4-3		15:45-15:59			19.0		3.95
5	5-1	2018.06.24	10:20-10:34	Tsuchuura-Itako	cloudy rainy	19.6	185±77	2.17
	5-2		10:25-10:39			19.5		2.02
	5-3		10:35-10:49			19.5		1.42
6	6-1	2018.06.24	15:27-15:41	Tsuchuura-Itako	cloudy sunny	22.8	287±76	2.66
	6-2		15:35-15:49			22.9		2.93
	6-3		15:42-15:56			23.0		2.41
7	7-1	2018.09.23	9:52-10:04	Tsuchuura-Tamatsukuri	sunny	23.2	577±186	5.18

(T_a, radiation and wind speed are average value of each segment measured by ship.)

Table 3 Data from Koshin observatory

Items	Equipment	Sampling time	Observation height	Average time
3 components wind speed, wind direction,	Sonic anemometer (Gill Instruments Ltd., R3A)	0.1 s	9.80 m	Last 10 min
Water surface temperature	Infrared radiation thermometer (Minorta, CML-303N)	5 s	4.27 m	Last 10 min
Upward long wave radiation	4-component radiometer (Kipp & Zonen B.V., CNR-1)	5 s	4.29 m	Last 10 min

Table 4 Water temperature from observatories around Lake Kasumigaura

Observatory	Longititude	Lattitude	Equipment	Sampling time	Observation height	Average time
Koshin	140.407	36.04	Platinum resistance thermometer	1 s	-0.5 m	Last 20 min
Asooki	140.4867	36.04	Platinum resistance thermometer	1 s	-0.5 m	Last 20 min
Hirayama	140.3423	36.1396	Platinum resistance thermometer	1 s	-0.5 m	Last 20 min
Kakeumaoki	140.2467	36.0539	Platinum resistance thermometer	1 s	-0.5 m	Last 20 min
Kamayaoki	140.5692	36.0065	Platinum resistance thermometer	1 s	-0.5 m	Last 20 min

Table 5 Wind speed from observatories around Lake Kasumigaura

Observatory	Longititude (°)	Lattitude (°)	Equipment	Sampling time	Observation height	Average time
Asooki	140.4867	35.9588	Windmill with wind vane anemometer	0.25 s	9.5 m	Last 10 min
Itako	140.5433	35.935	Windmill with wind vane anemometer	0.25 s	7.8 m	Last 10 min
Odaka	140.4581	36.0188	Windmill with wind vane anemometer	0.25 s	6.5 m	Last 10 min
Tsuchiura	140.2172	36.074	Windmill with wind vane anemometer	0.25 s	10 m	Last 10 min
Hokota	140.5046	36.152	Windmill with wind vane anemometer	0.25 s	10 m	Last 10 min
Wanigawa	140.6135	35.9271	Windmill with wind vane anemometer	0.25 s	8 m	Last 10 min
Tamatsukuri	140.4026	36.0954	Windmill with wind vane anemometer	0.25 s	11 m	Last 10 min
Azumamura	140.4526	35.9443	Windmill with wind vane anemometer	0.25 s	41 m	Last 10 min

Table 6 Quality flags for stationarity (Foken et al., 2005; Wei, 2003)

Class	Flags
1 2	Excellent
3 4 5	Normal
6 7 8	Low
9	Bad

Table 7 Condition of steady state

Run		Class ($\overline{\boldsymbol{w'q'}}$)	Class ($\overline{\boldsymbol{w't'}}$)
1	1-1	1	2
	1-2	1	2
	1-3	1	2
	1-4	1	1
	1-5	1	1
2	2-1	1	1
	2-2	2	2
	2-3	1	1
	2-4	1	1
	2-5	1	2
3	3-1	1	1
	3-2	1	2
	3-3	1	2
	3-4	1	3
	3-5	1	1
4	4-1	1	1
	4-2	1	1
	4-3	1	3
5	5-1	2	1
	5-2	2	1
	5-3	6	1
6	6-1	2	5
	6-2	4	2
	6-3	2	7
7	7-1	4	4

Table 8 Condition of spectrum analysis

Run	spectrum analysis
1	O
2	O
3	O
4	O
5	O
6	O
7	O

○: dats is good for calculating fluxes.

Table 9 Condition of trend

Run	trend
1	
2	
3	
4	
5	√
6	
7	

Table 10 Conditions of R_n and G

Run	Mean value of R_n (W/m^2)	Mean value of G (W/m^2)
1	245	3
2	142	-119
3	501	322
4	189	29
5	178	98
6	175	97
7	562	309

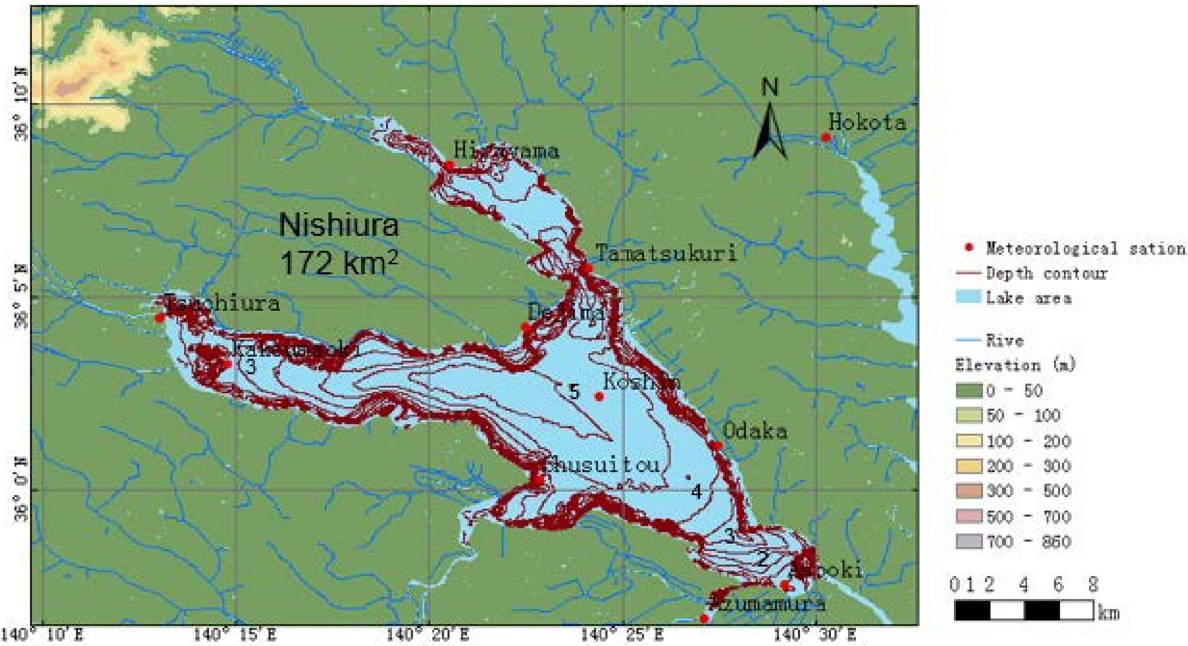

Fig. 1 Topographic map of Lake Kasumigaura

Fig. 2 Pleasure boat (https://www.ibarakiguide.jp/db-kanko/lacusmarina.html)

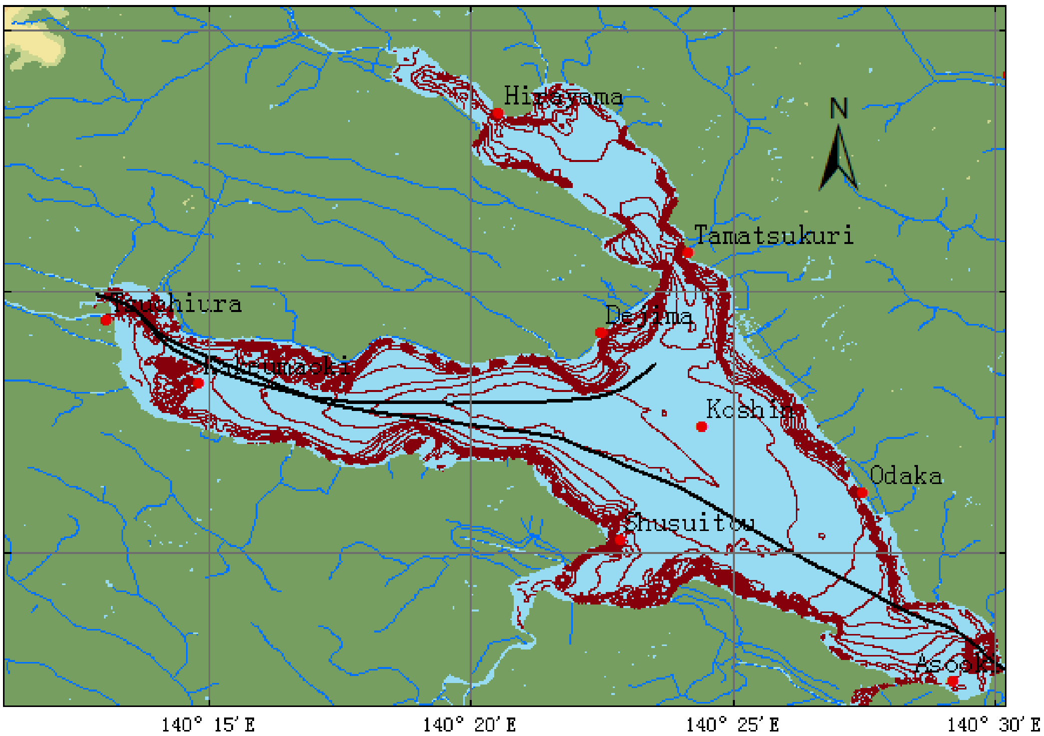

Fig. 3 Ship courses

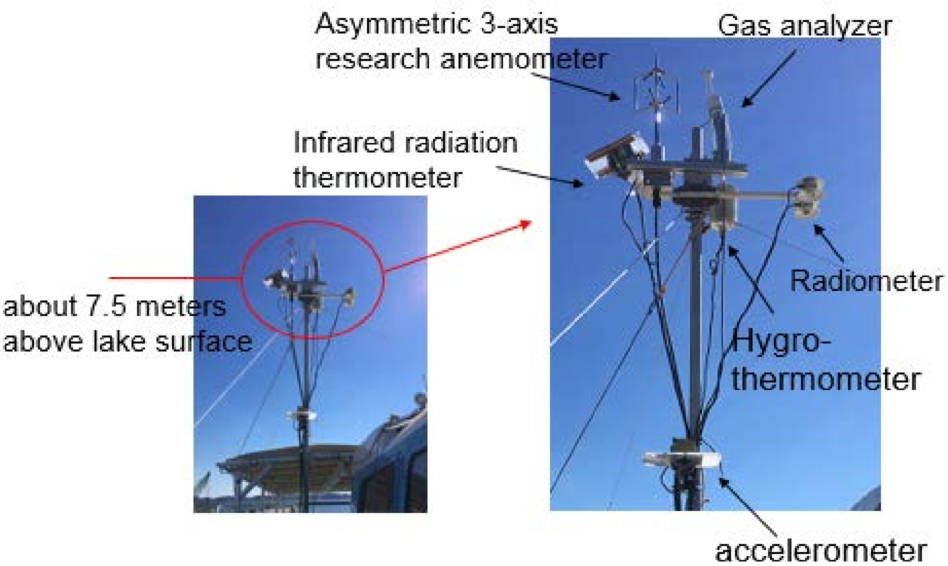

Fig. 4 Instruments on ship

Fig. 5 Koshin Observatory (Photo was taken on 2017.12.11)

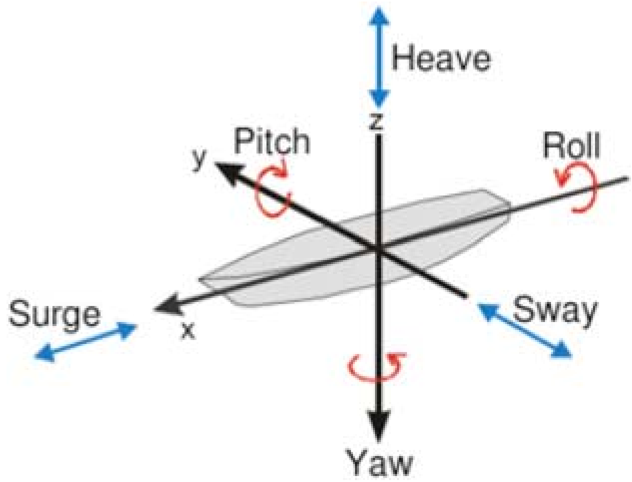

Fig. 6 Ship motion (Lee et al., 2016)

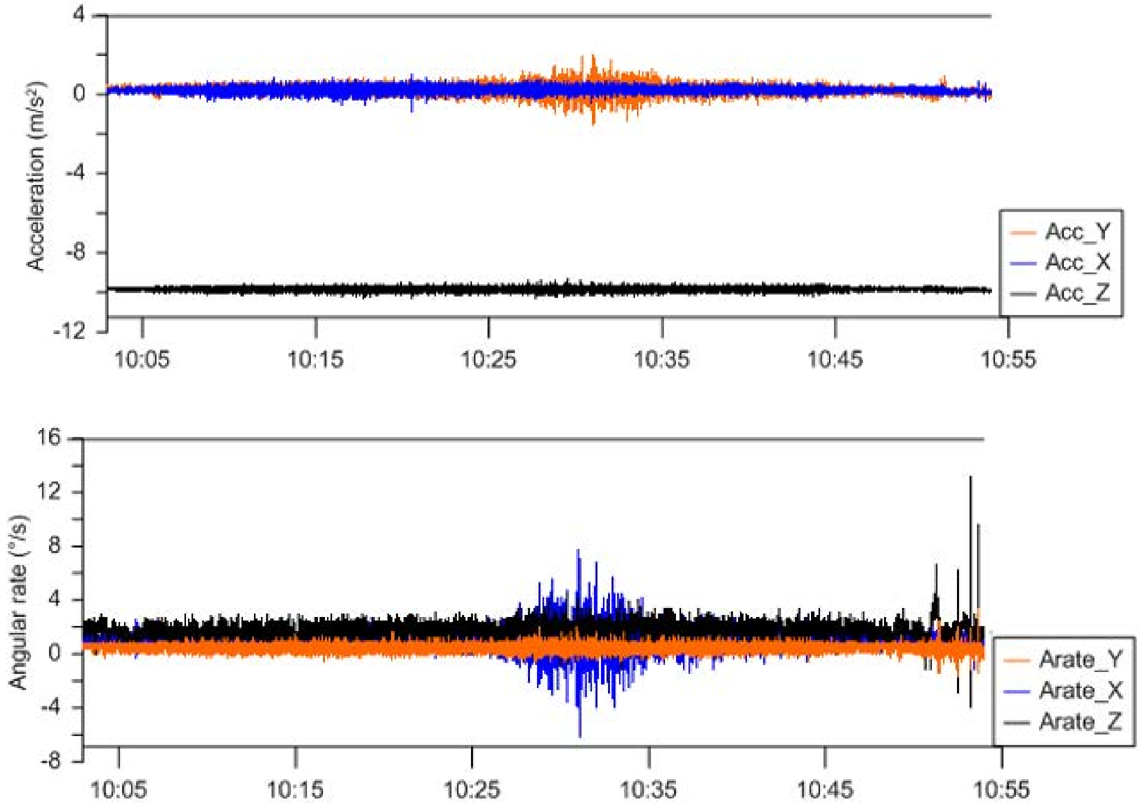

Fig. 7 Three accelerations and angular rates of ship (raw data)

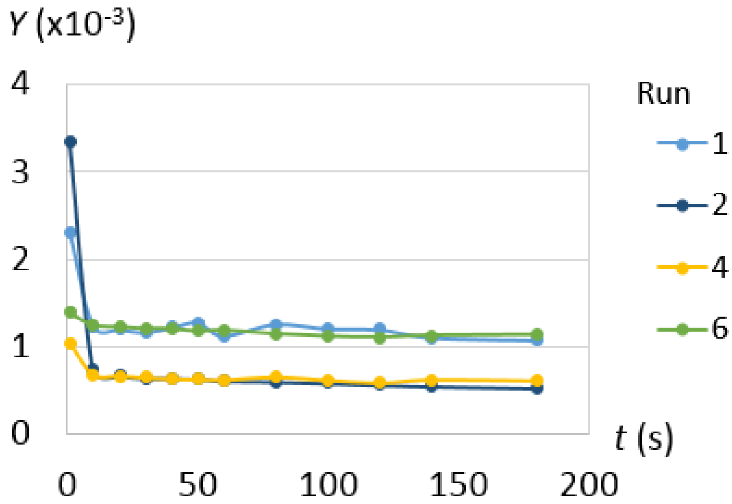
Y (x10-3)
4
3
2
1
0
Run
1
2
4
6
t (s)
0
50
100
150
200

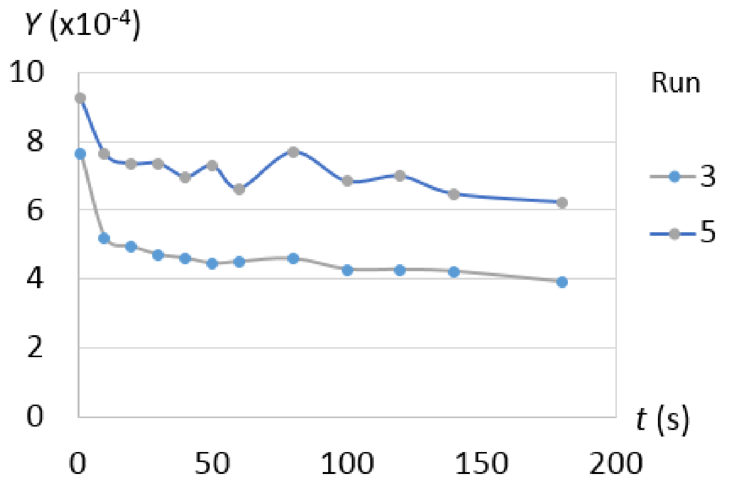
Y (x10-4)
10
8
6
4
2
0
Run
3
5
t (s)
0
50
100
150
200

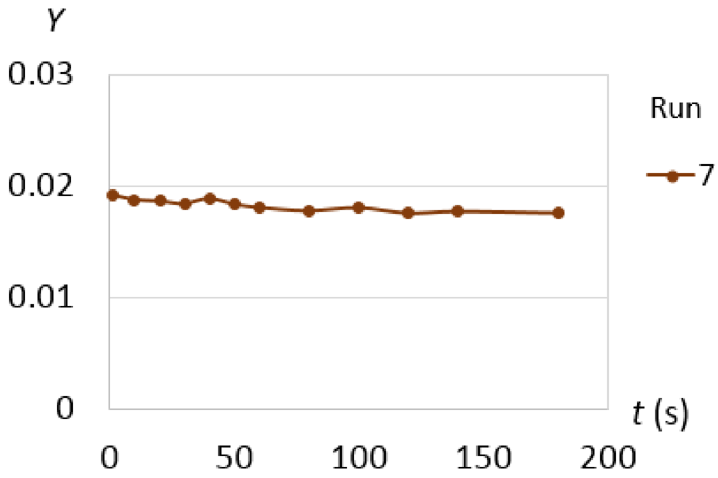

Fig. 8 Mean square deviations of longitudinal accelerations with different averaging time

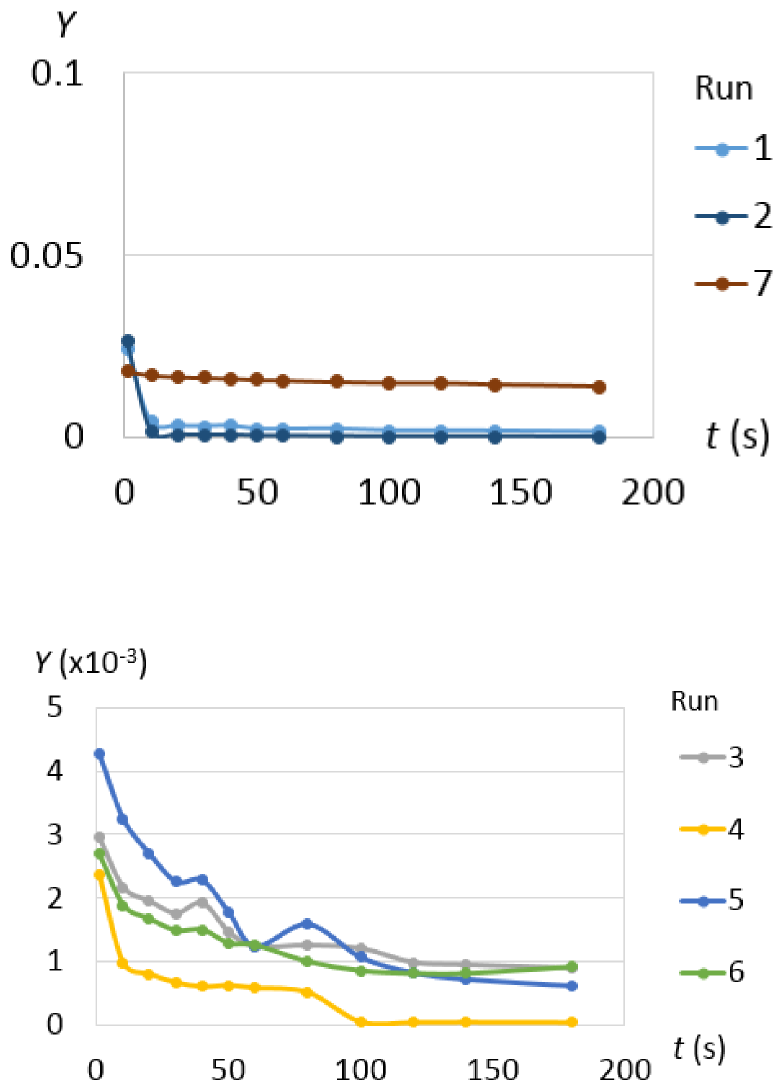

Fig. 9 The same as Fig. 8 but for lateral accelerations

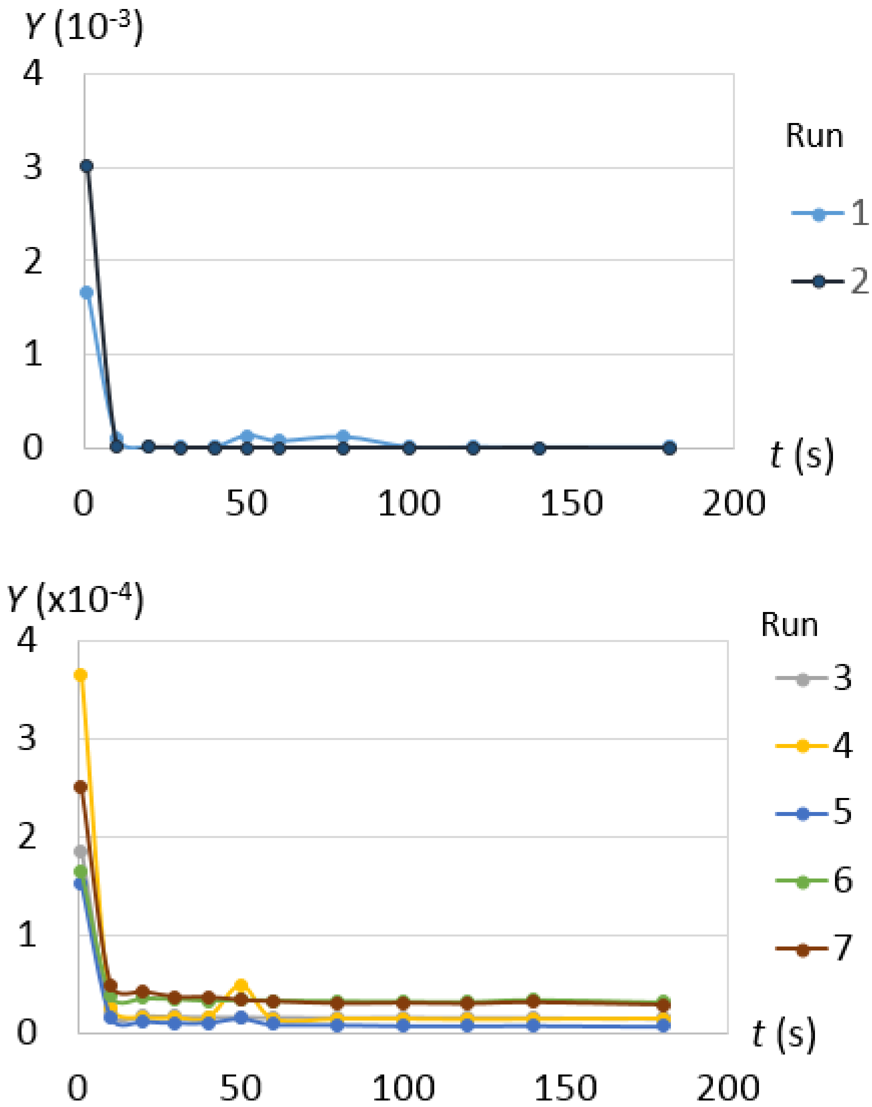

Fig. 10 The same as Fig. 8 but for vertical accelerations

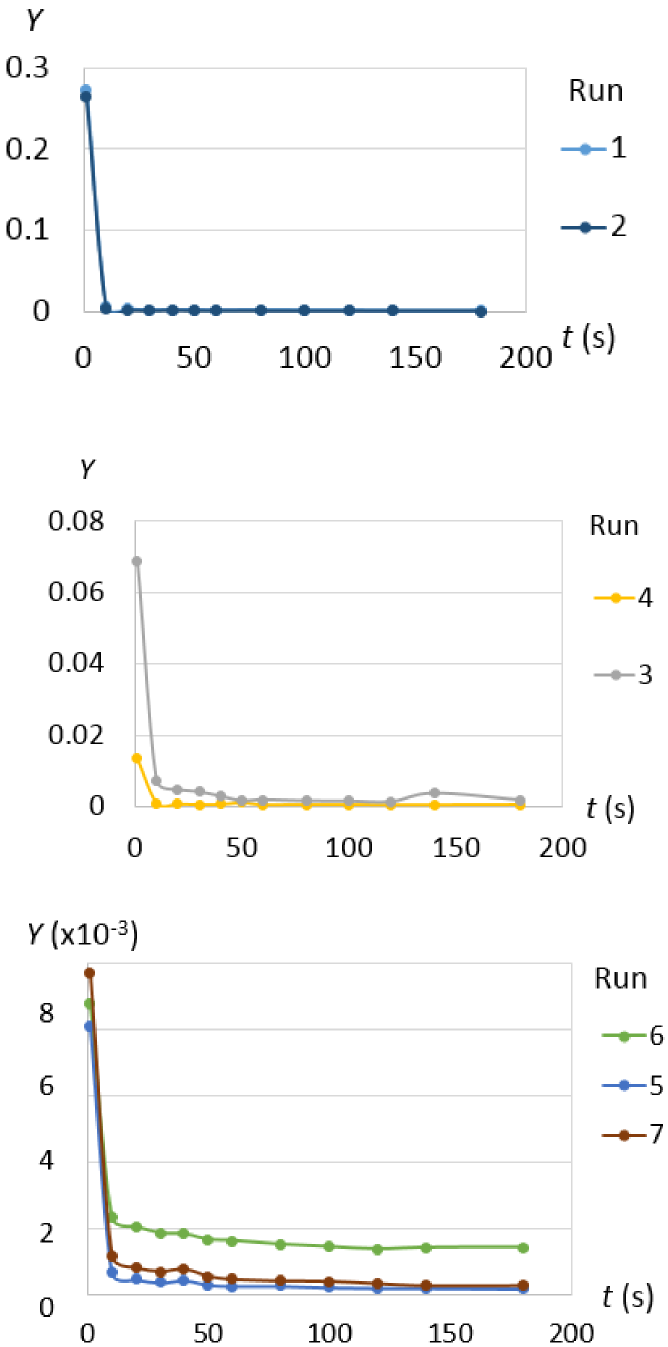

Fig. 11 Mean square deviations of longitudinal angular rates with different averaging time

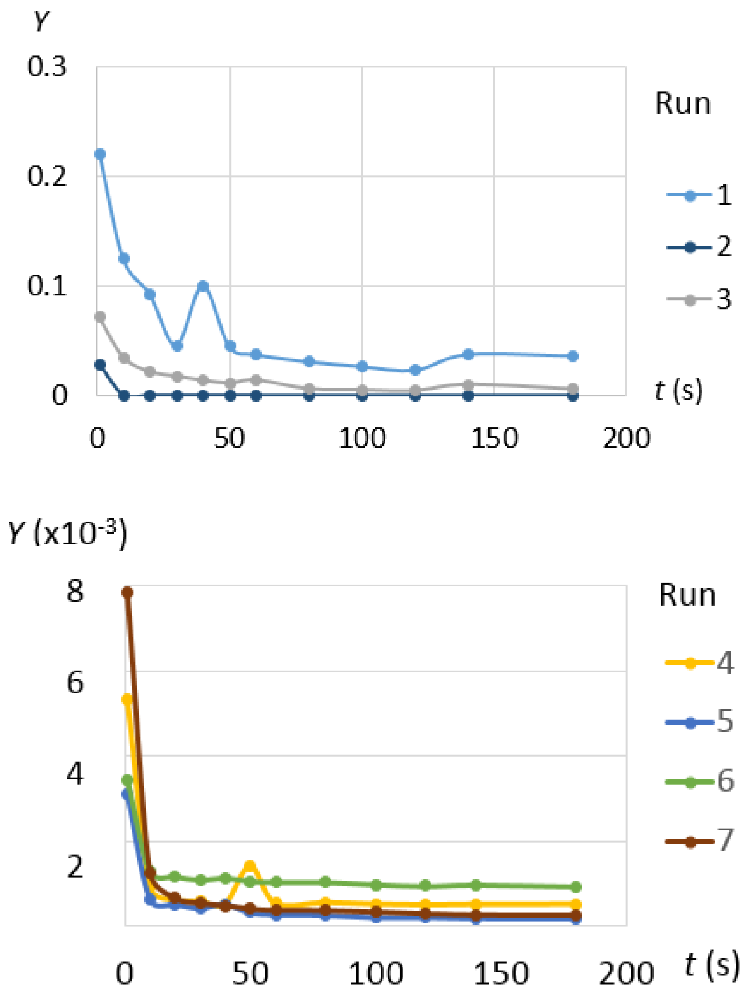

Fig. 12 The same as Fig. 11 but for lateral angular rates

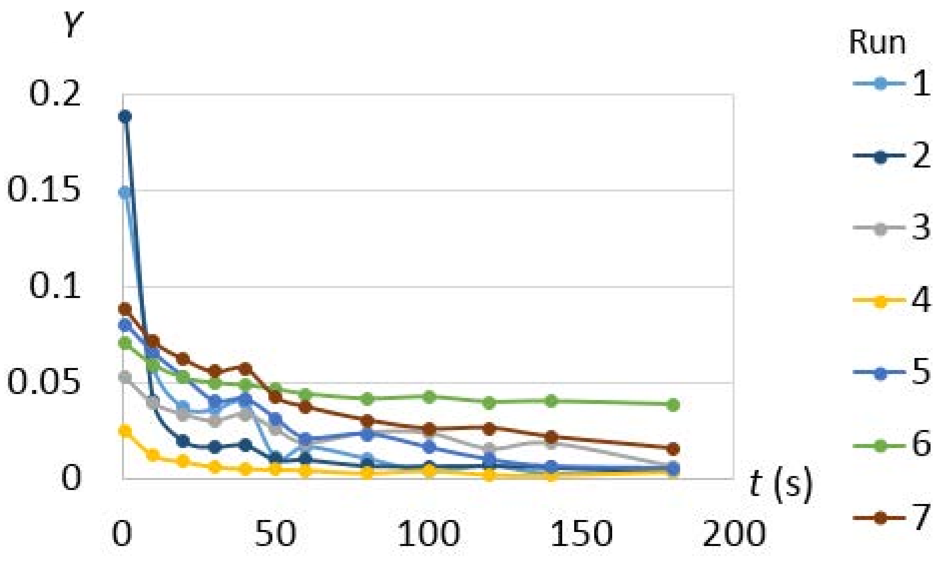

Fig. 13 The same as Fig. 11 but for vertical angular rates

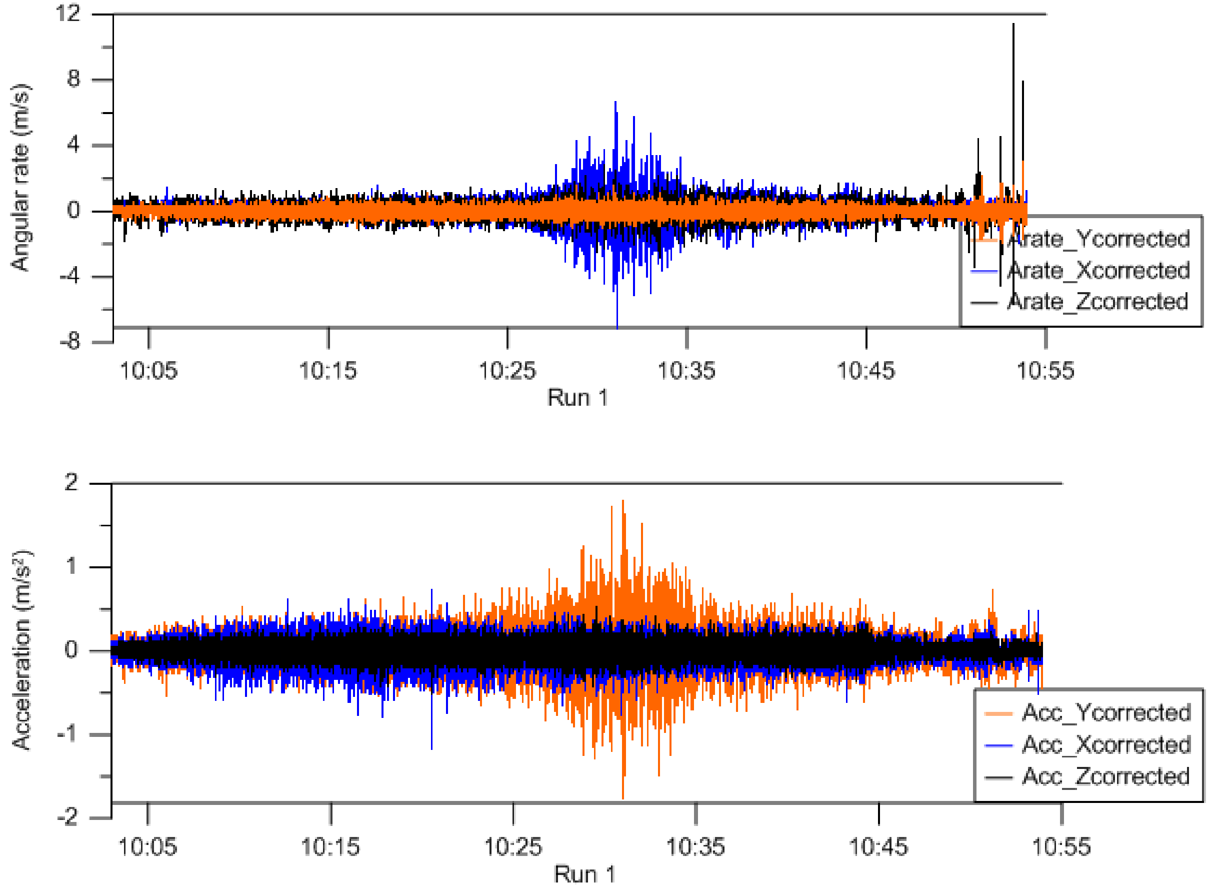

Fig. 14 An example of three angular rates and three accelerations after correction (Run 1)

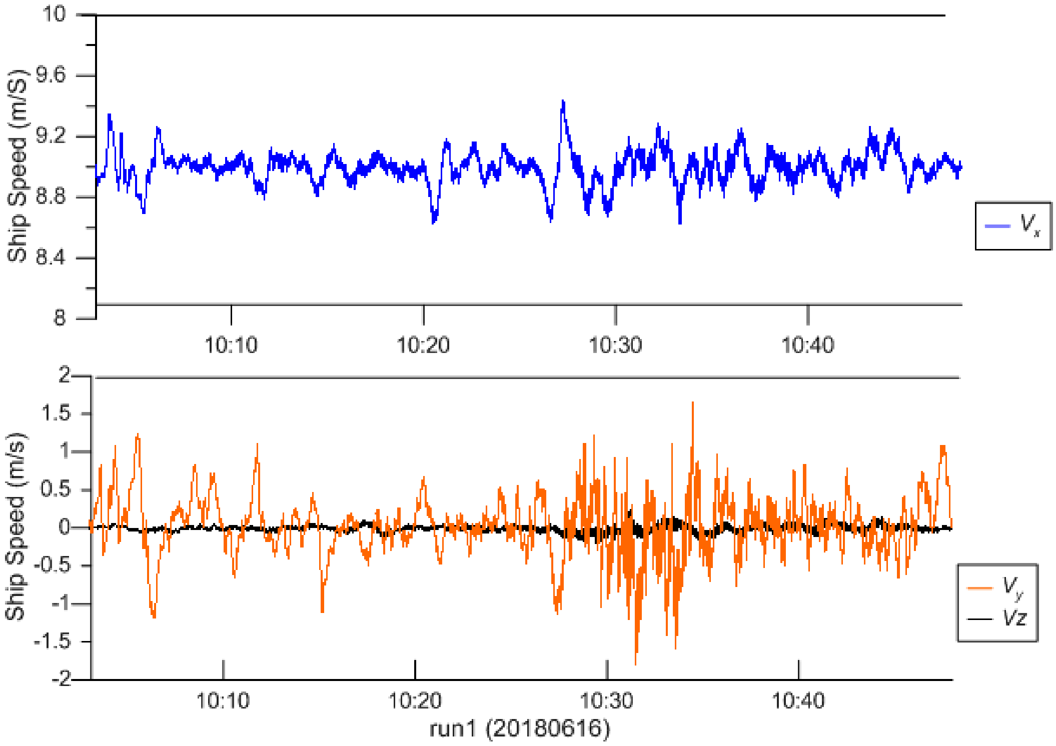

Fig. 15 An example of ship speed (Run1)

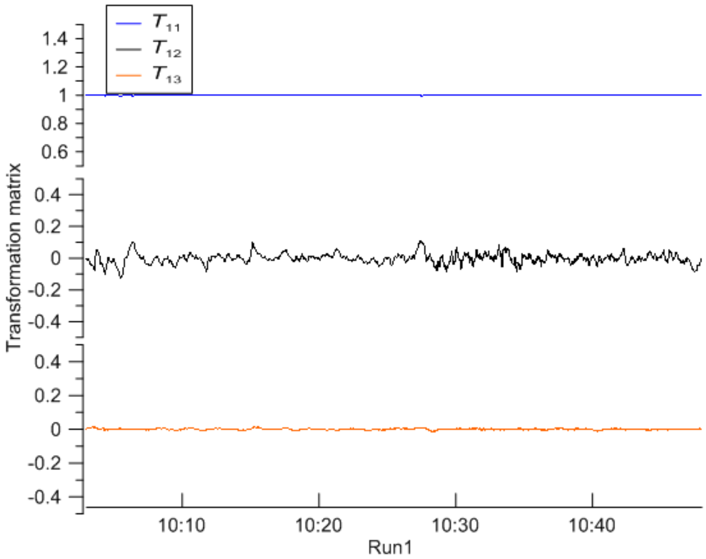
T_{11}
T_{12}
T_{13}
Transformation matrix
1.4
1.2
1
0.8
0.6
0.4
0.2
0
-0.2
-0.4
0.4
0.2
0
-0.2
-0.4
10:10
10:20
10:30
10:40
Run1

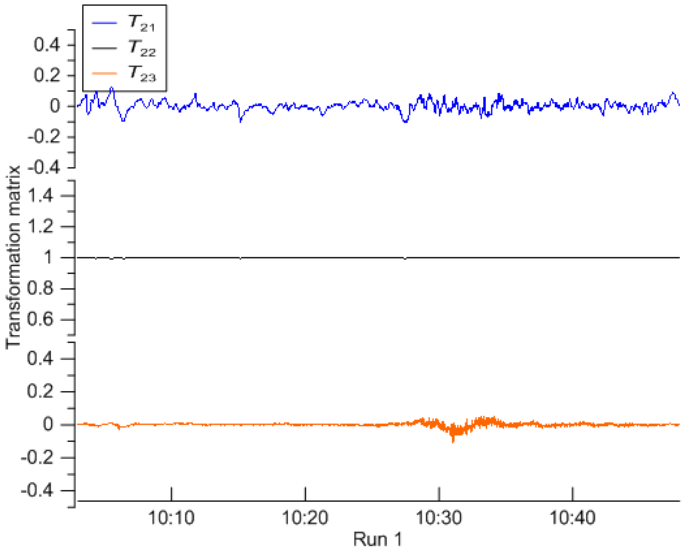
T_{21}
T_{22}
T_{23}
Transformation matrix
0.4
0.2
0
-0.2
-0.4
1.4
1.2
1
0.8
0.6
0.4
0.2
0
-0.2
-0.4
10:10
10:20
10:30
10:40
Run 1

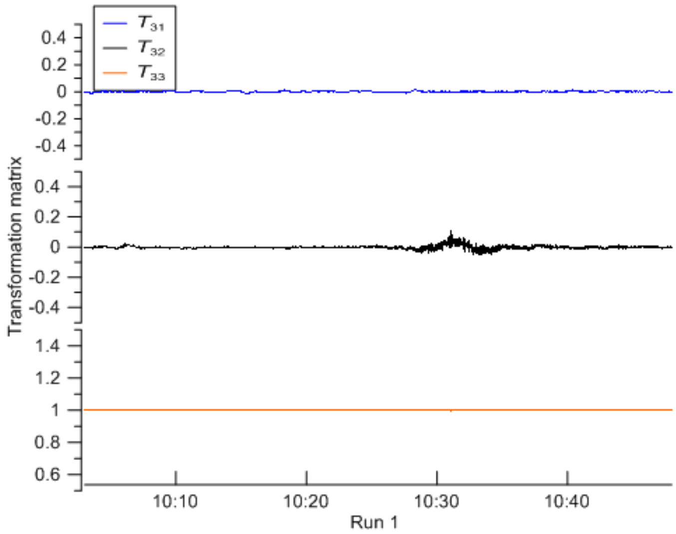

Fig. 16 An example of transformation matrix (Run1)

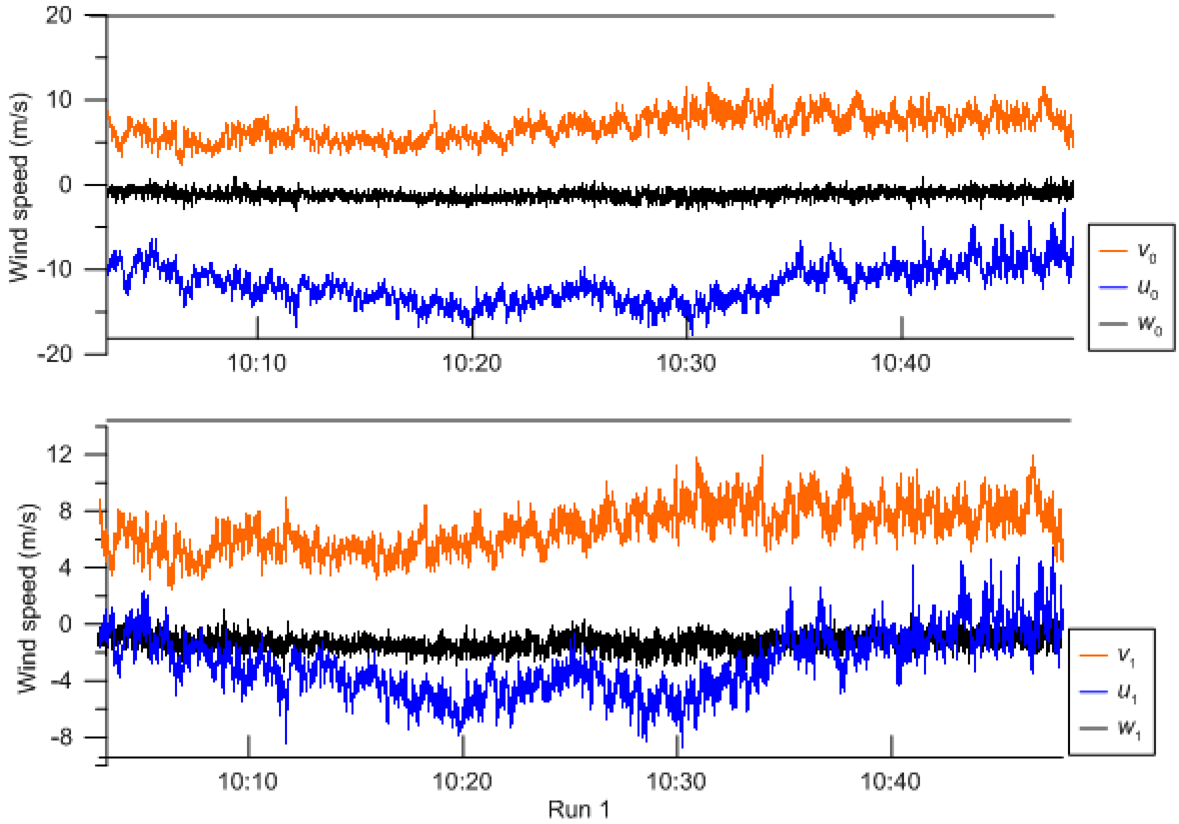

Fig. 17 Wind speeds observed from ship and after ship motion correction (Run 1)

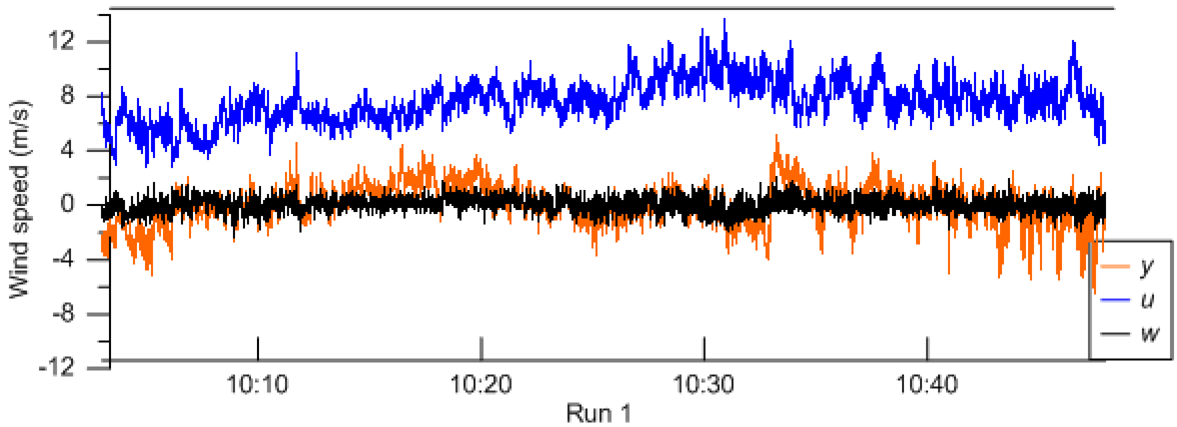

Fig. 18 An example of wind speed after correction of Run 1

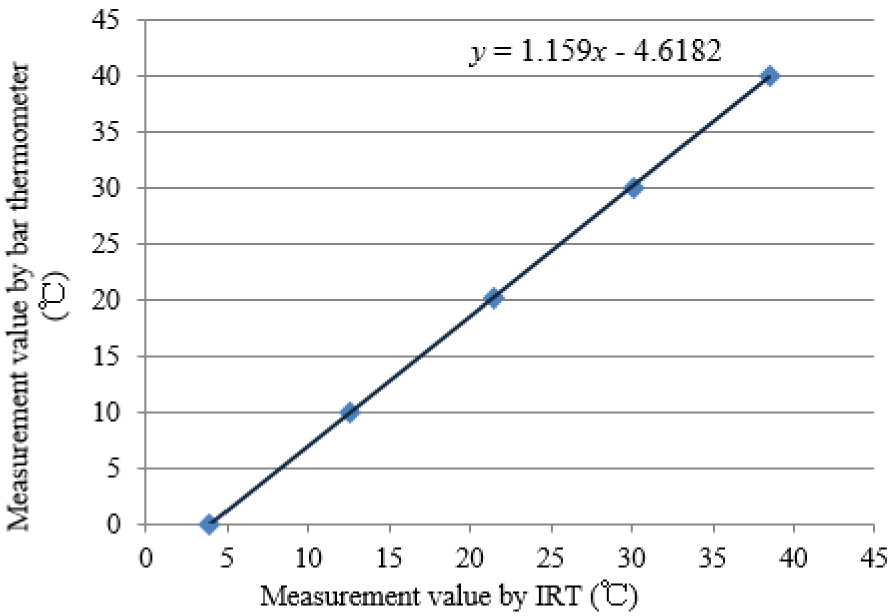

Fig. 19 Calibration of infrared radiation thermometer (IRT) (2018.02.05)

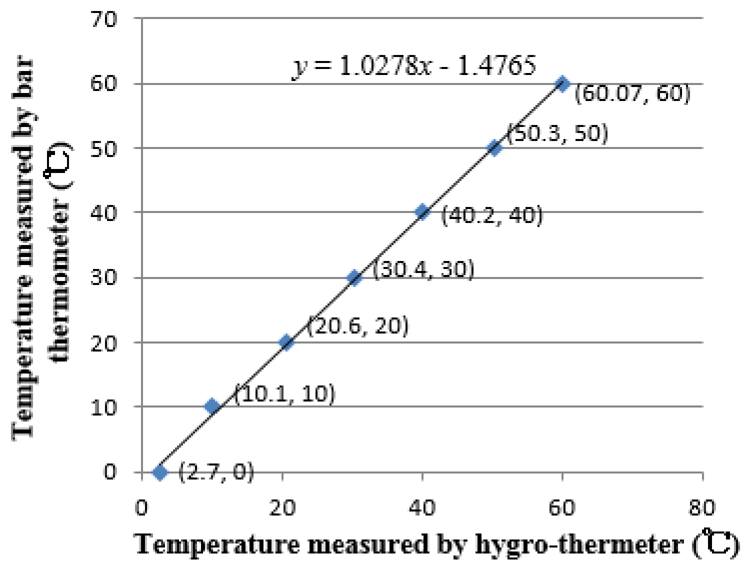

Fig. 20 Calibration of hygro-thermometer (for temperature) (2018.05.29)

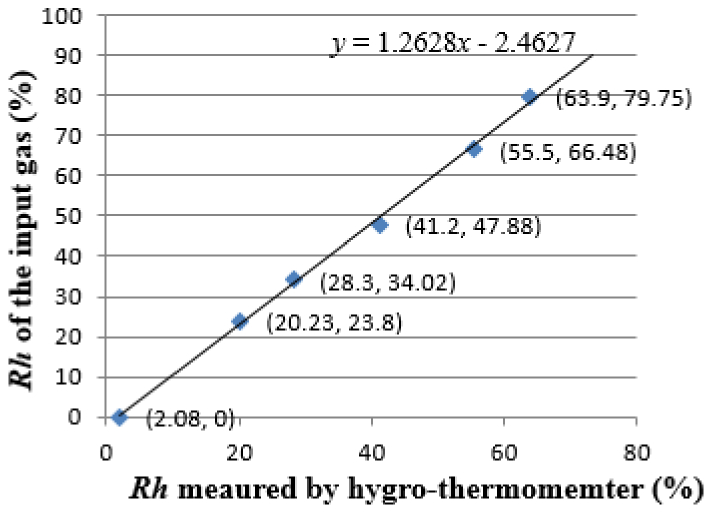

Fig. 21 Calibration of hygro-thermometer (for humidity) (2018.05.29)

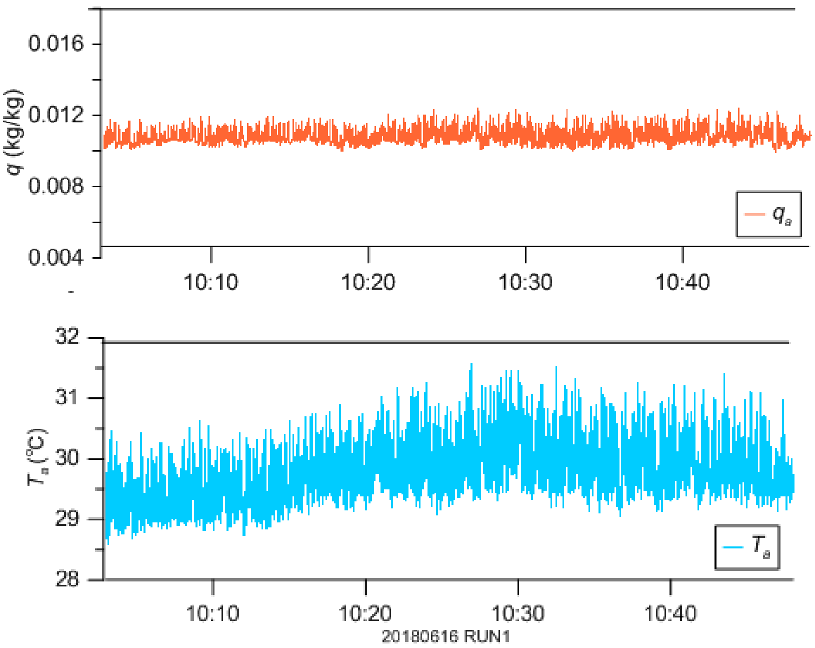

Fig. 22 An example of q_a, T_a from Run1 (raw data)

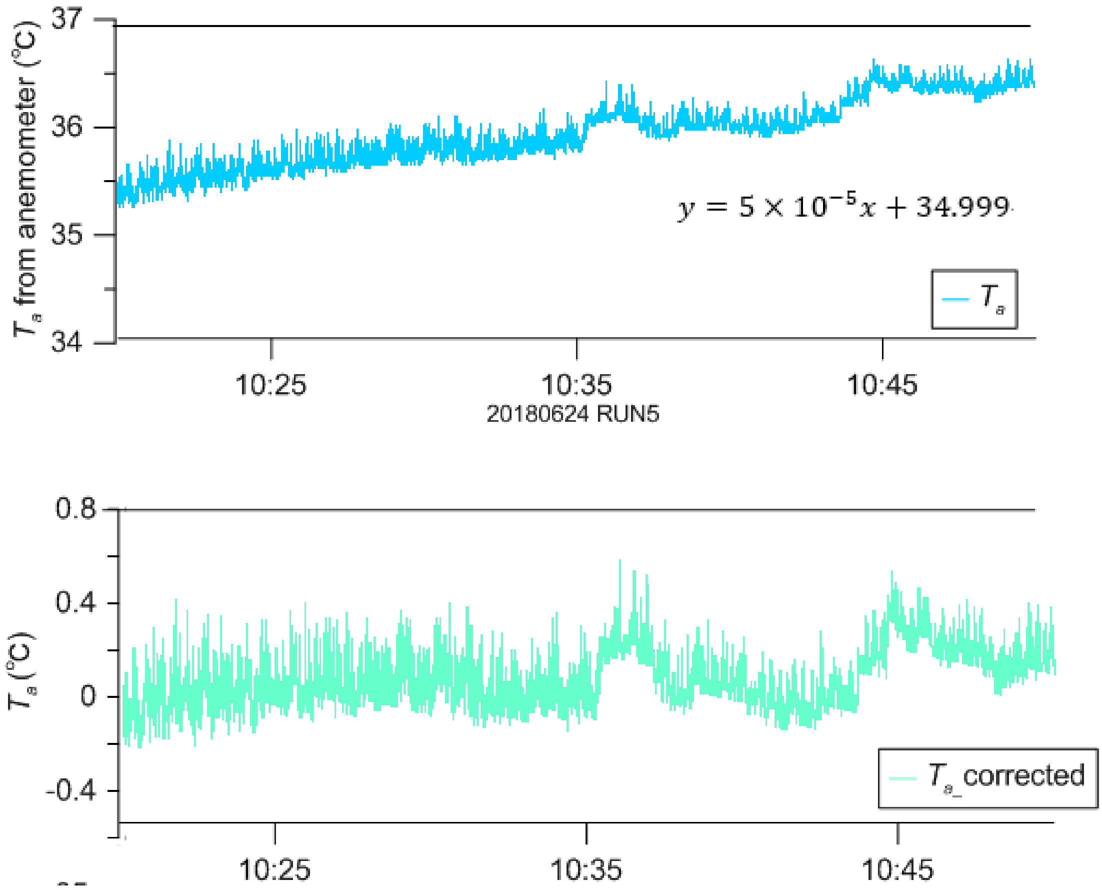

Fig. 23 Trend of T_a and trend removed

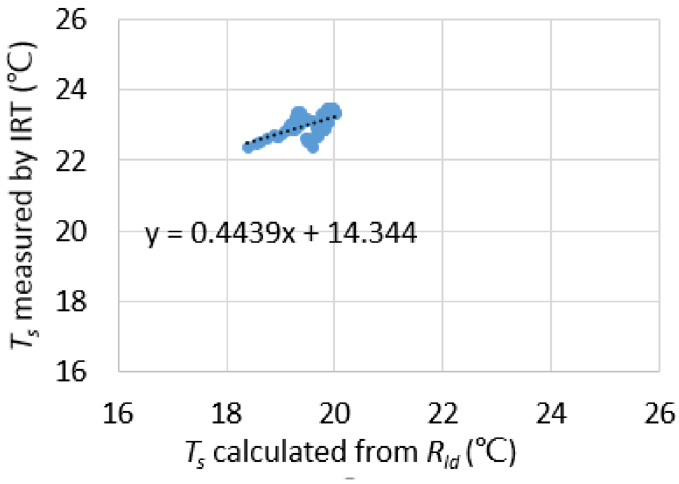

Fig. 24 The comparison of T_s measured by IRT and T_s calculated from R_{ld}

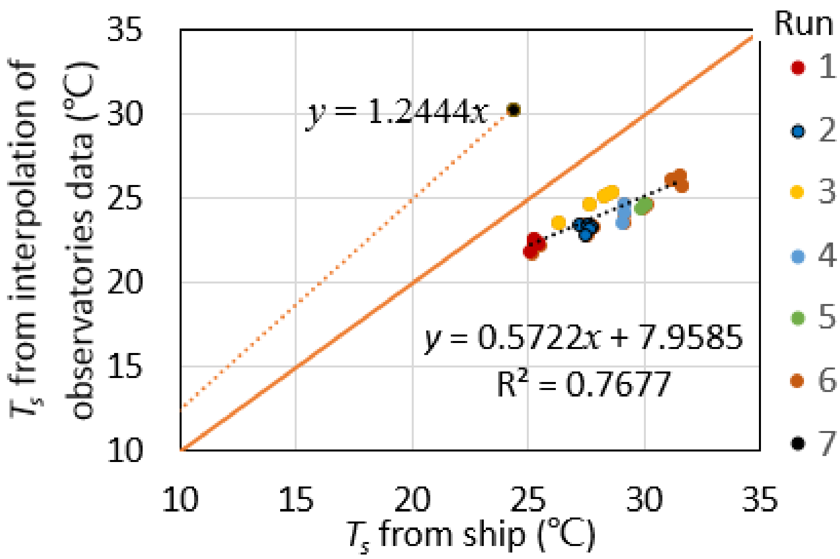

Fig. 25 T_s from interpolation of observatories data and ship

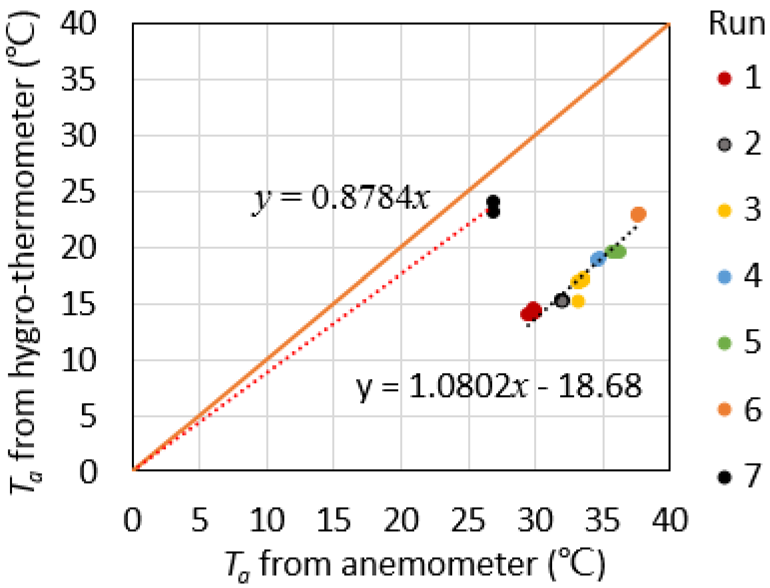

Fig. 26 T_a from anemometer and hygro-thermometer

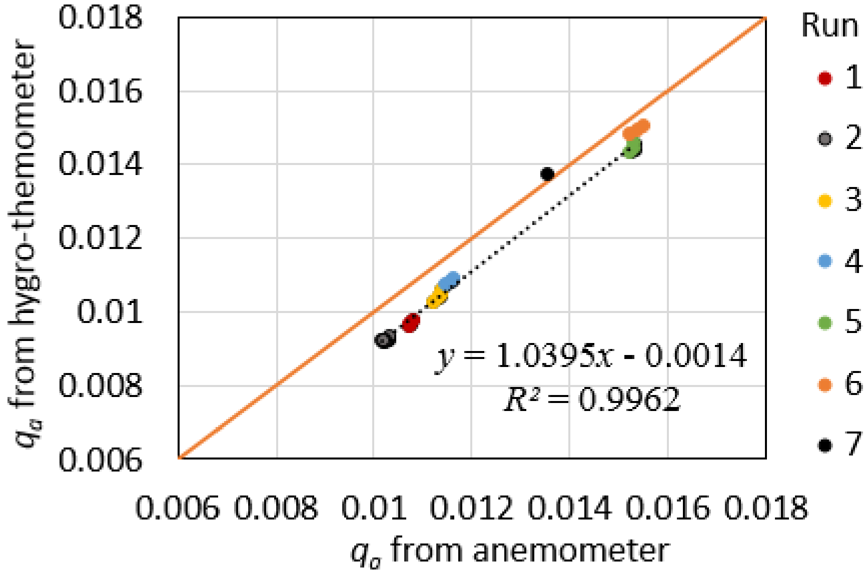

Fig. 27 q_a from anemometer and hygro-thermometer

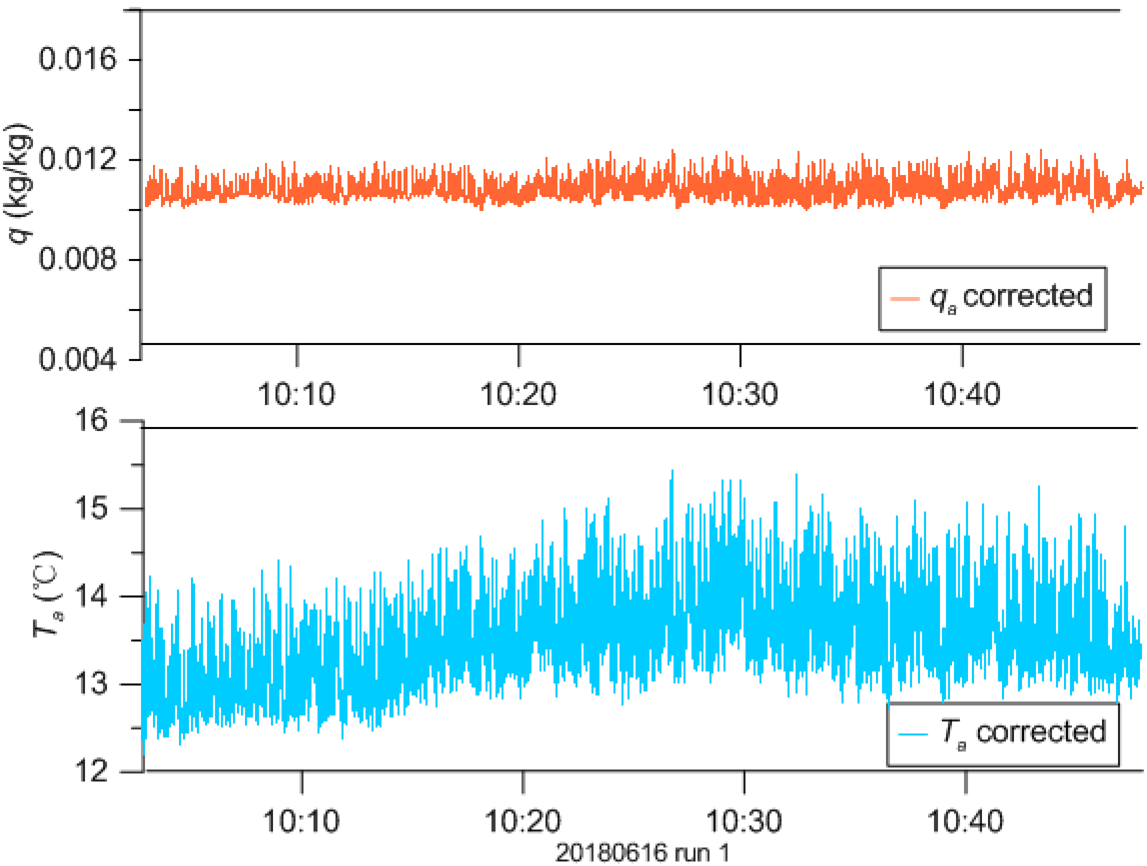

Fig. 28 An example of q_a and T_a from Run1 (after correction)

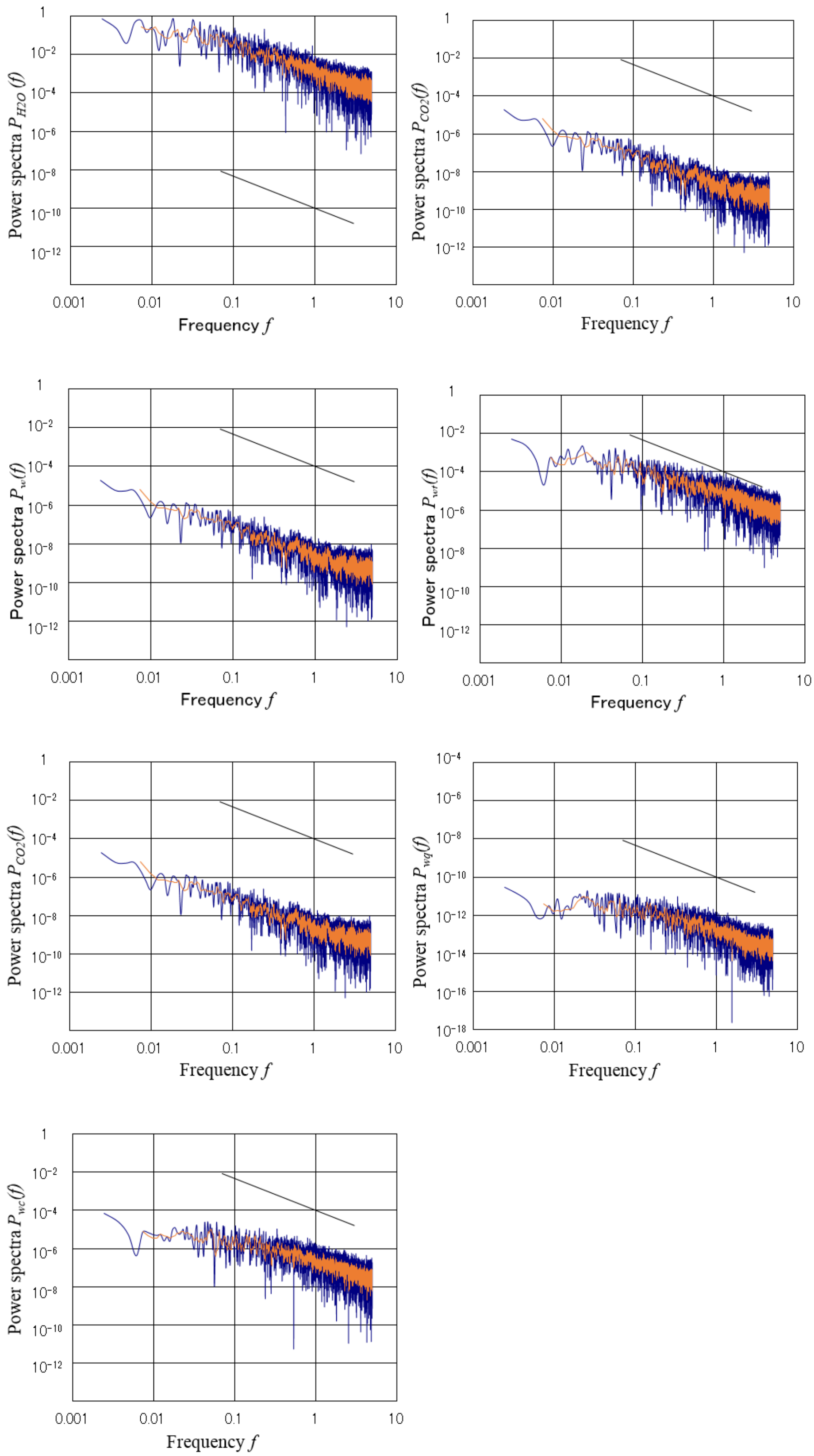

Fig. 29 An example of spectral analysis of Run 1 (The slope of solid line is -5/3)

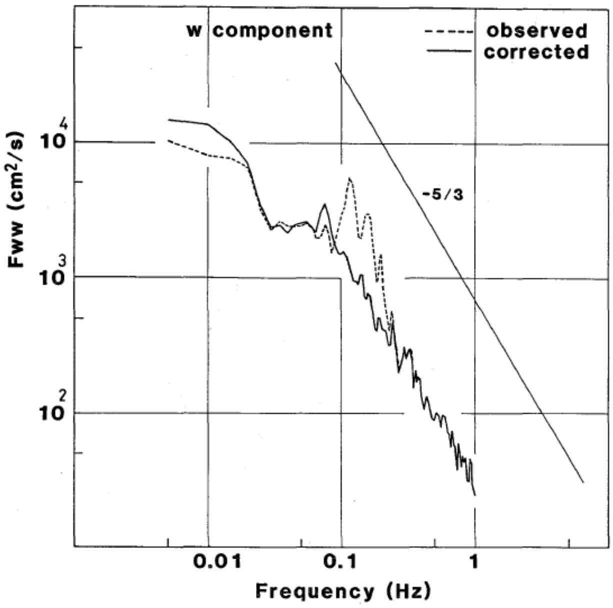

Fig. 30 Spectra of observed and corrected vertical wind speed (Fujitani, 1985)

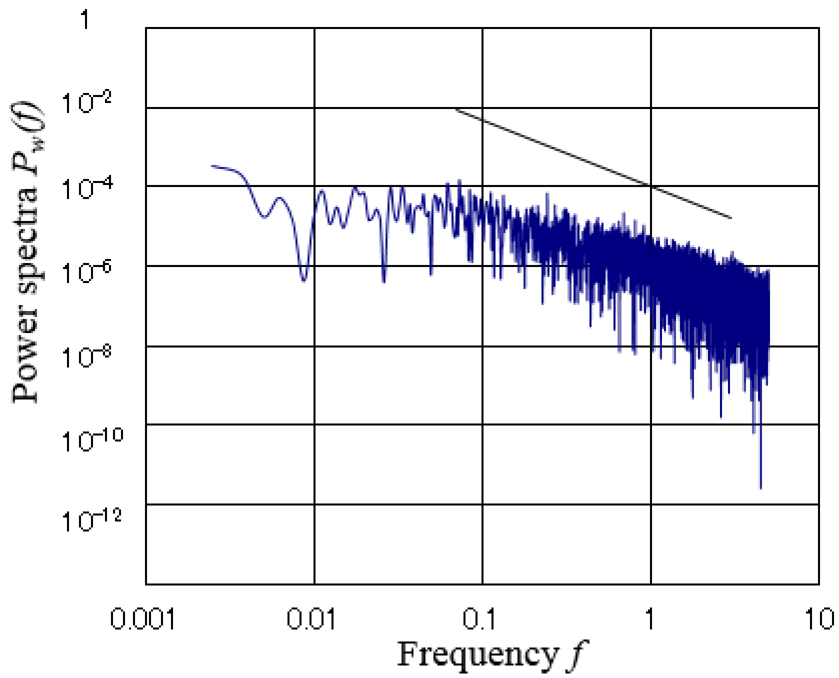

Fig. 31 Spectra of observed vertical wind speed (An example of Run 1)

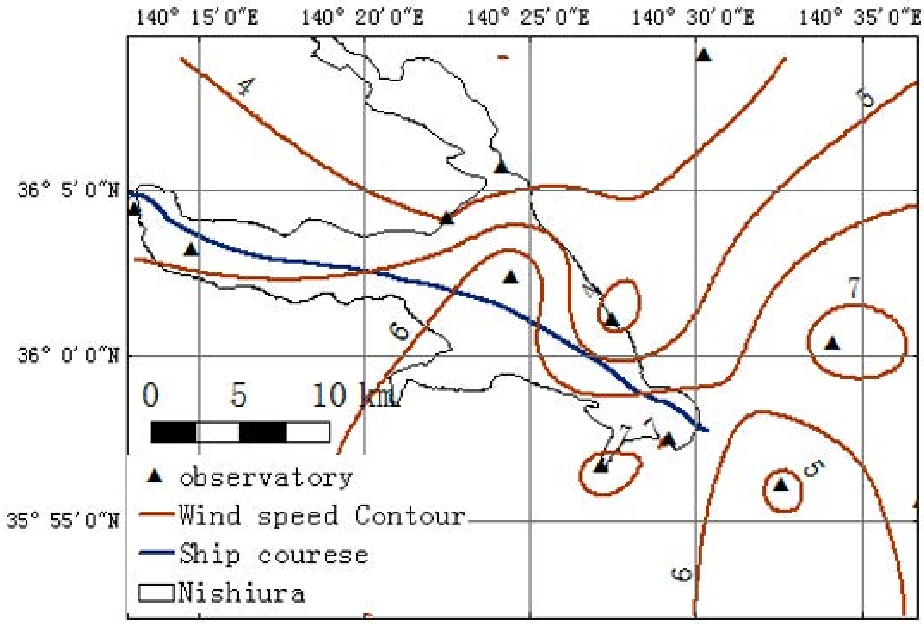

Fig. 32 An example of interpolation of wind speed (Run 1)

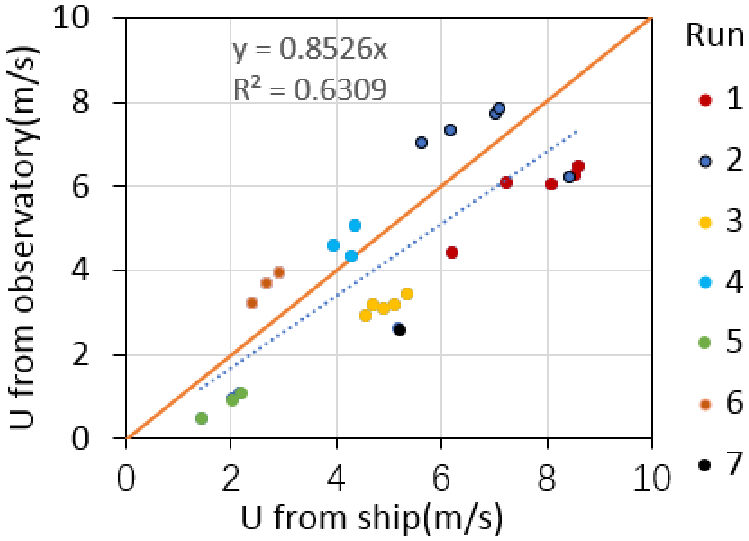

Fig. 33 Wind speed from observatory and ship

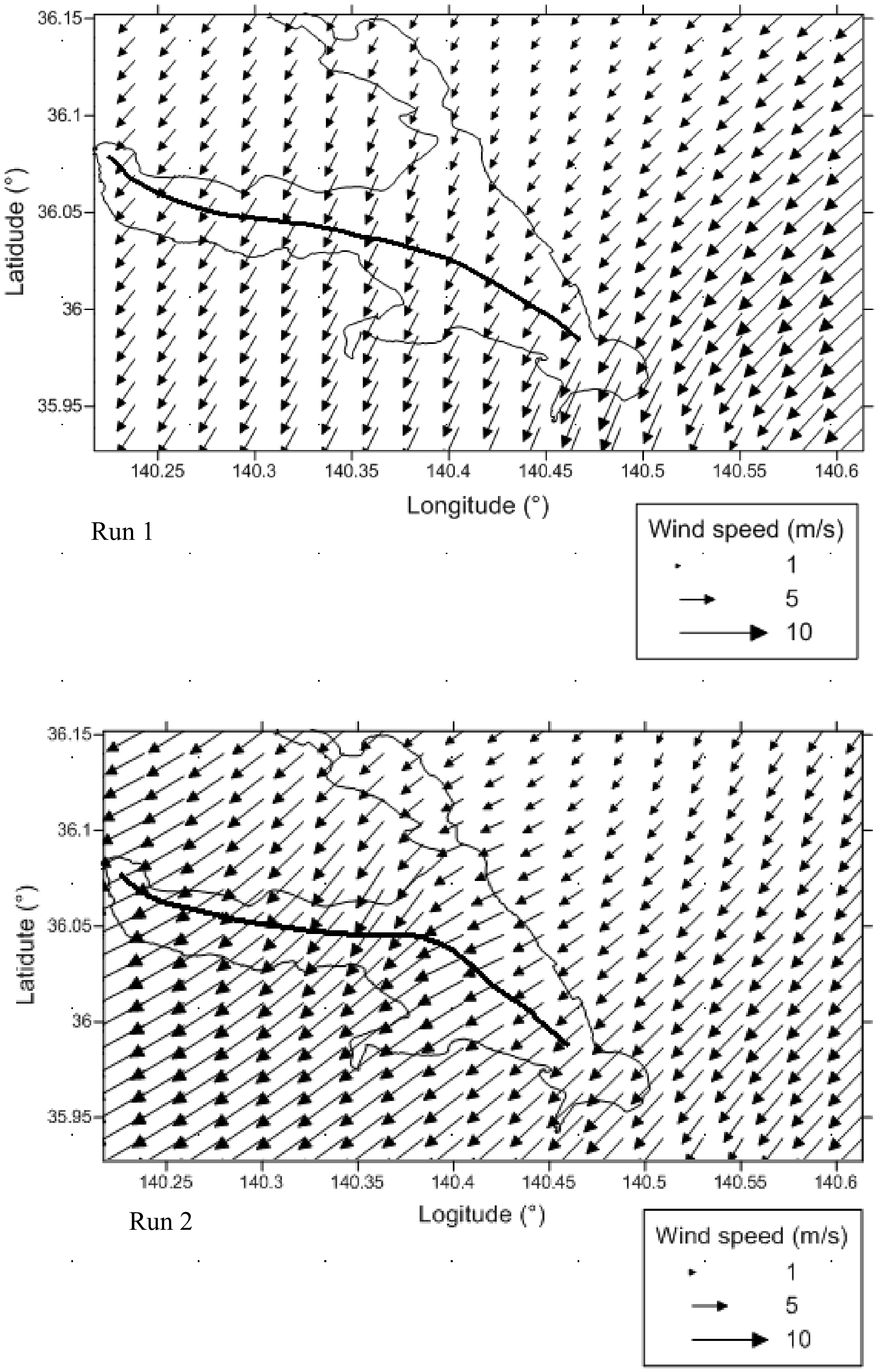

Fig. 34 Wind direction from interpolation of Run 1 and Run 2

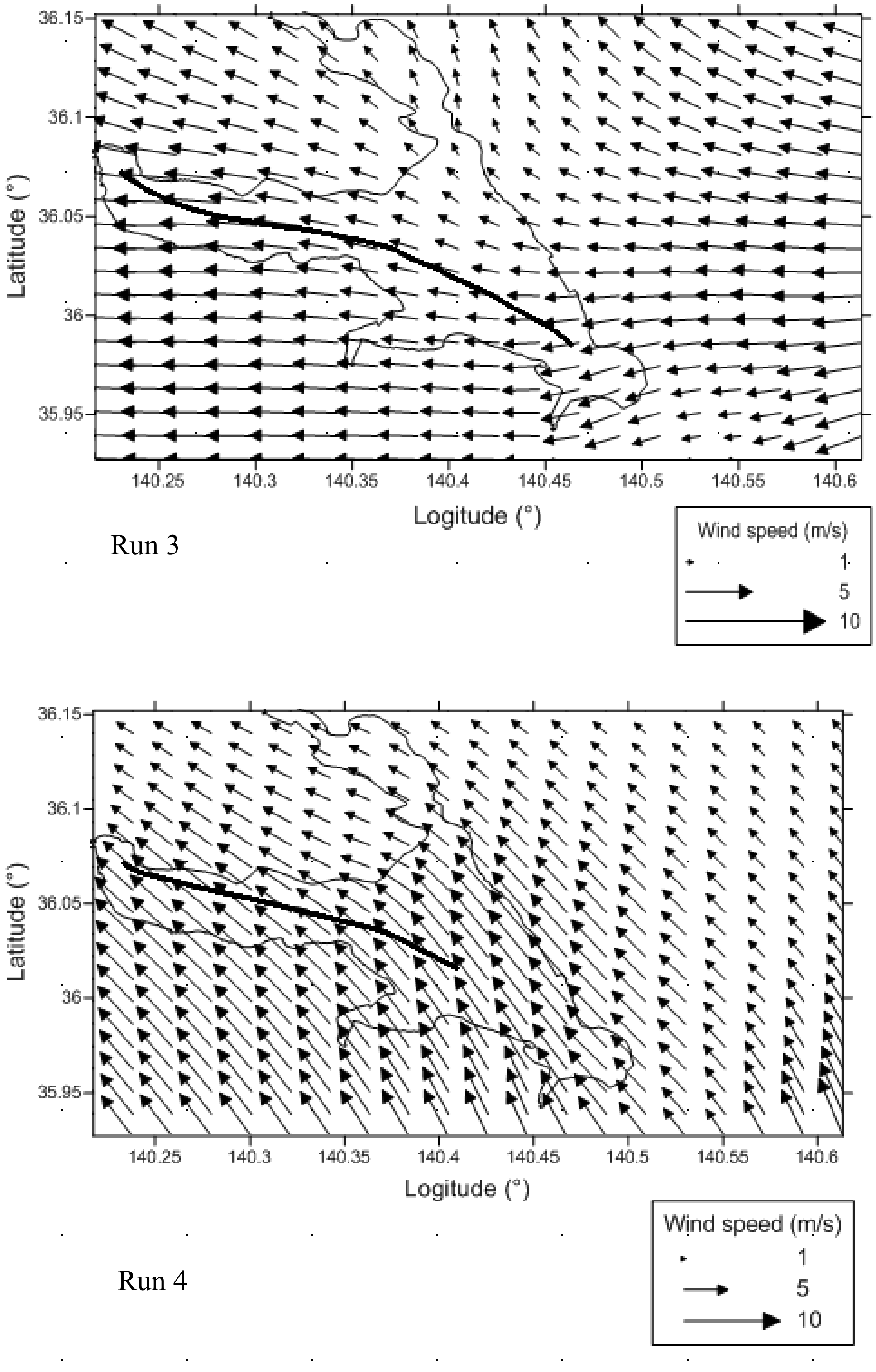

Fig. 35 The same as Fig. 24 but for Run 3 and Run 4

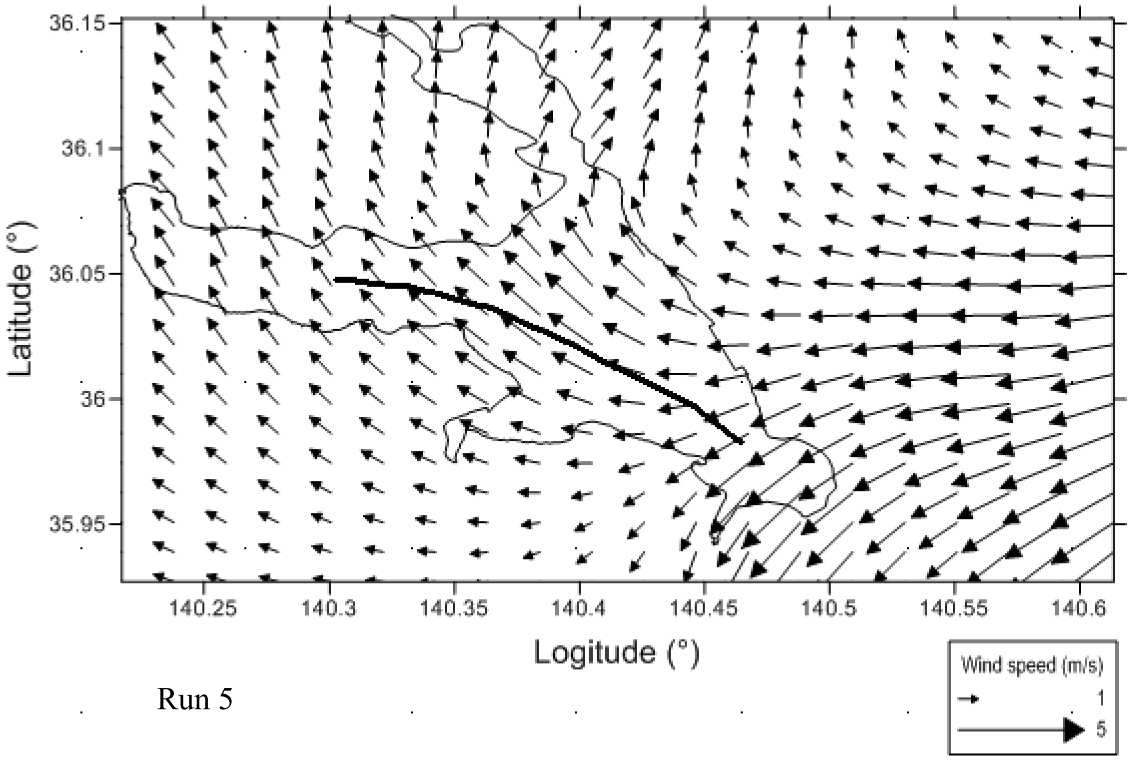

Run 5

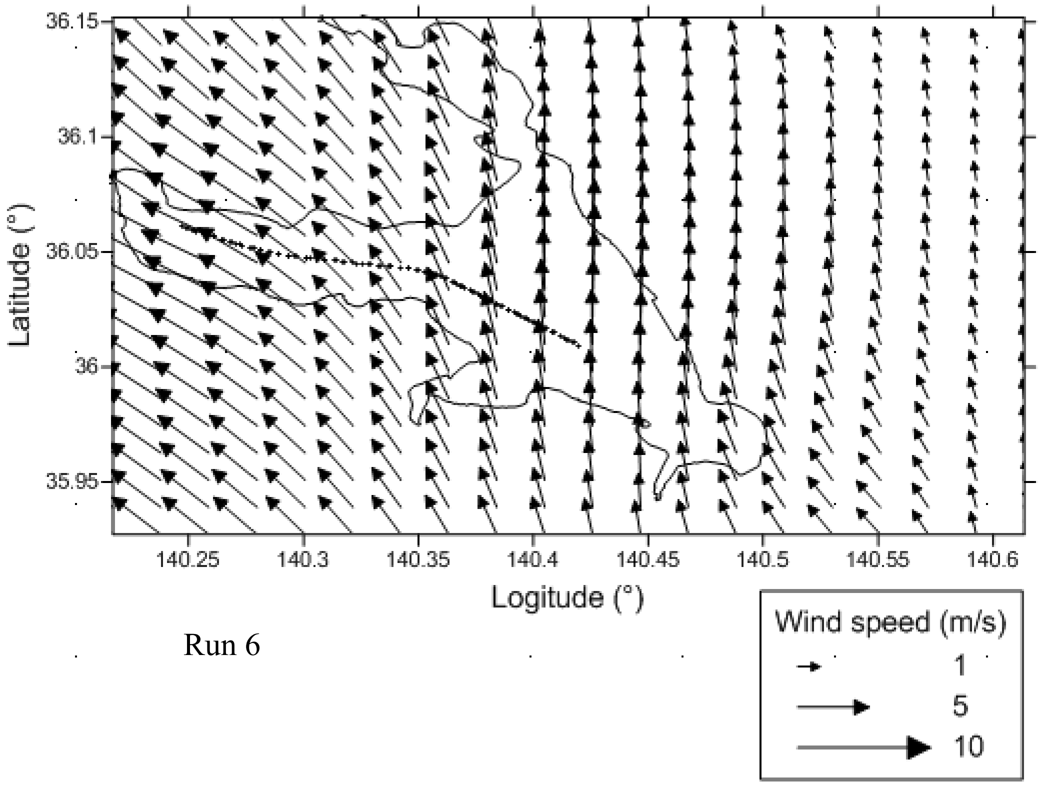

Run 6

Fig. 36 The same as Fig. 25 but for Run 5 and Run 6

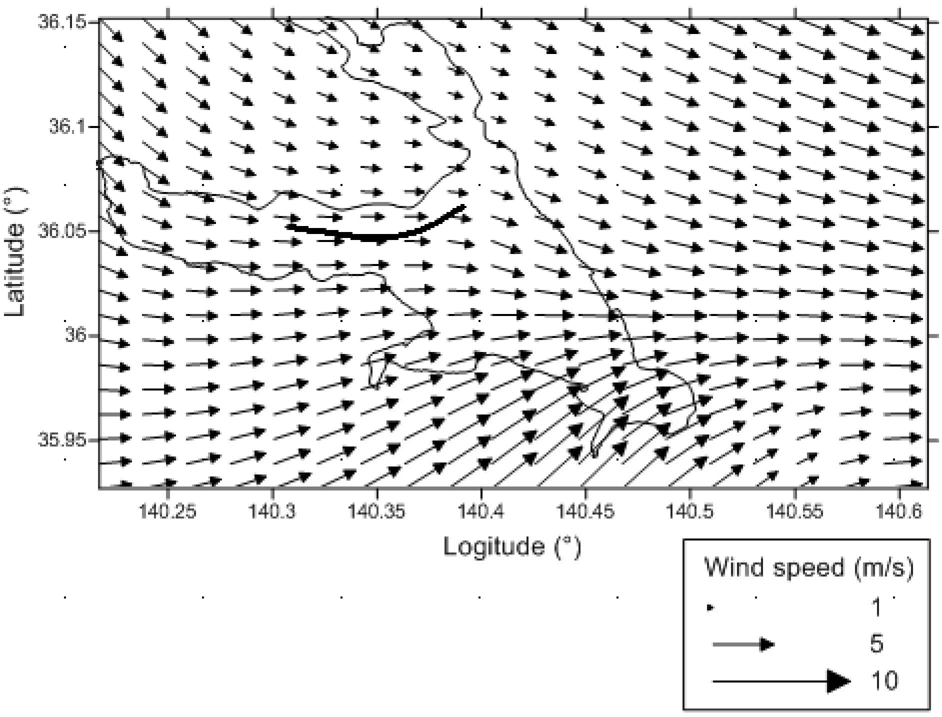

Fig. 37 The same as Fig. 25 but for Run 7

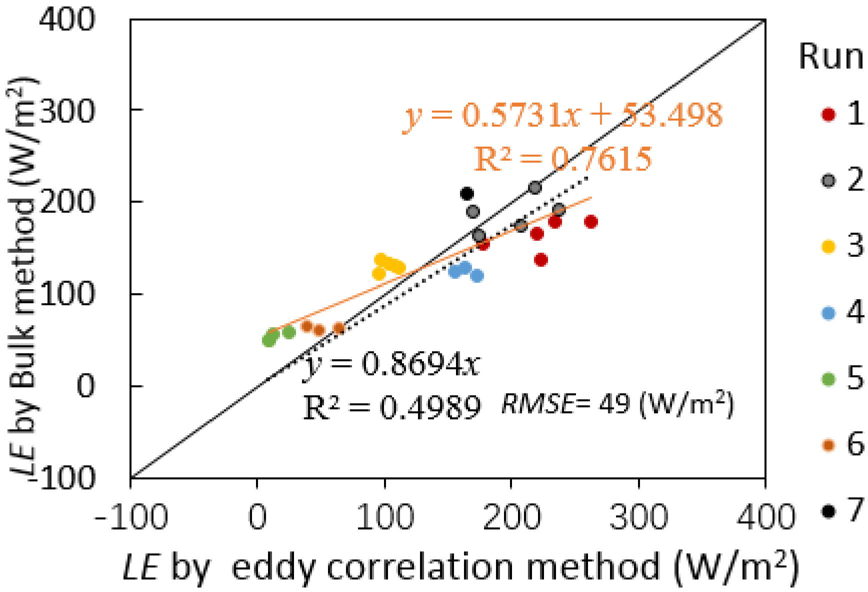

Fig. 38 Comparison of *LE* by the two methods

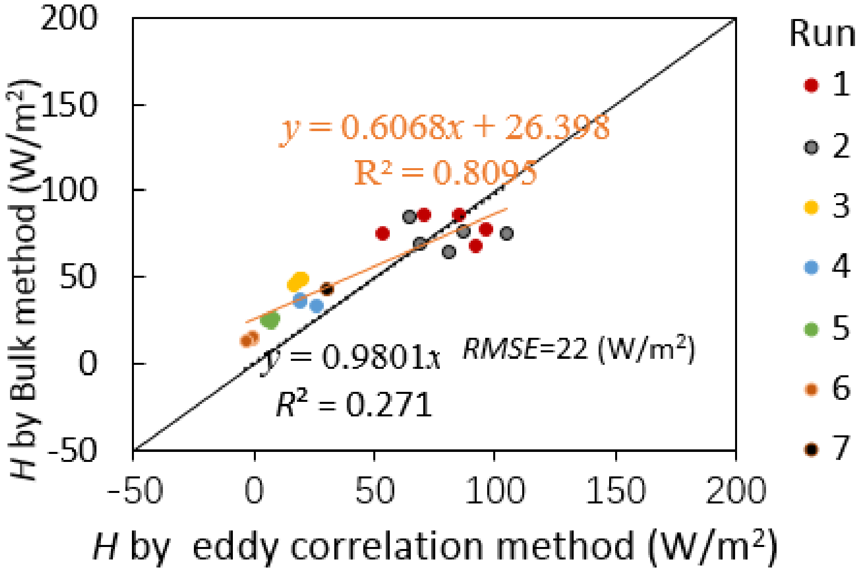

Fig. 39 Comparison of *LE* by the two methods

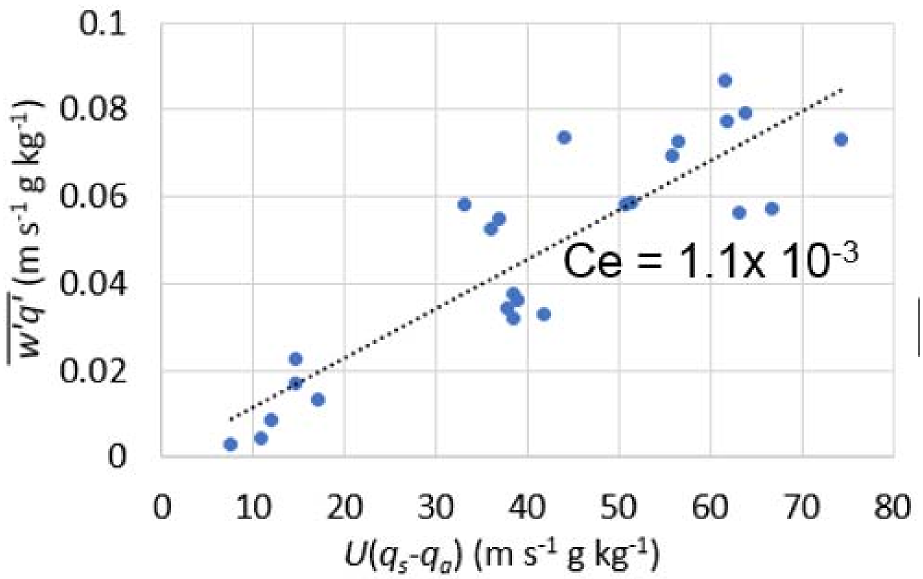

Fig. 40 Covariance of specific humidity and vertical speed plotted against the product of mean wind speed and lake-air difference

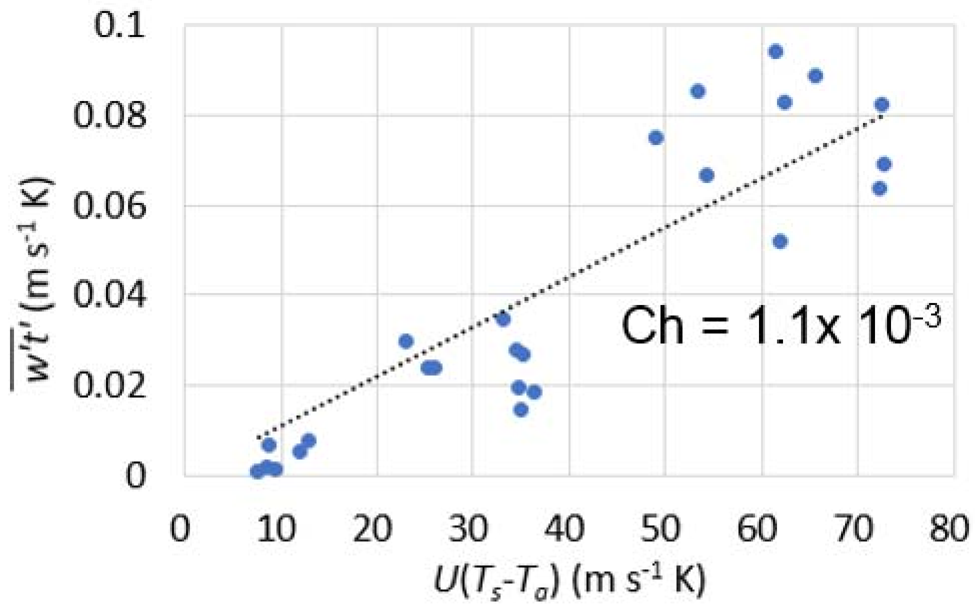

Fig. 41 The same as Fig. 40 but for temperature

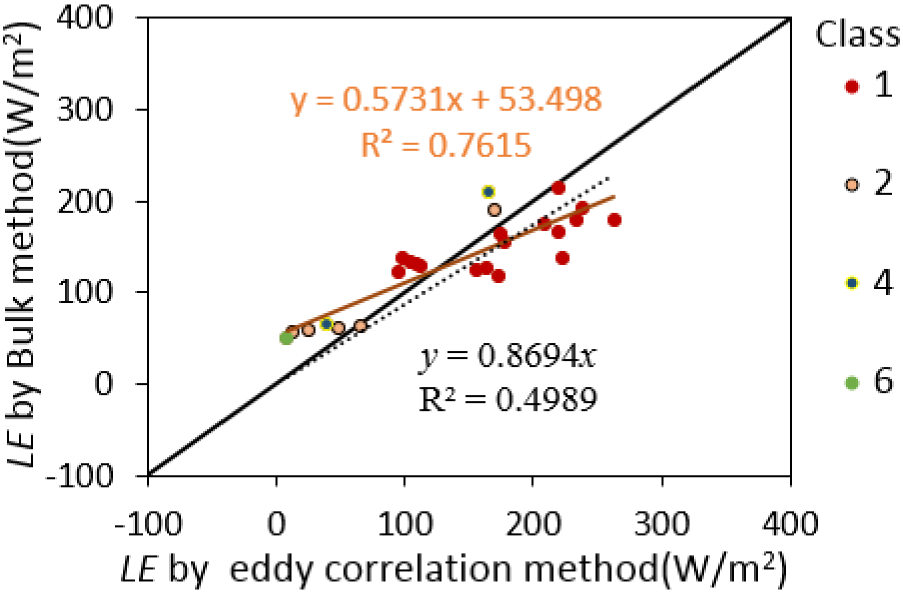

Fig. 42 Comparison of *LE* by the two methods

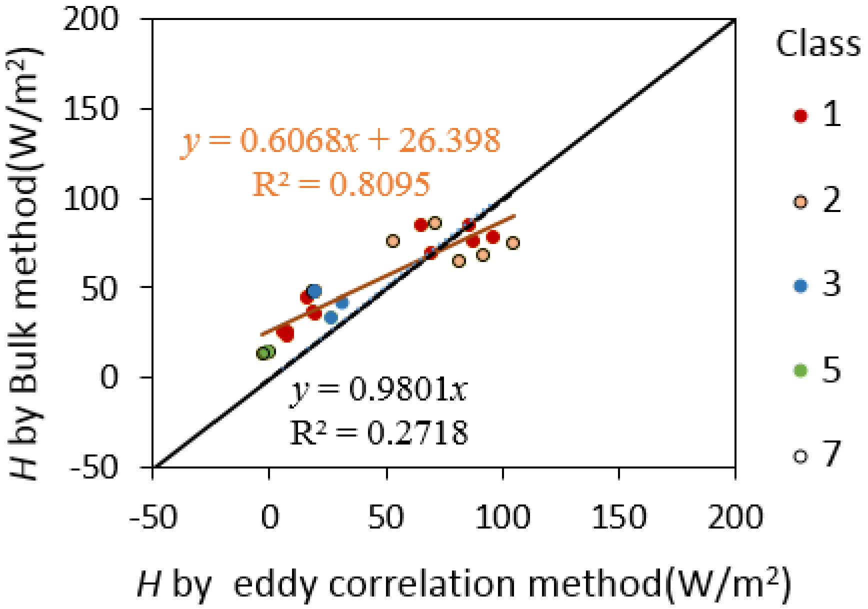

Fig. 43 Comparison of *H* by the two methods

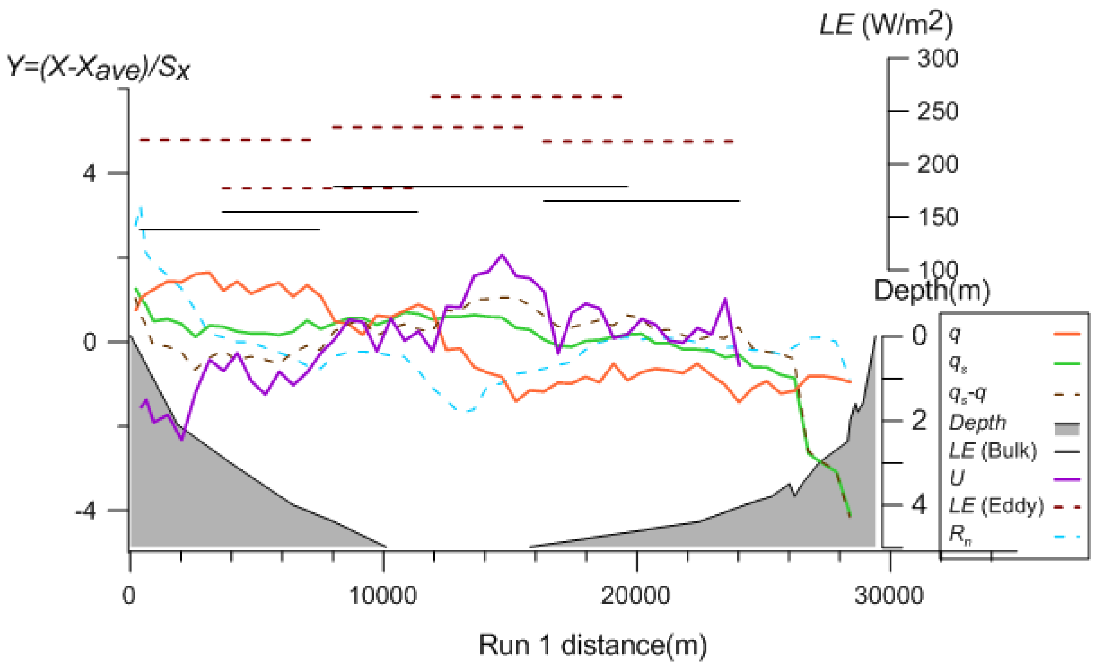

Fig. 44 The spatial distribution of *LE* (Run 1)

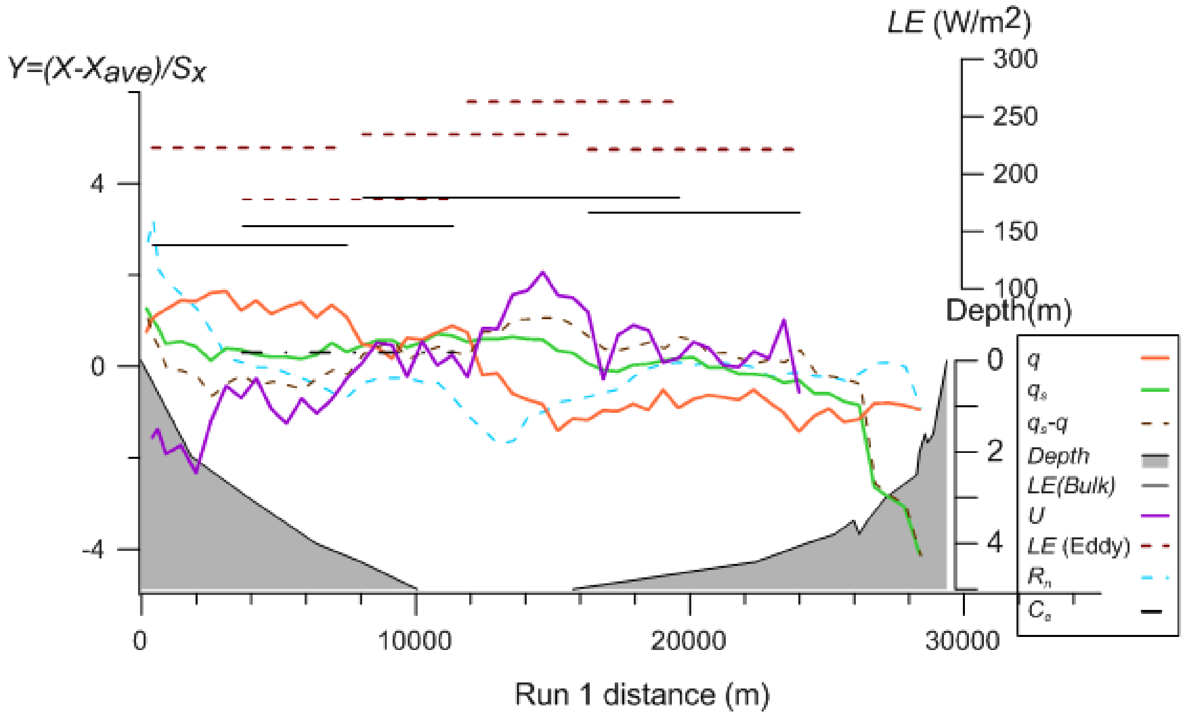

Fig. 45 The spatial distribution of *H* (Run 1)

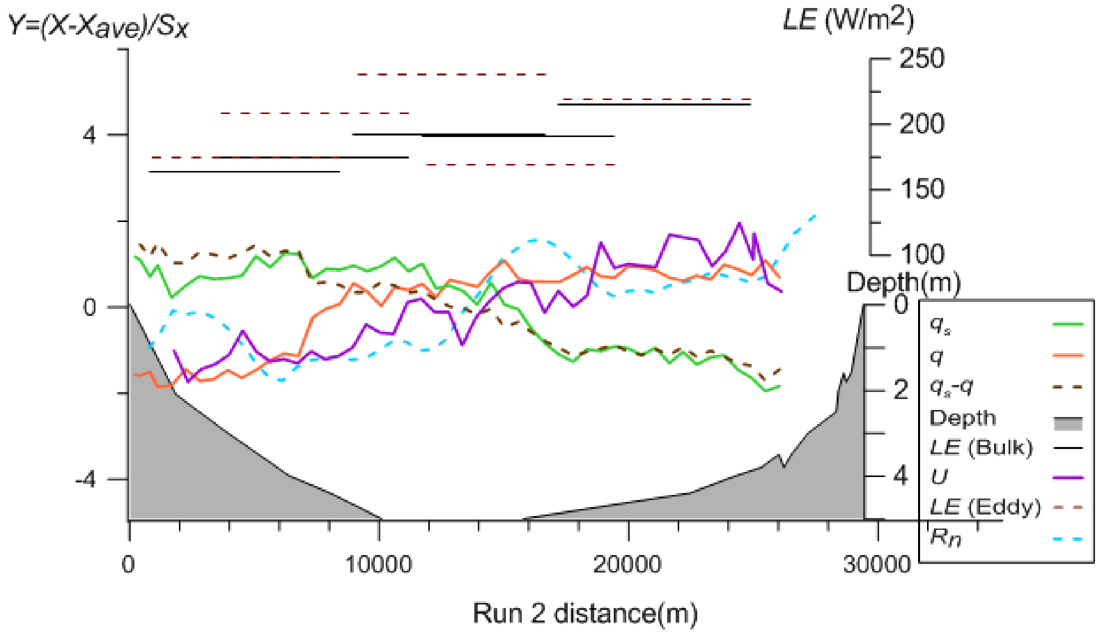

Fig. 46 The spatial distribution of *LE* (Run 2)

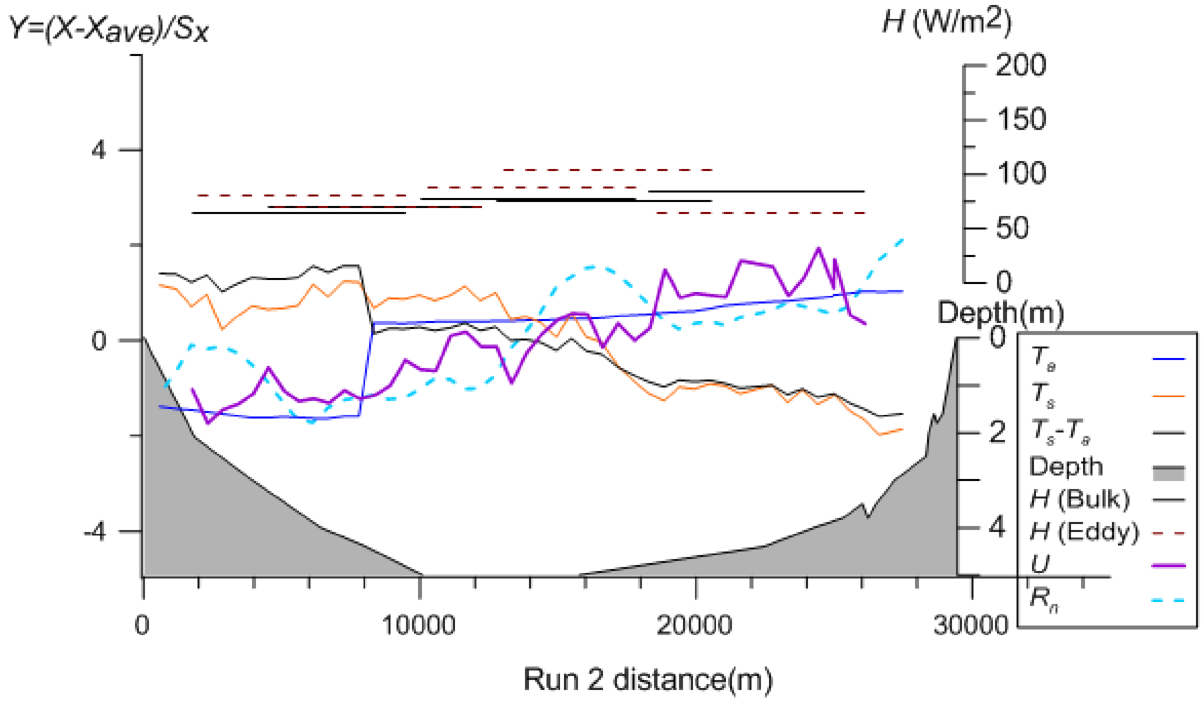

Fig. 47 The spatial distribution of *H* (Run 2)

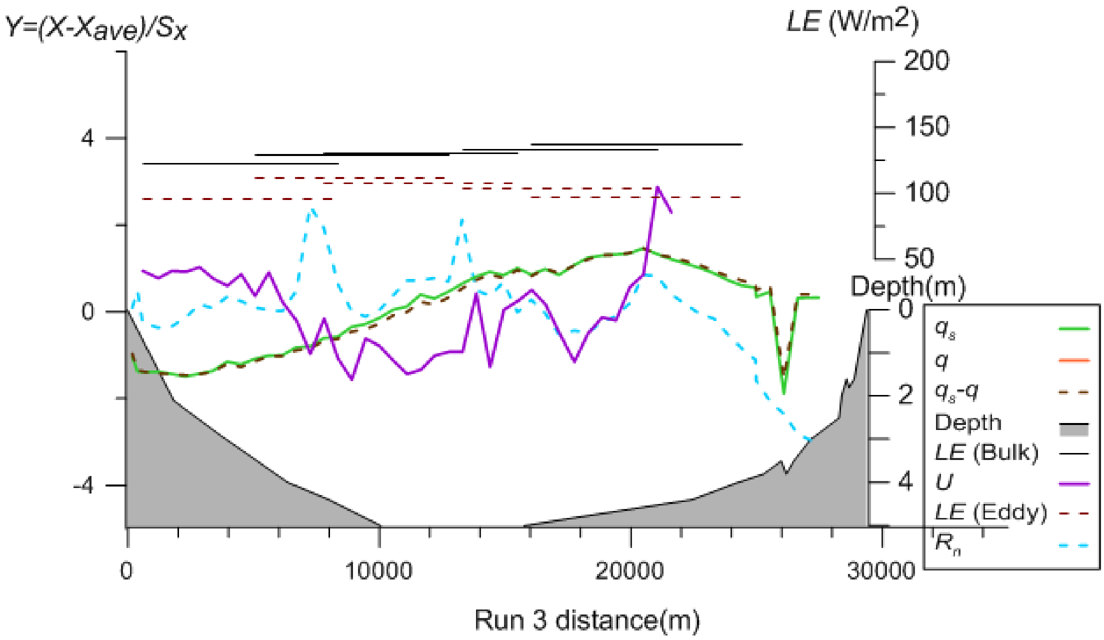

Fig. 48 The spatial distribution of *LE* (Run 3)

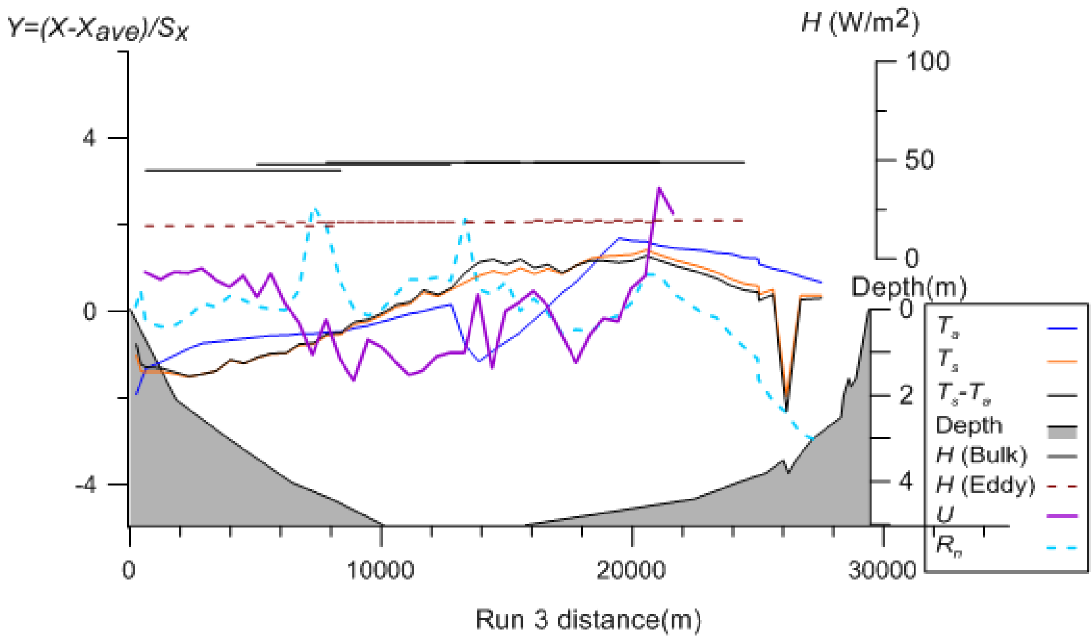

Fig. 49 The spatial distribution of *H* (Run 3)

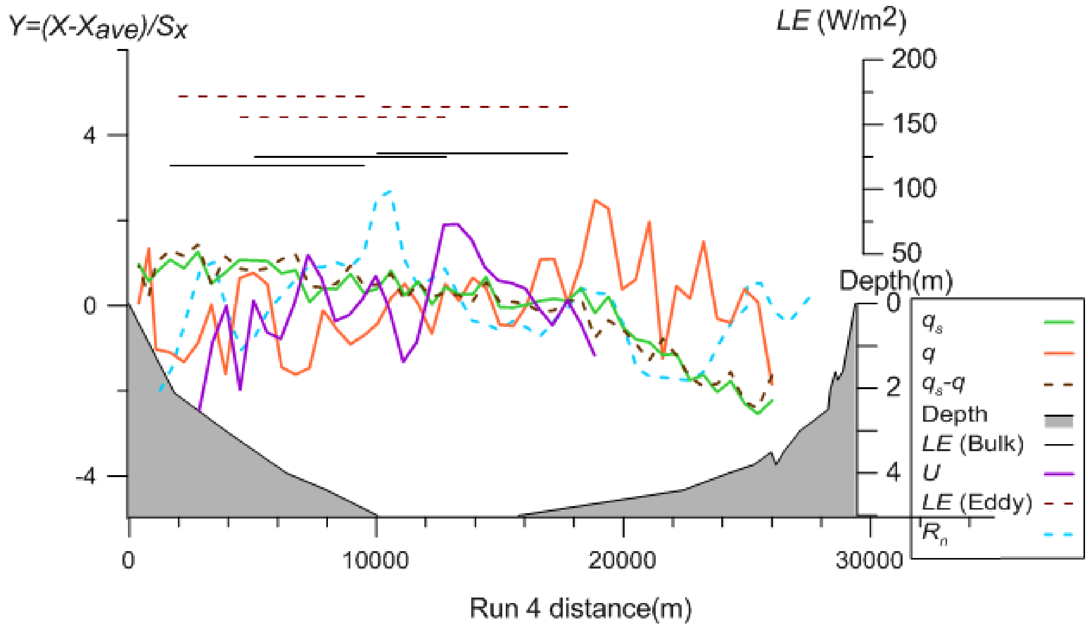

Fig. 50 The spatial distribution of *LE* (Run 4)

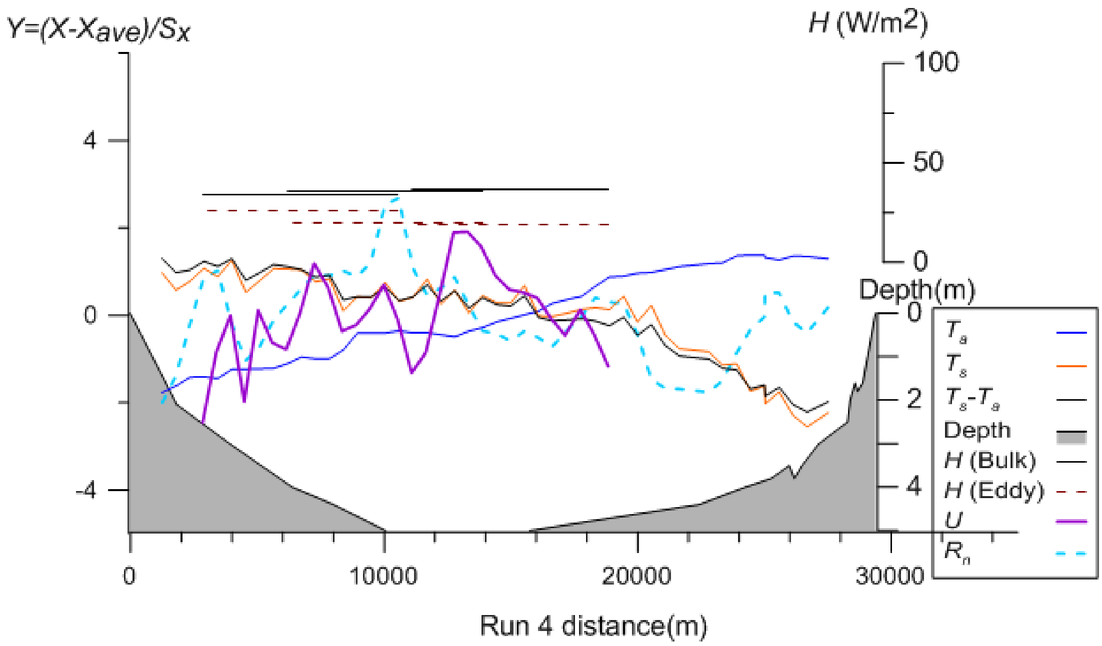

Fig. 51 The spatial distribution of *H* (Run 4)

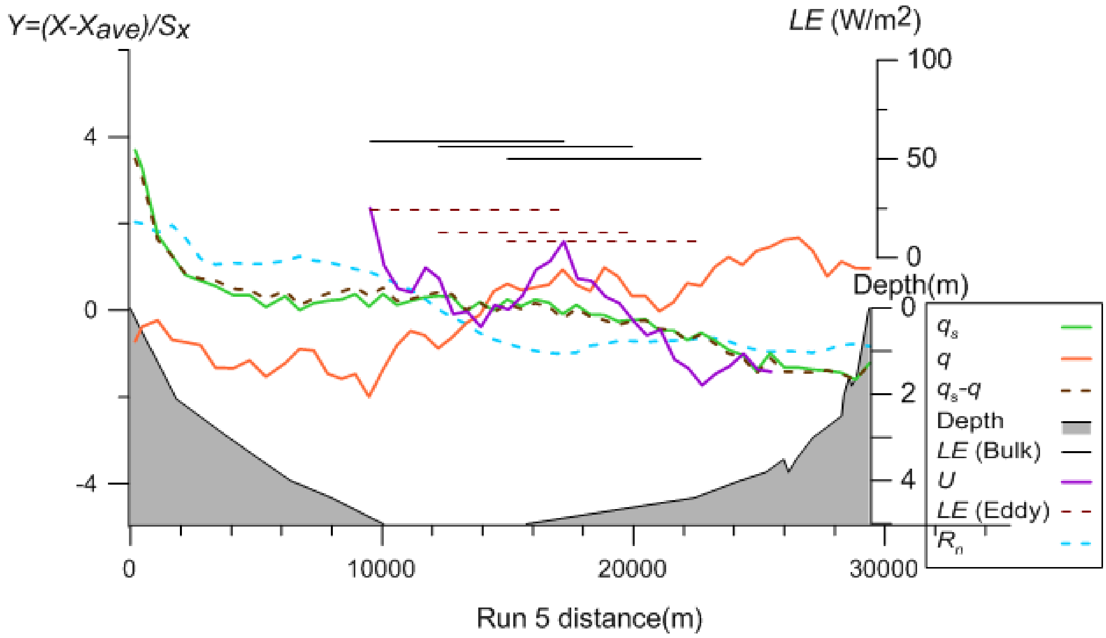

Fig. 52 The spatial distribution of *LE* (Run 5)

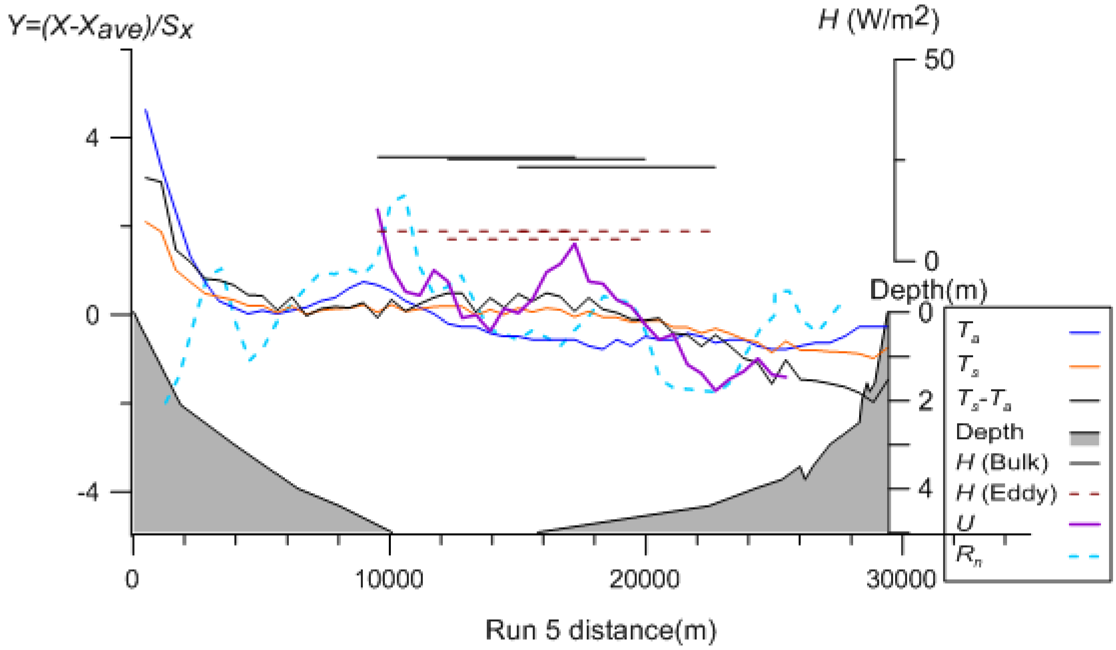

Fig. 53 The spatial distribution of *H* (Run 5)

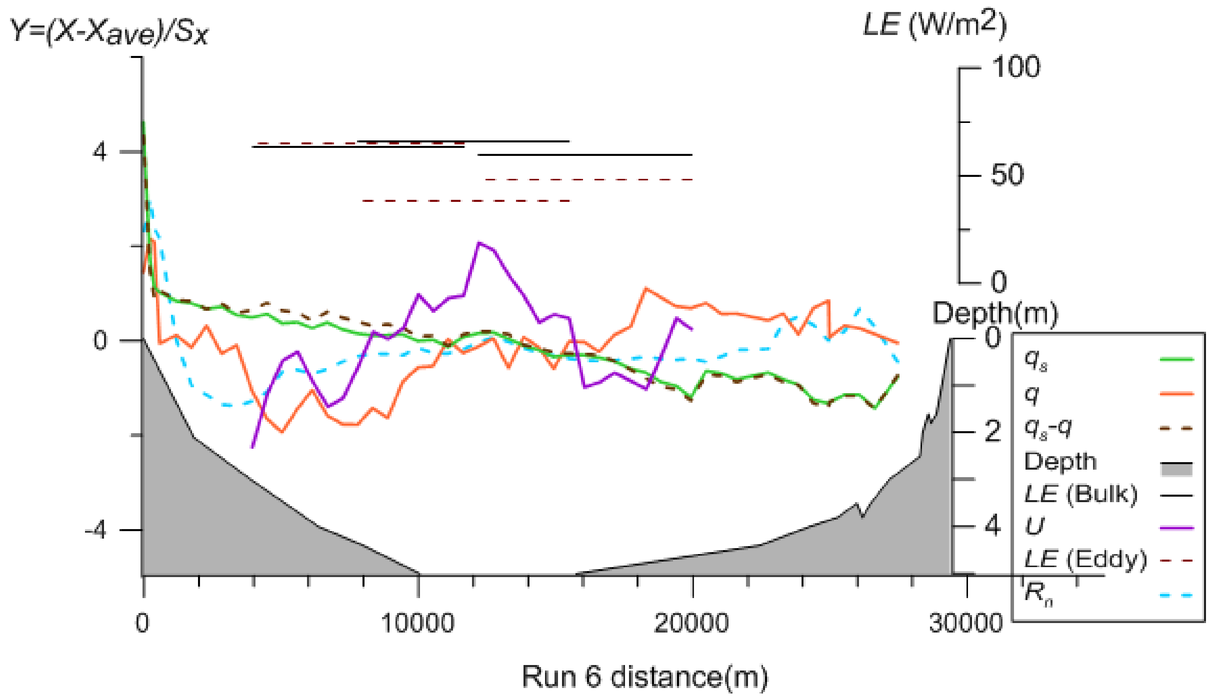

Fig. 54 The spatial distribution of *LE* (Run 6)

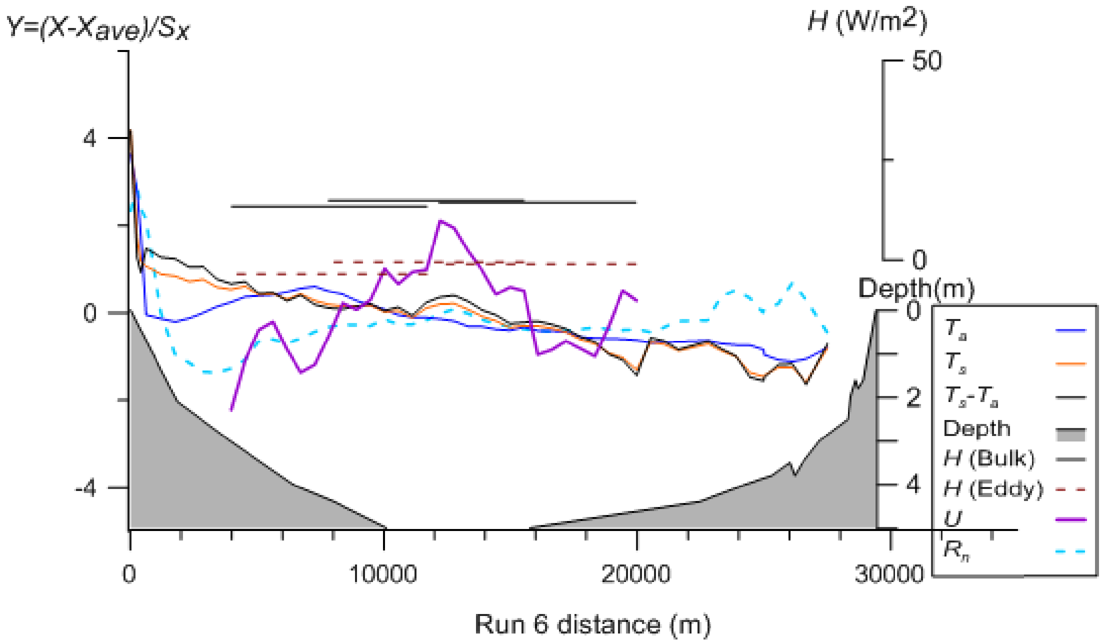

Fig. 55 The spatial distribution of *H* (Run 6)

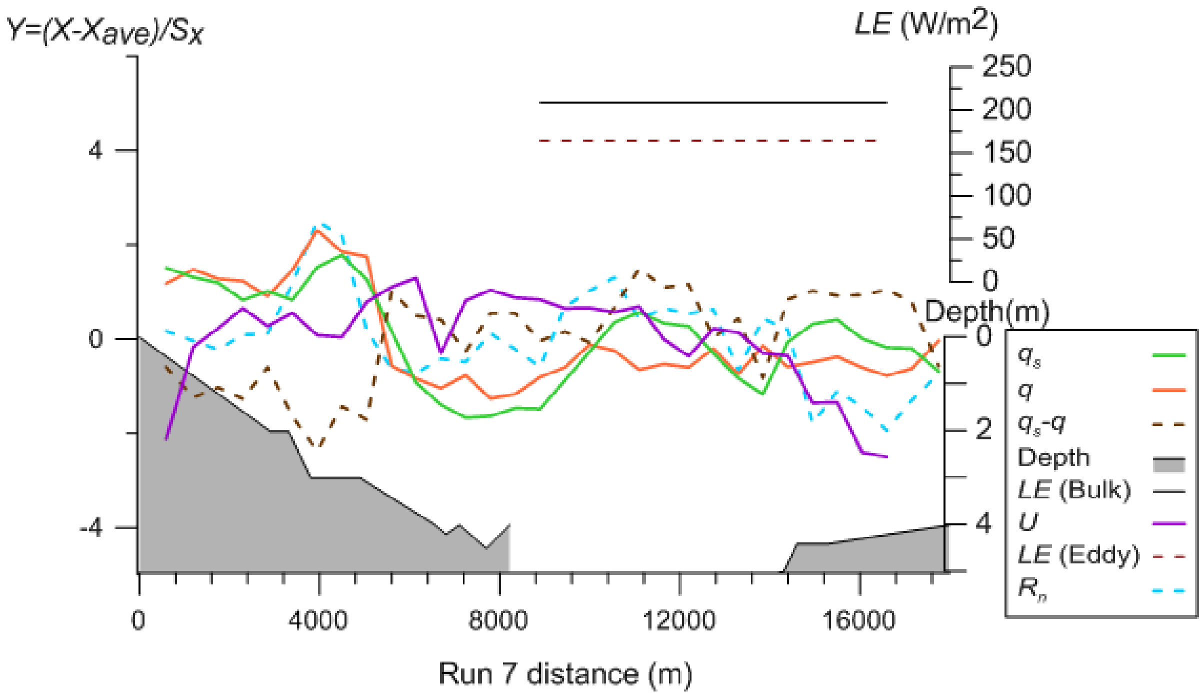

Fig. 56 The spatial distribution of *LE* (Run 7)

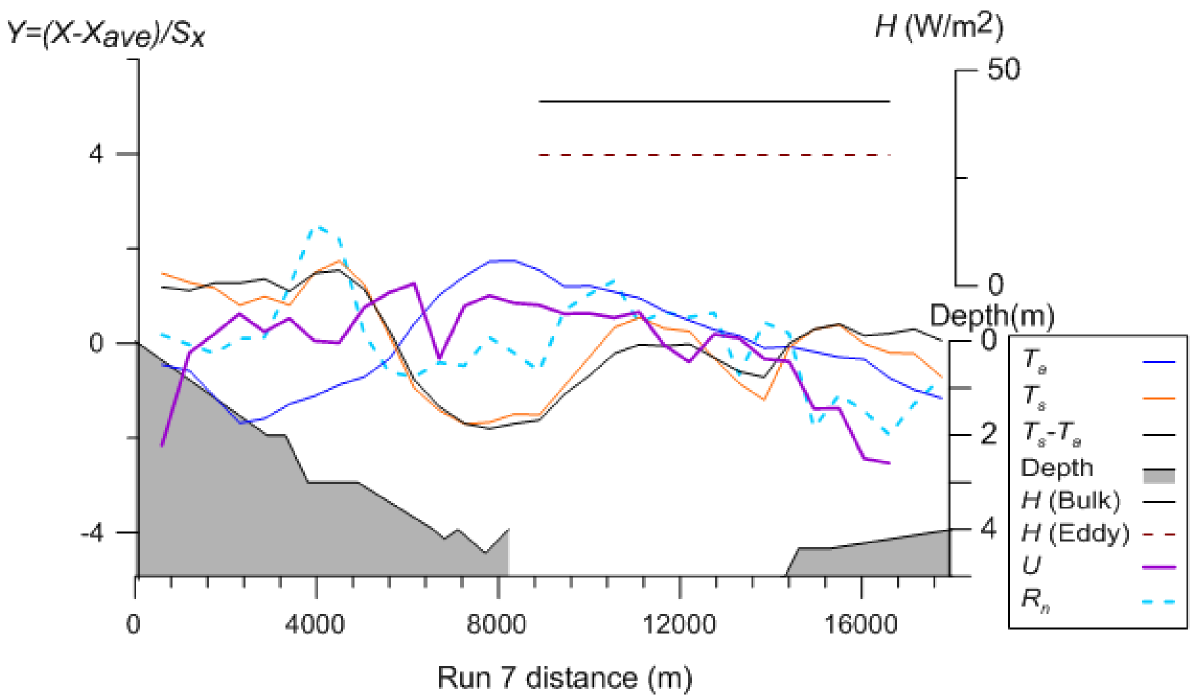

Fig. 57 The spatial distribution of *H* (Run 7)

Appendix A

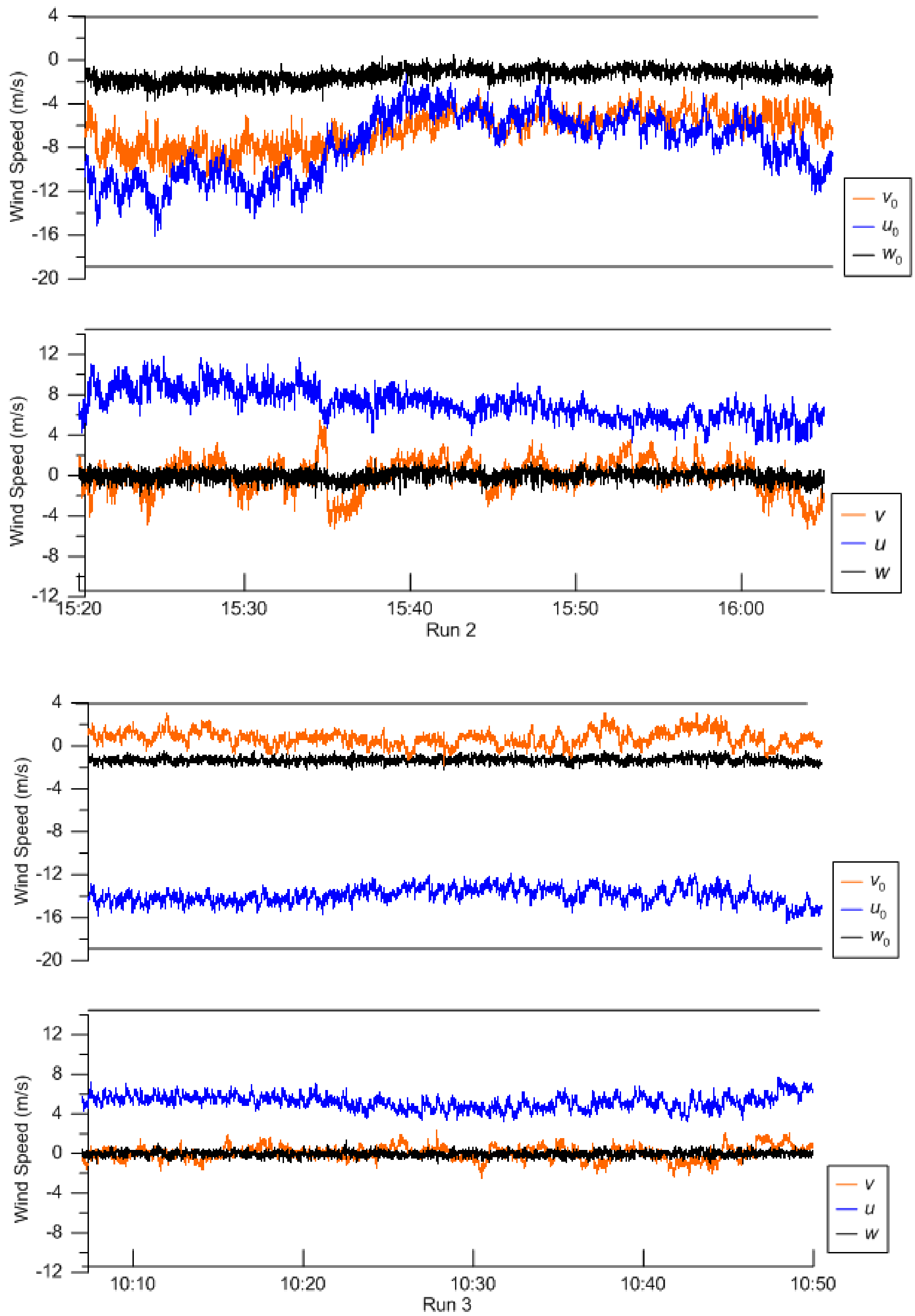

Fig. A-1 Observed and corrected wind speeds of Run 2 and Run 3

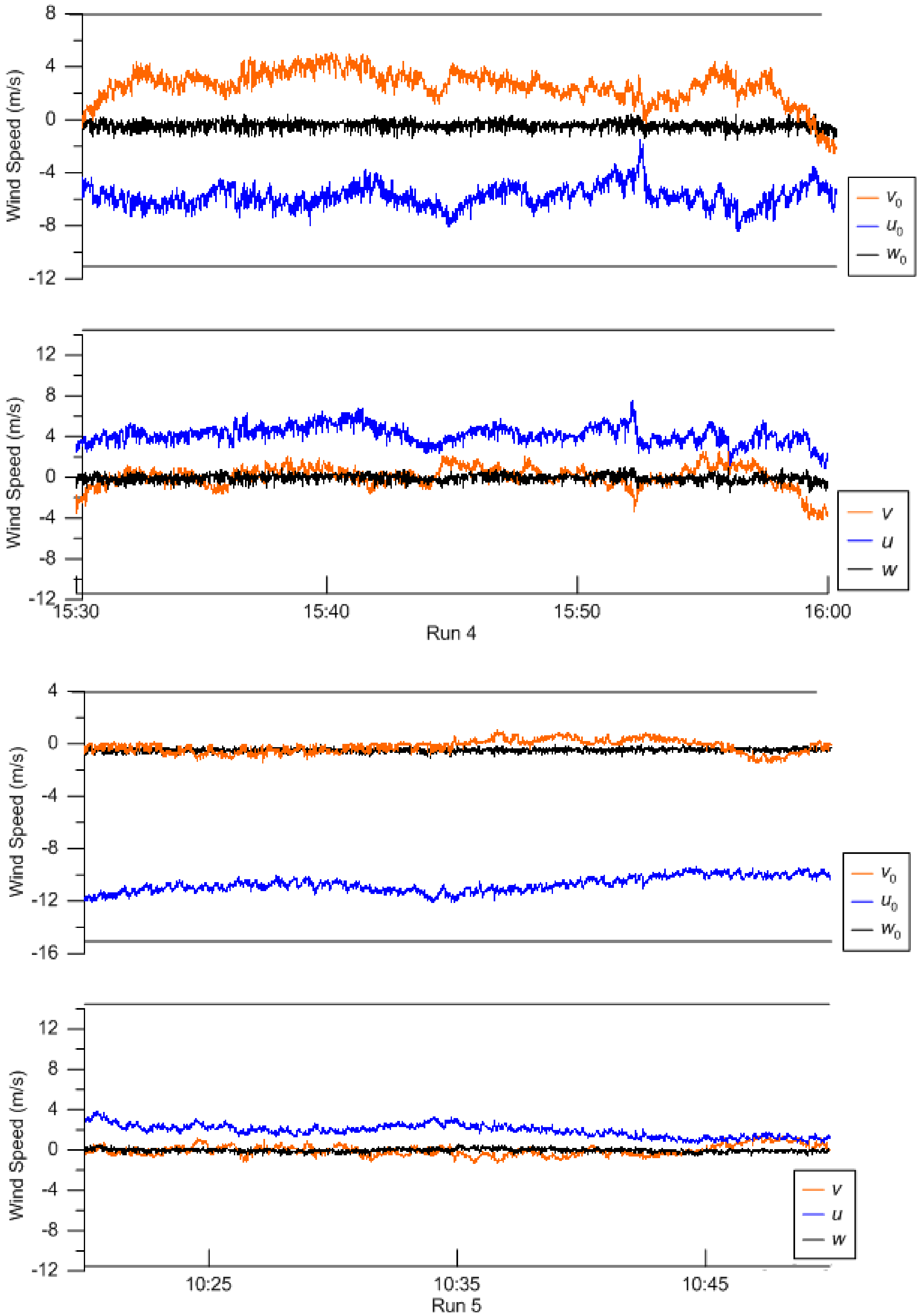

Fig. A-2 The same as Fig. A-1 but for Run 4 and Run 5

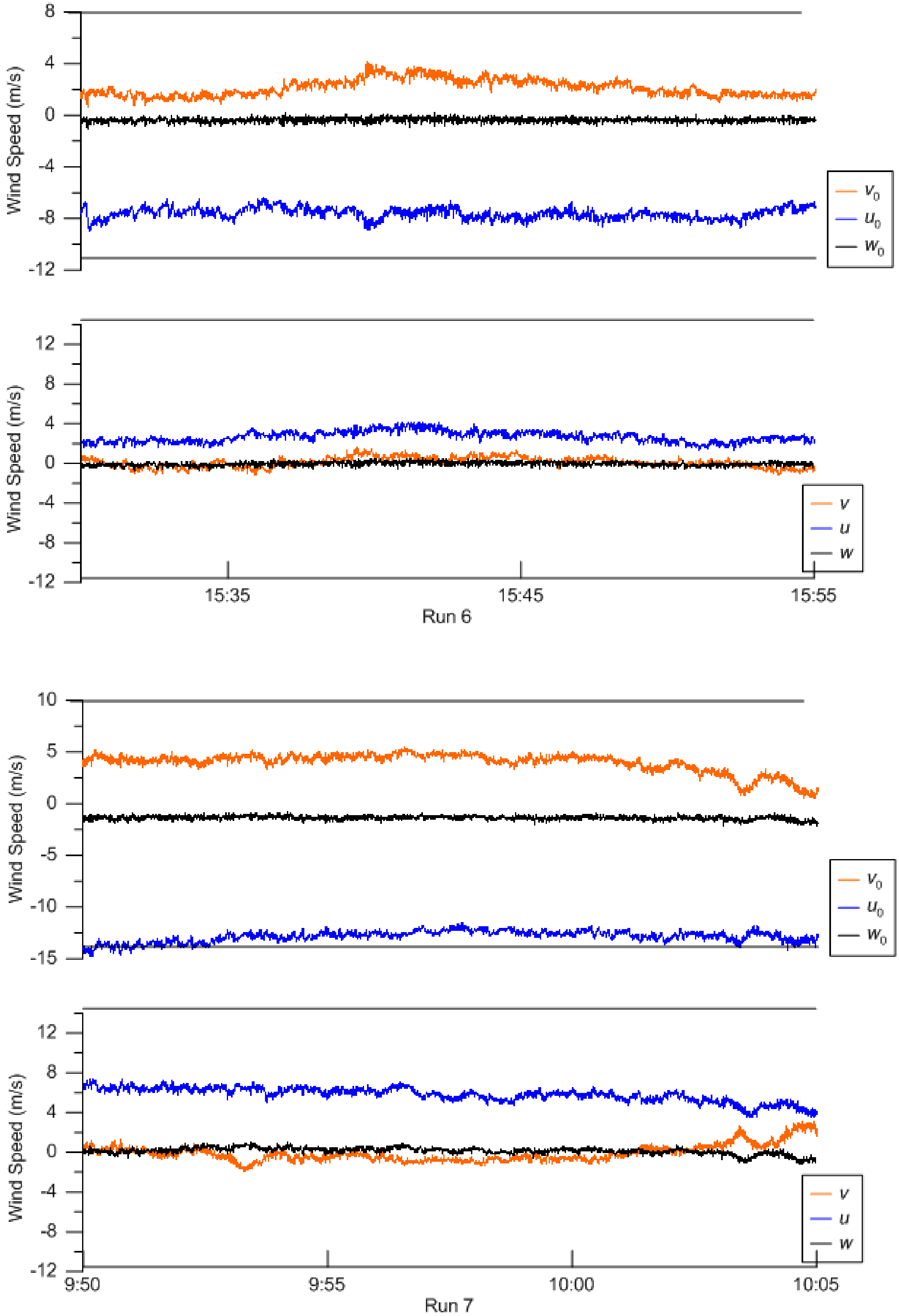

Fig. A-3 The same as Fig. A-1 but for Run 6 and Run 7

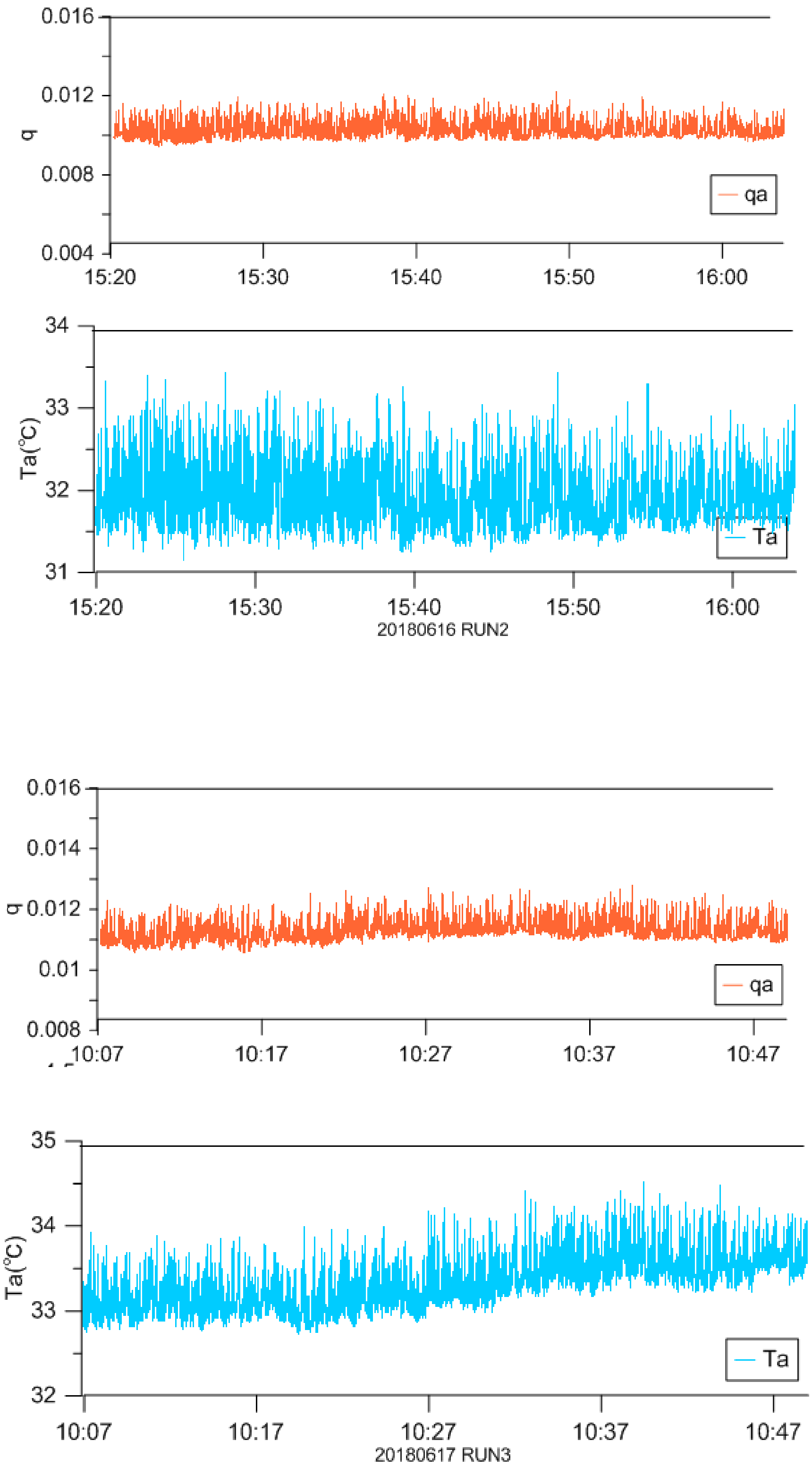

Fig. A-4 q_a and T_a of Run 2 and Run 3 (raw data)

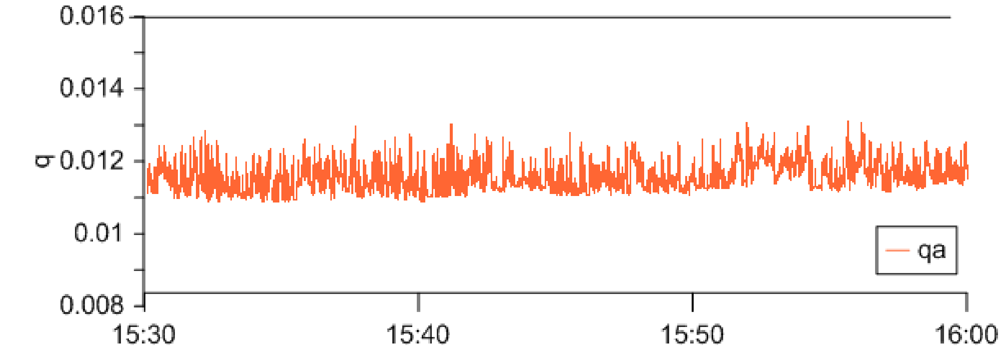

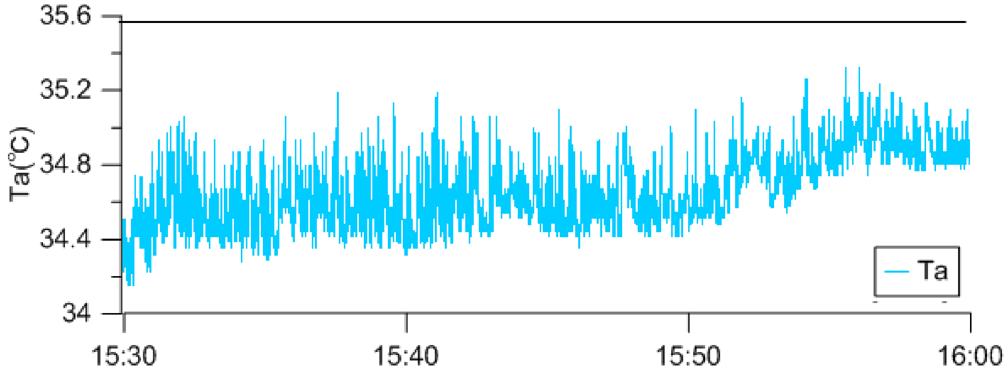

20180617 RUN4

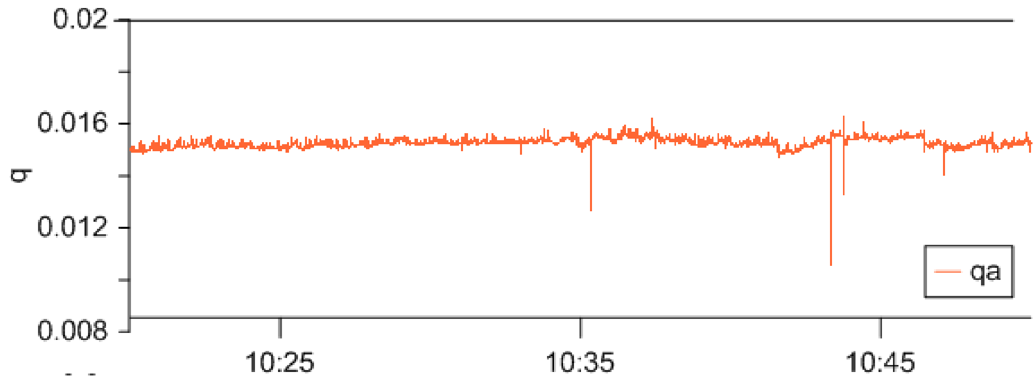

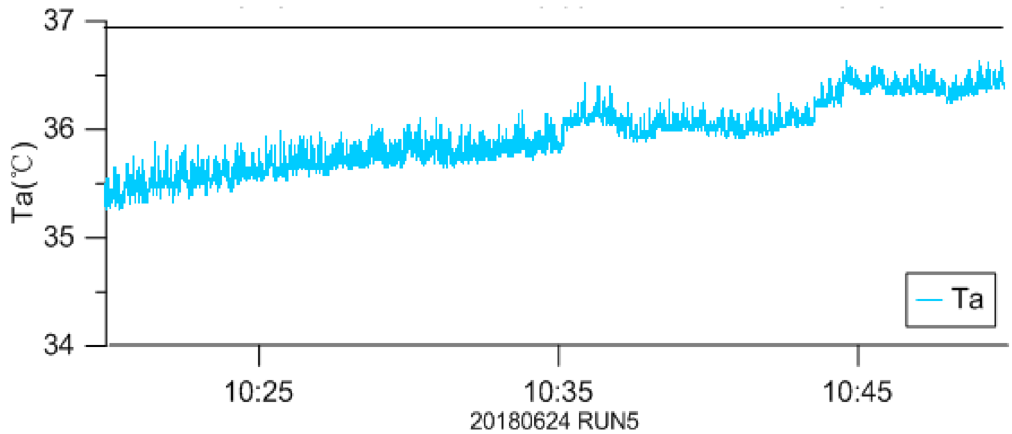

Fig. A-5 The same as Fig. A-4 but for Run 4 and Run 5

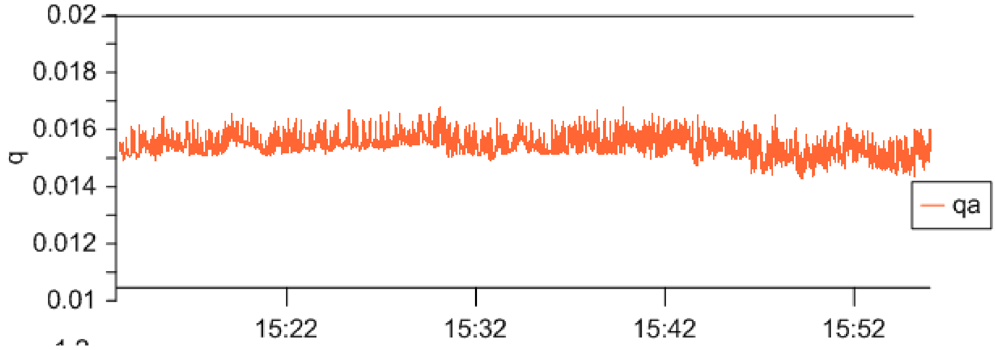

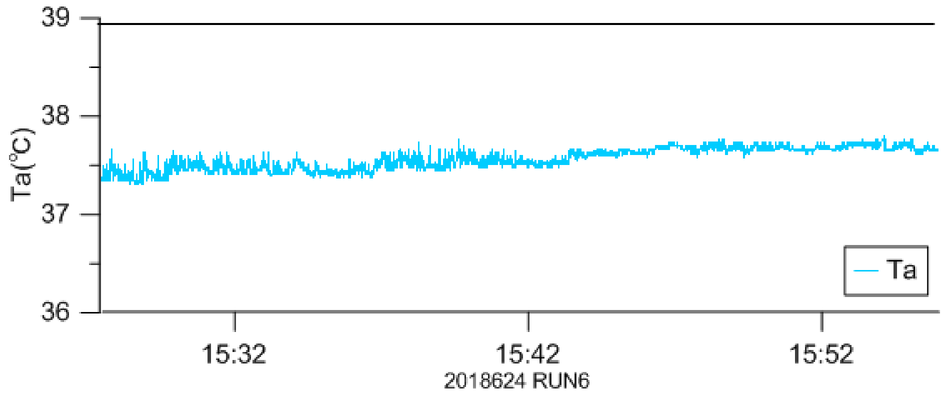

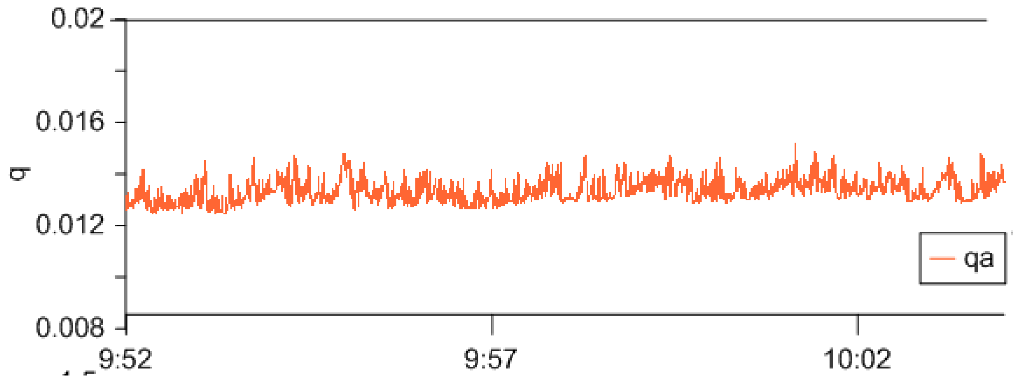

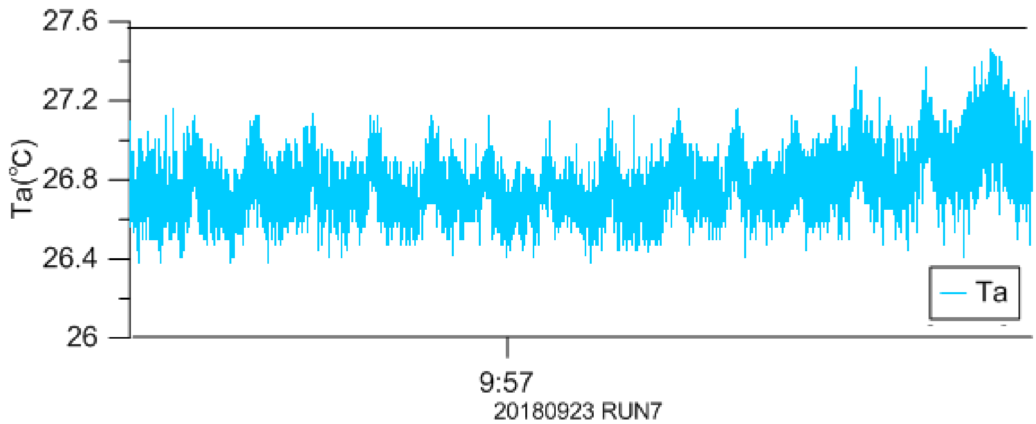

Fig. A-6 The same as Fig. A-4 but for Run 6 and Run 7

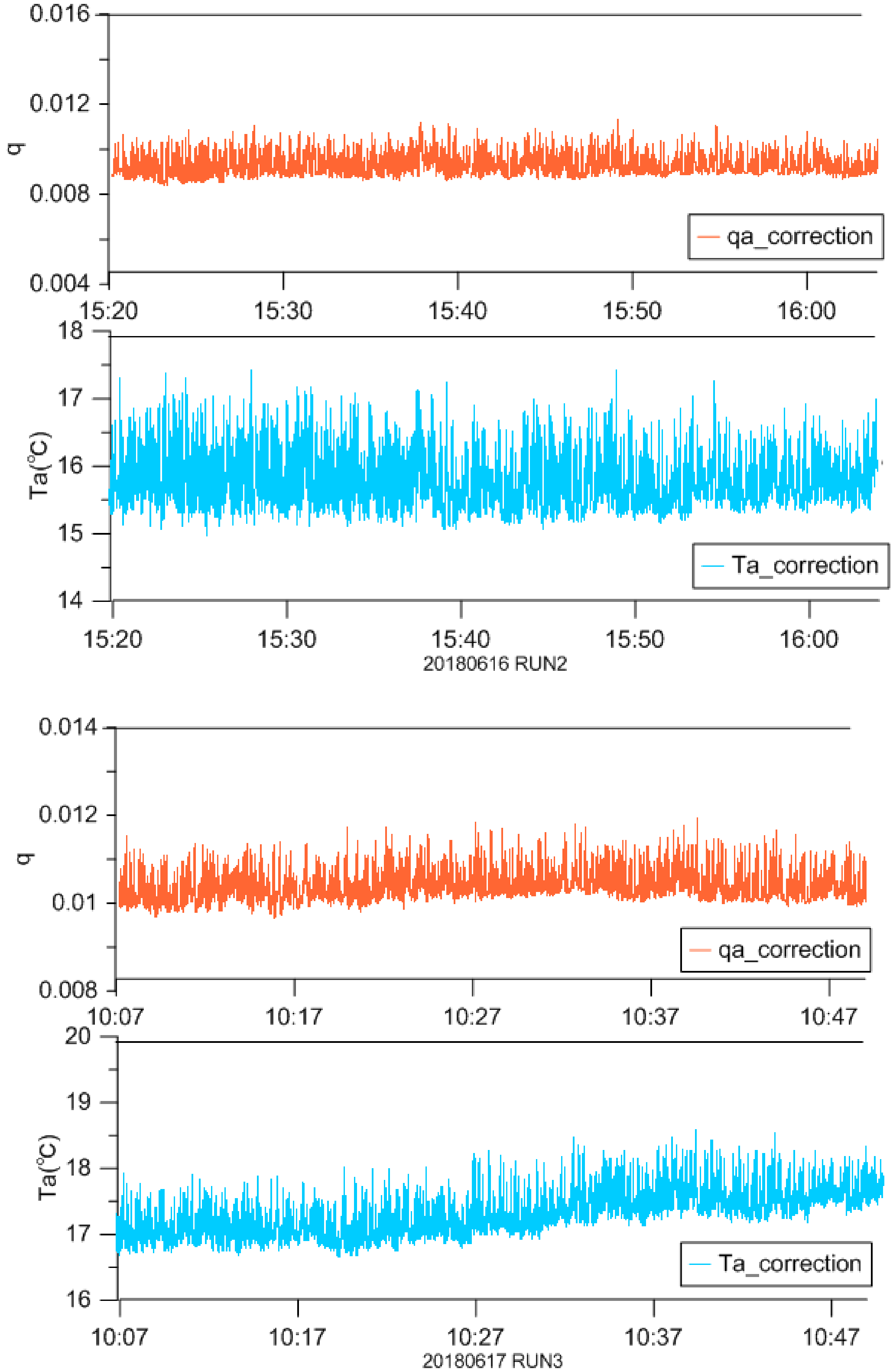

Fig. A-7 Corrected q_a and T_a of Run 2 and Run 3

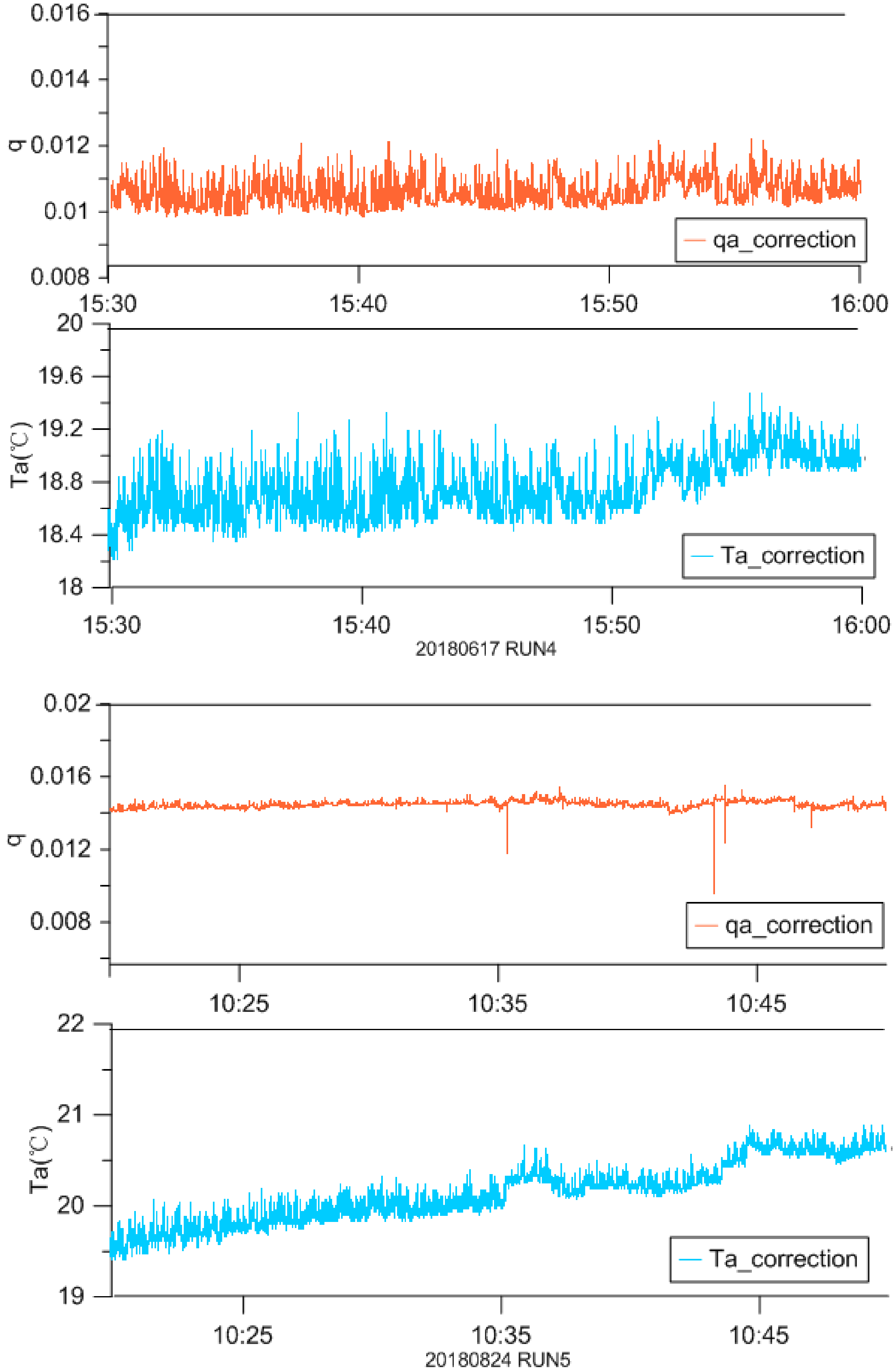

Fig. A-8 The same as Fig. A-7 but for Run 4 and Run 5

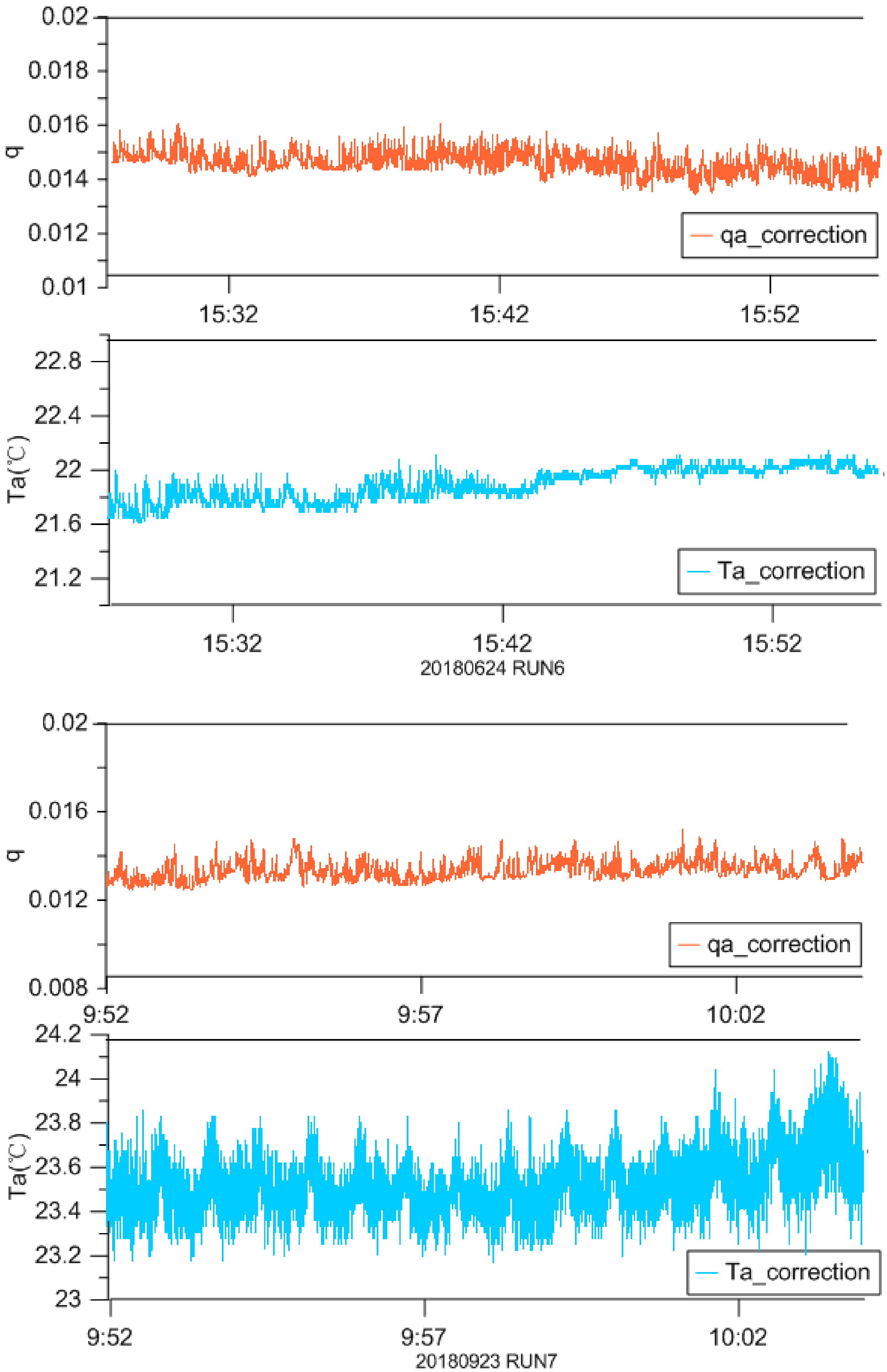

Fig. A-9 The same as Fig. A-7 but for Run 6 and Run 7

Appendix B

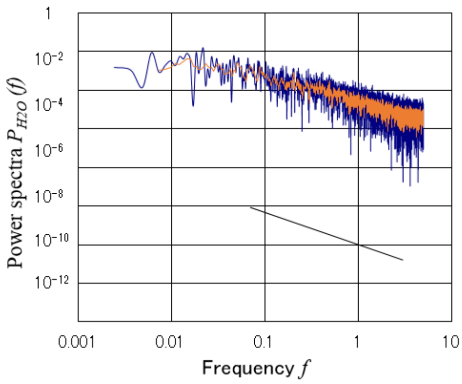
Power spectra $P_{H2O}(f)$
1
10^{-2}
10^{-4}
10^{-6}
10^{-8}
10^{-10}
10^{-12}
0.001
0.01
0.1
1
10
Frequency f

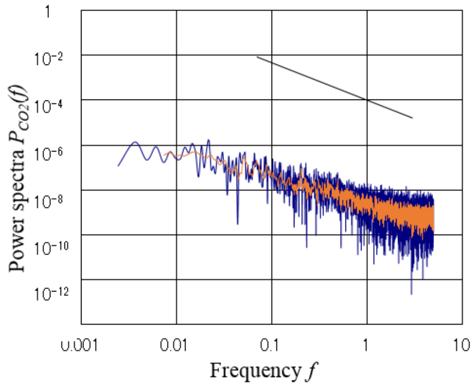
Power spectra $P_{CO2}(f)$
1
10^{-2}
10^{-4}
10^{-6}
10^{-8}
10^{-10}
10^{-12}
0.001
0.01
0.1
1
10
Frequency f

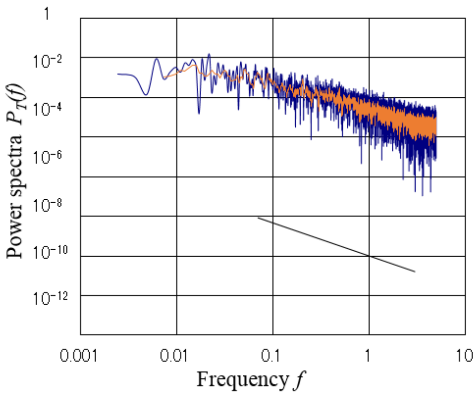
Power spectra $P_T(f)$
1
10^{-2}
10^{-4}
10^{-6}
10^{-8}
10^{-10}
10^{-12}
0.001
0.01
0.1
1
10
Frequency f

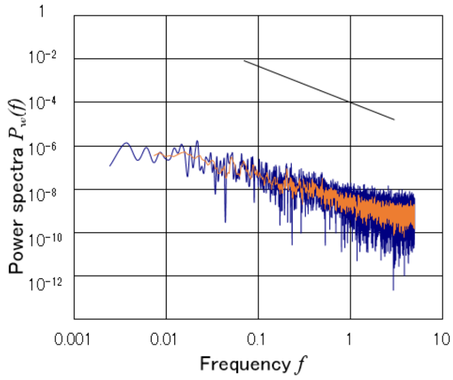
Power spectra $P_w(f)$
1
10^{-2}
10^{-4}
10^{-6}
10^{-8}
10^{-10}
10^{-12}
0.001
0.01
0.1
1
10
Frequency f

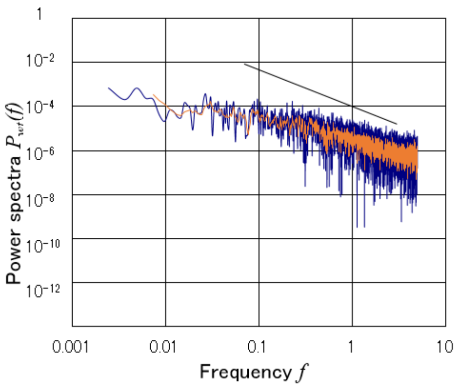
Power spectra $P_{wr}(f)$
1
10^{-2}
10^{-4}
10^{-6}
10^{-8}
10^{-10}
10^{-12}
0.001
0.01
0.1
1
10
Frequency f

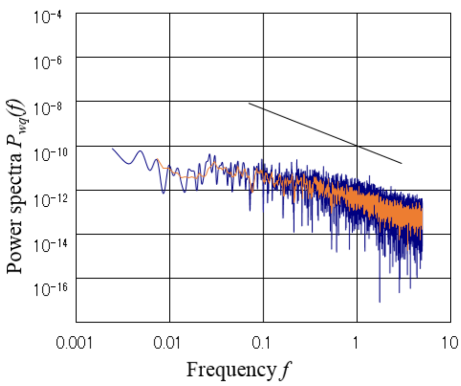
Power spectra $P_{wq}(f)$
10^{-4}
10^{-6}
10^{-8}
10^{-10}
10^{-12}
10^{-14}
10^{-16}
0.001
0.01
0.1
1
10
Frequency f

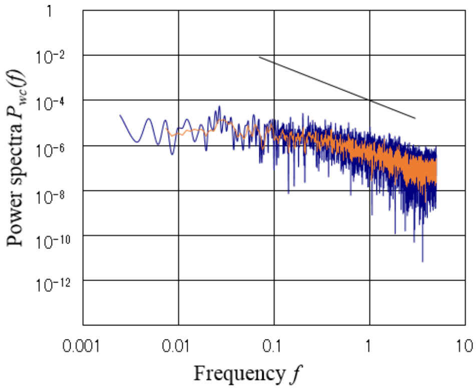

Fig. B-1 Spectrum analysis of Run 1-3

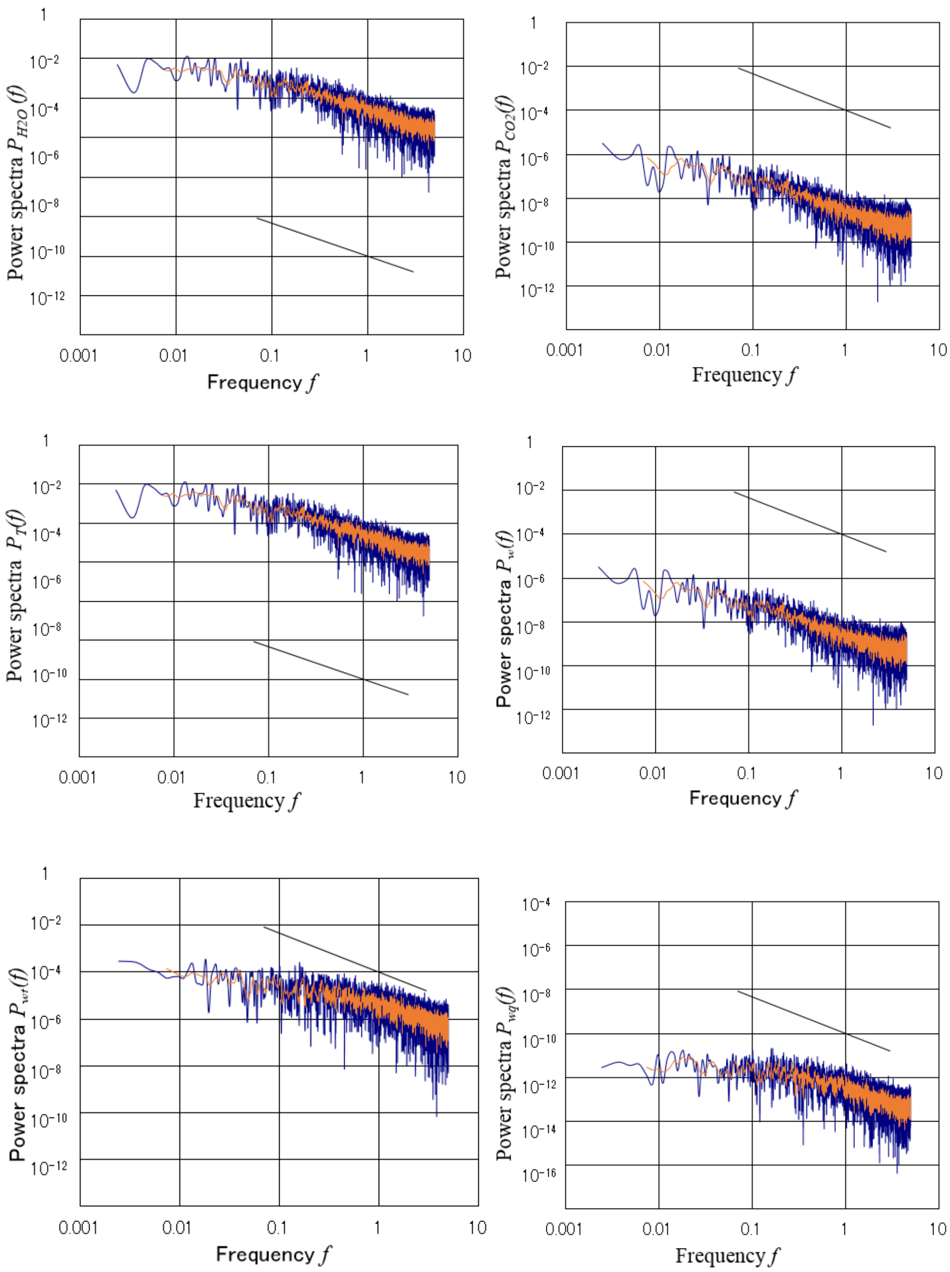

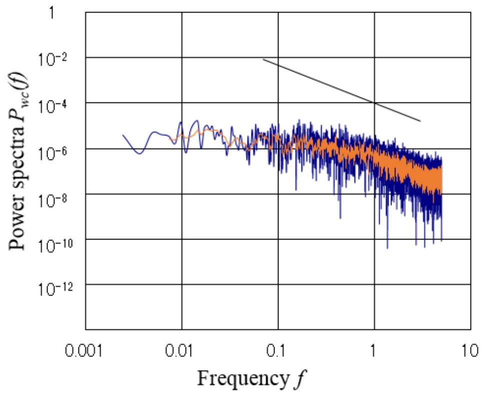

Fig. B-2 Spectrum analysis of Run 1-5

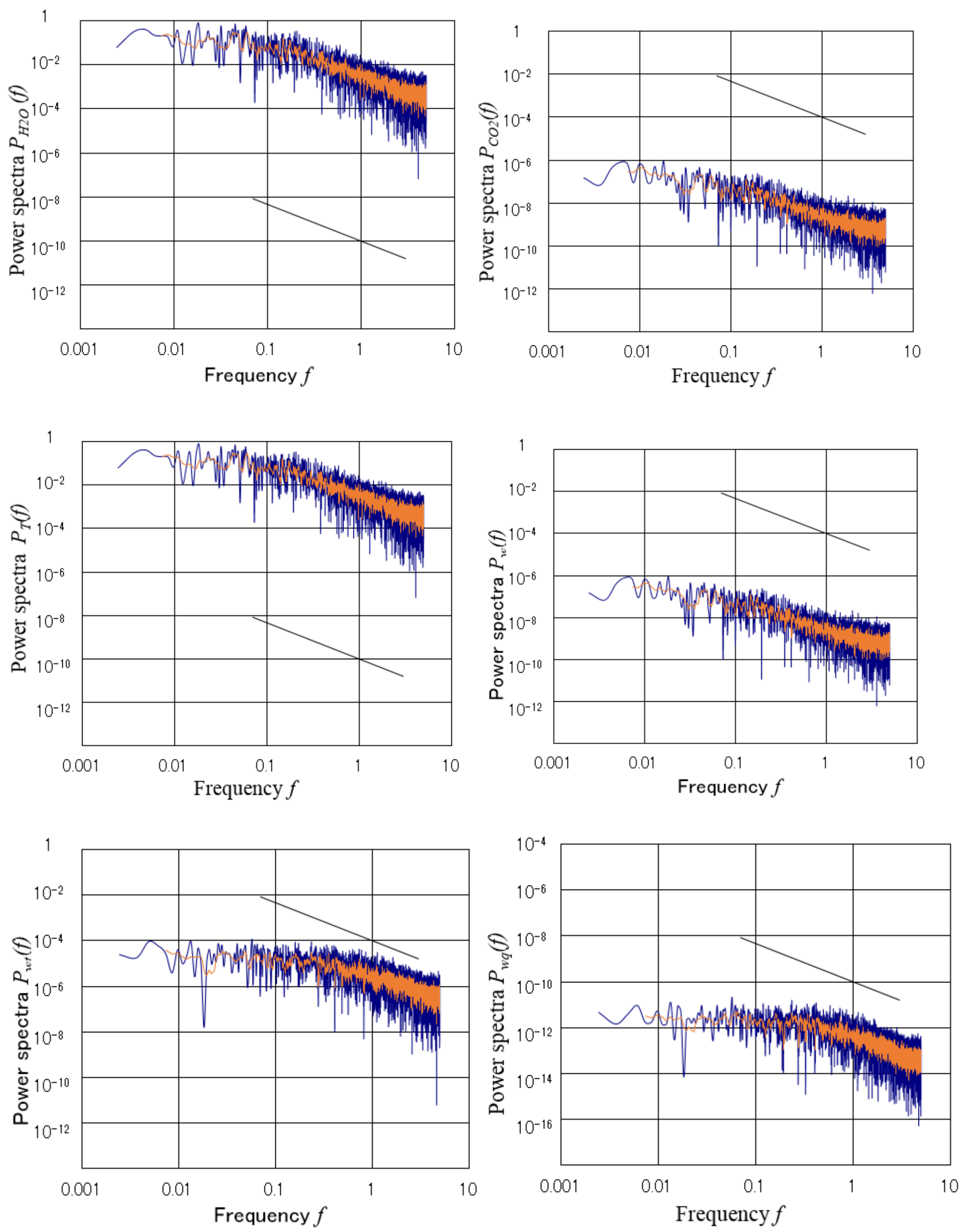

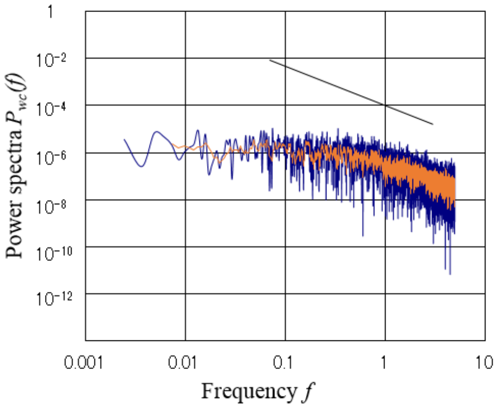

Fig. B-3 Spectrum analysis of Run 2-1

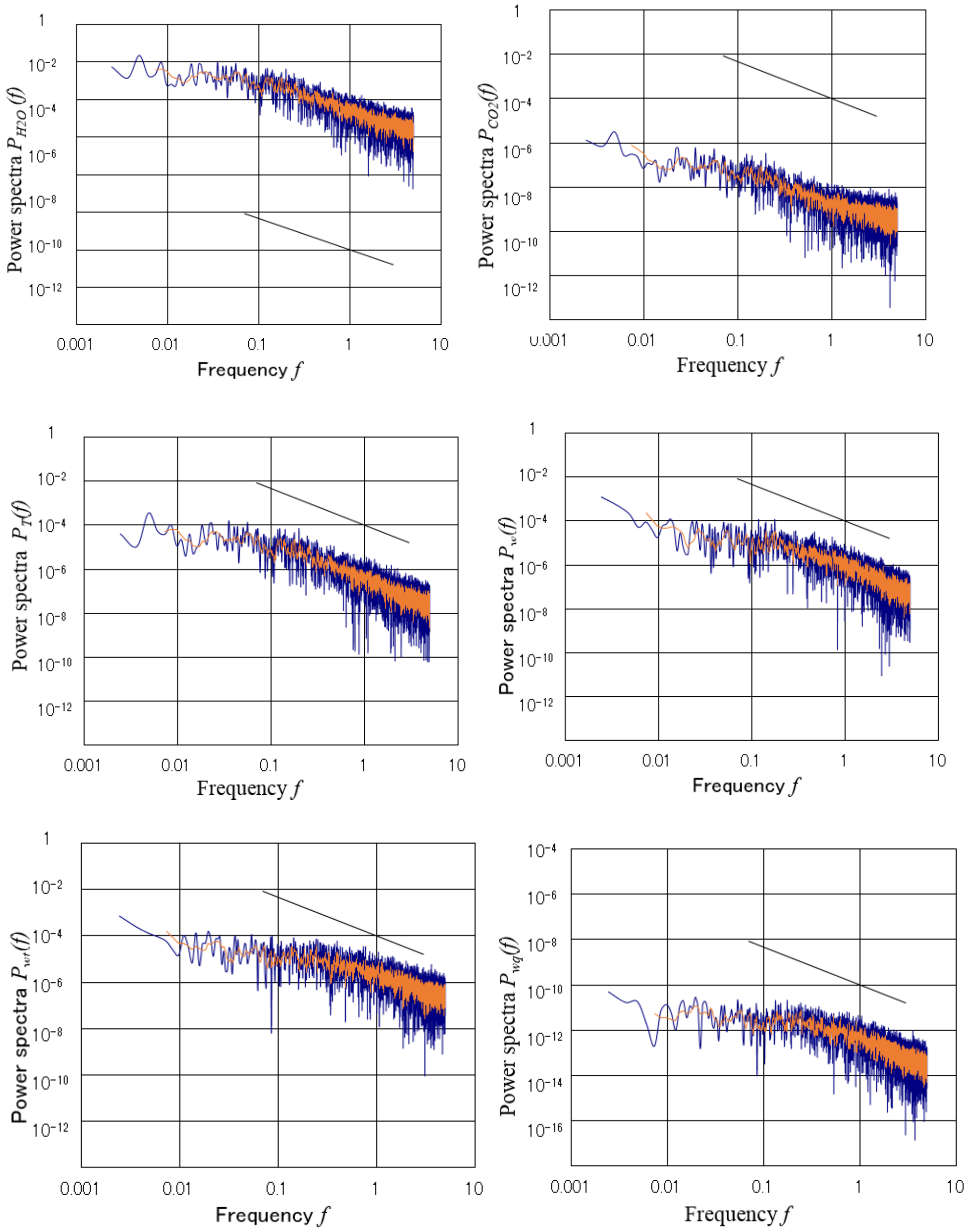

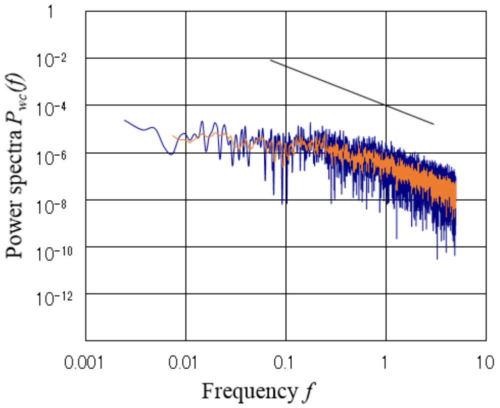

Fig. B-4 Spectrum analysis of Run 2-3

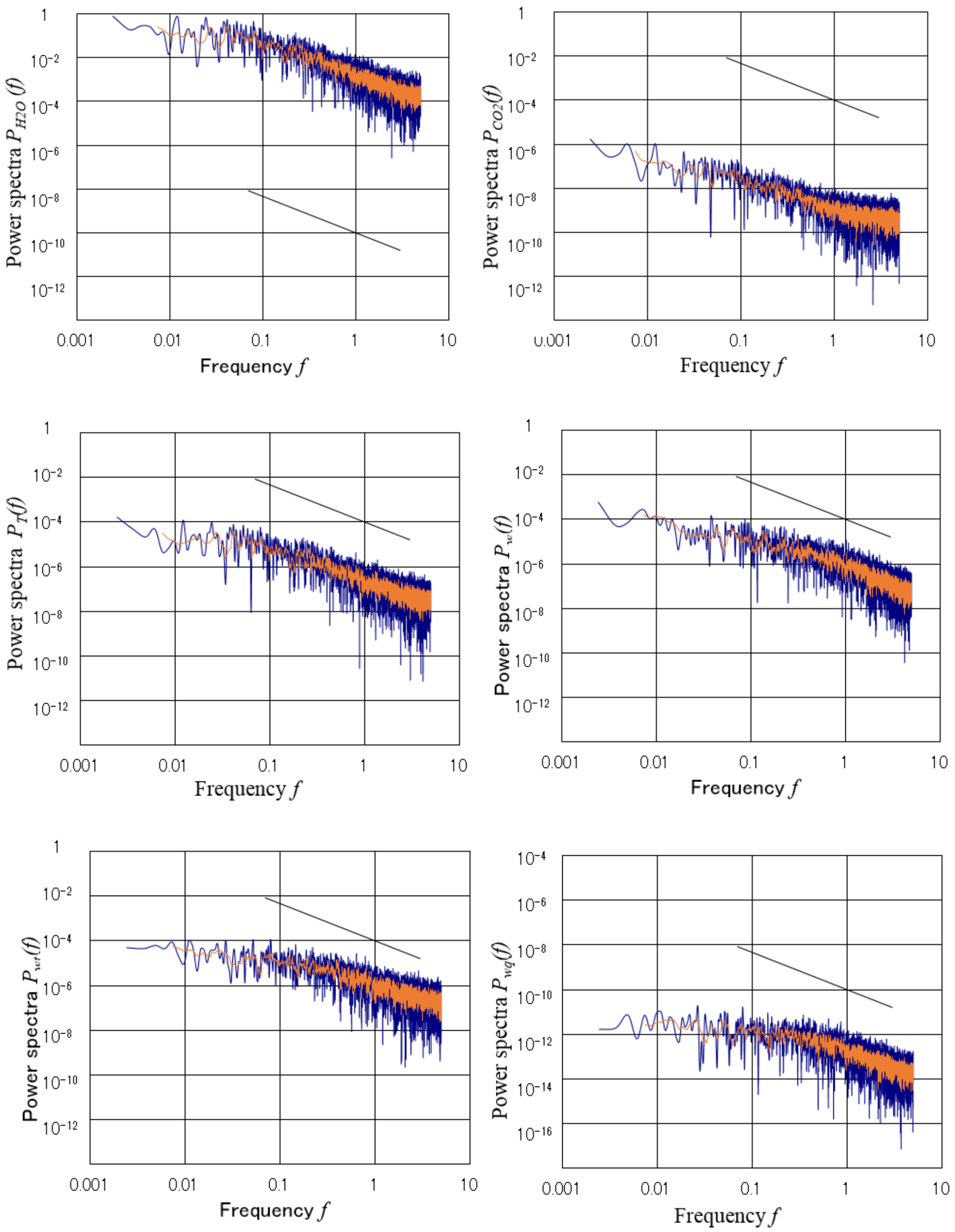

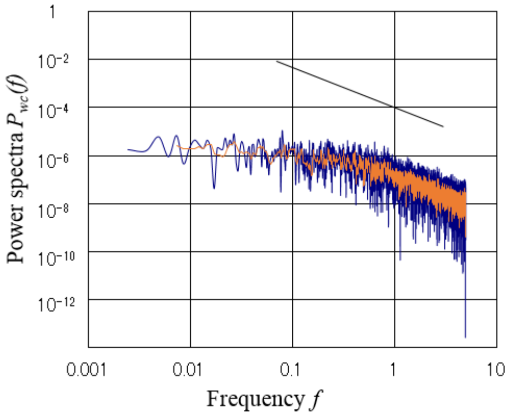

Fig. B-5 Spectrum analysis of Run 2-5

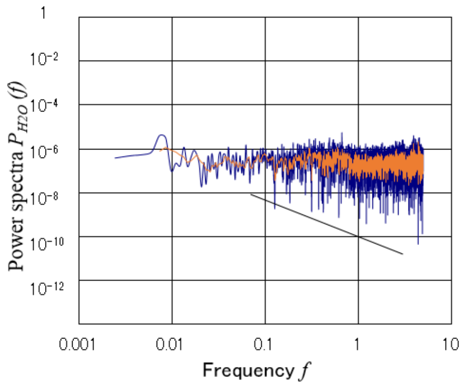

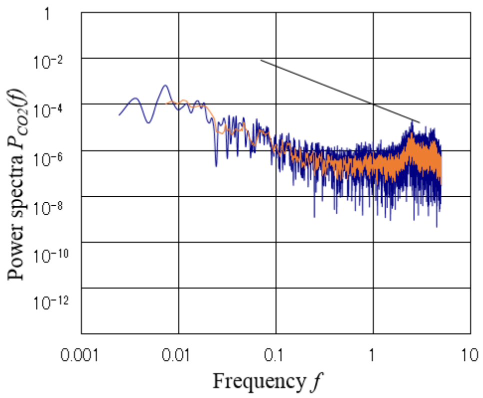

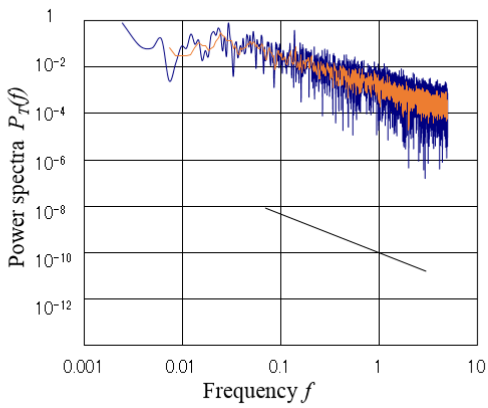

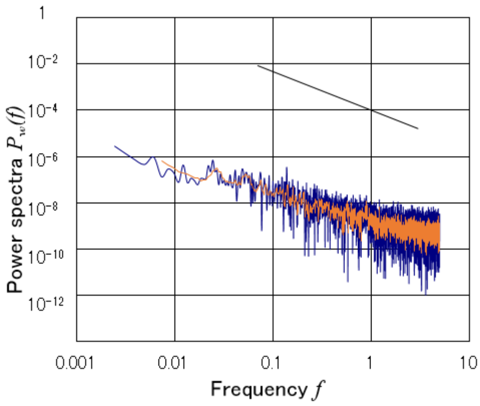

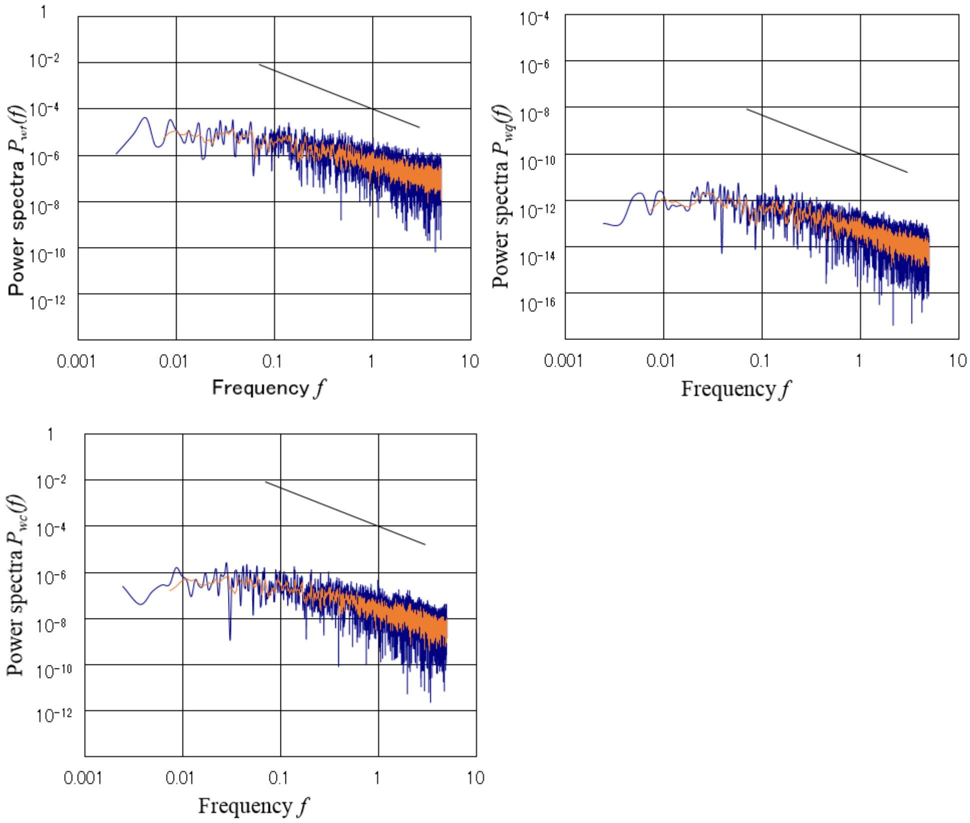

Fig. B- 6 Spectrum analysis of Run 3-1

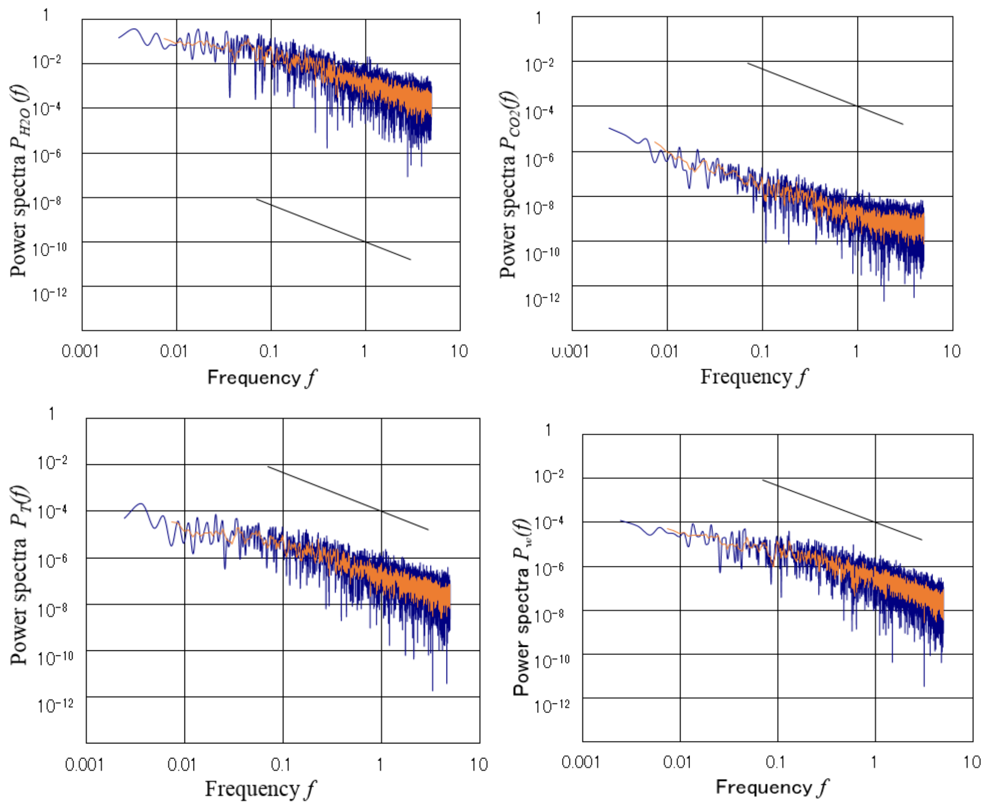

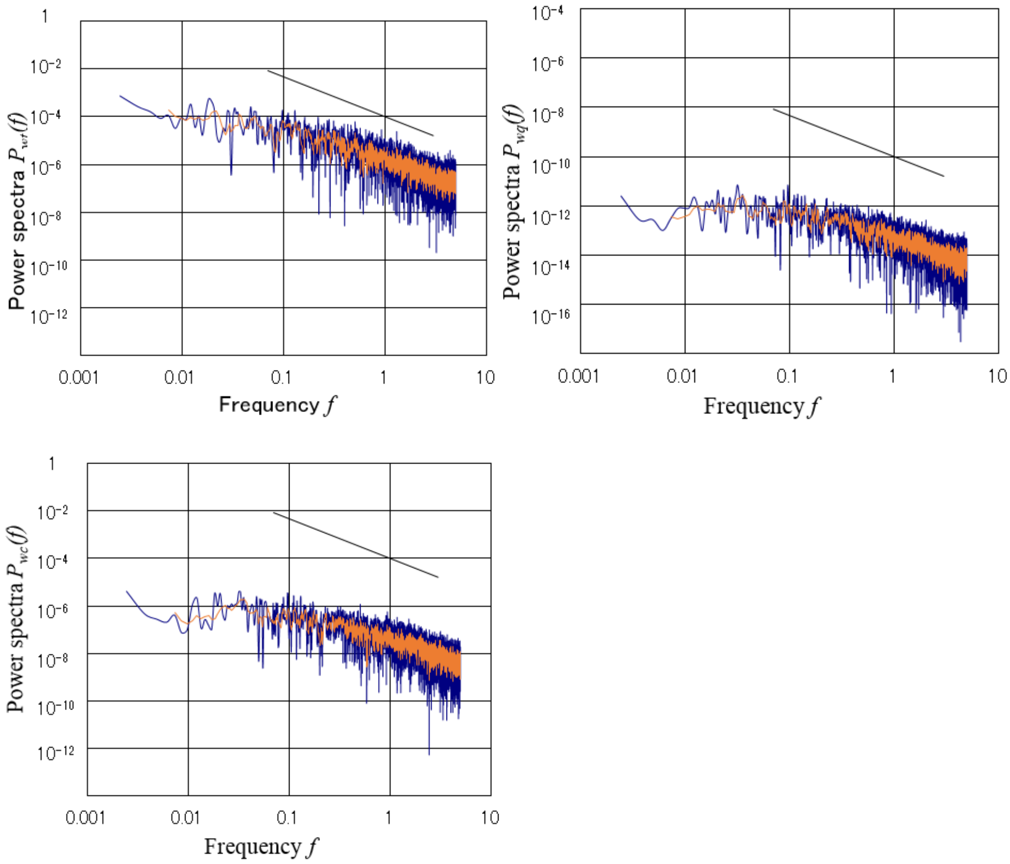

Fig. B-7 Spectrum analysis of Run 3-3

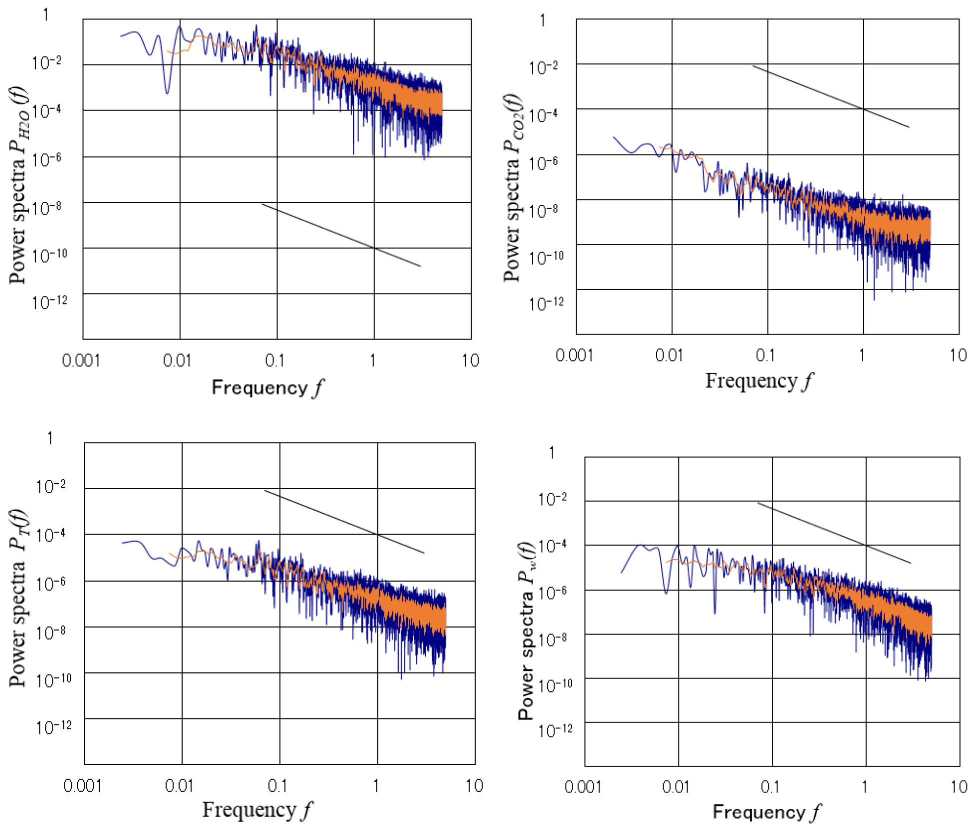

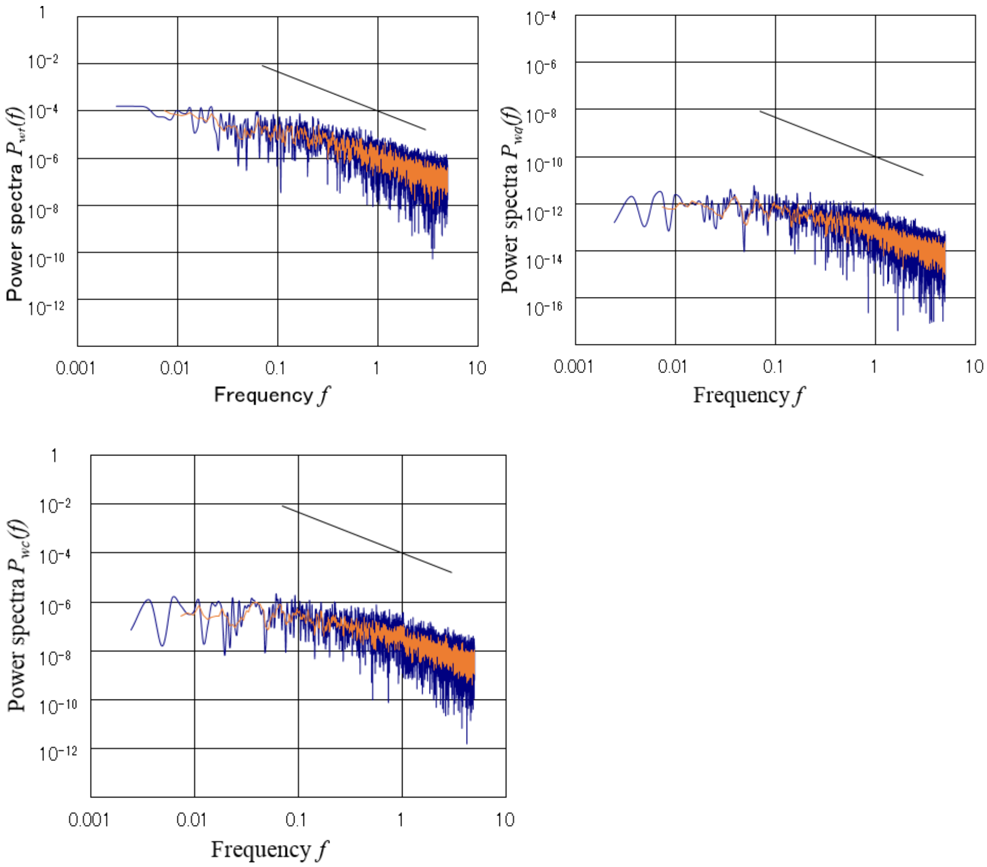

Fig. B-8 Spectrum analysis of Run 3-5

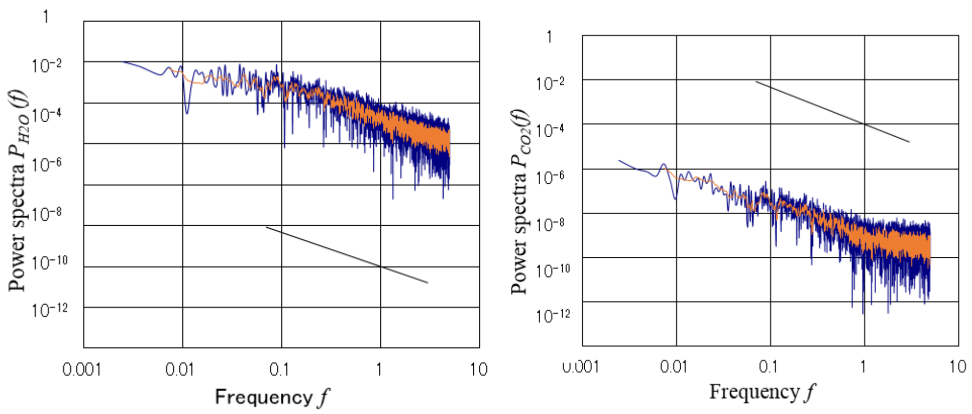

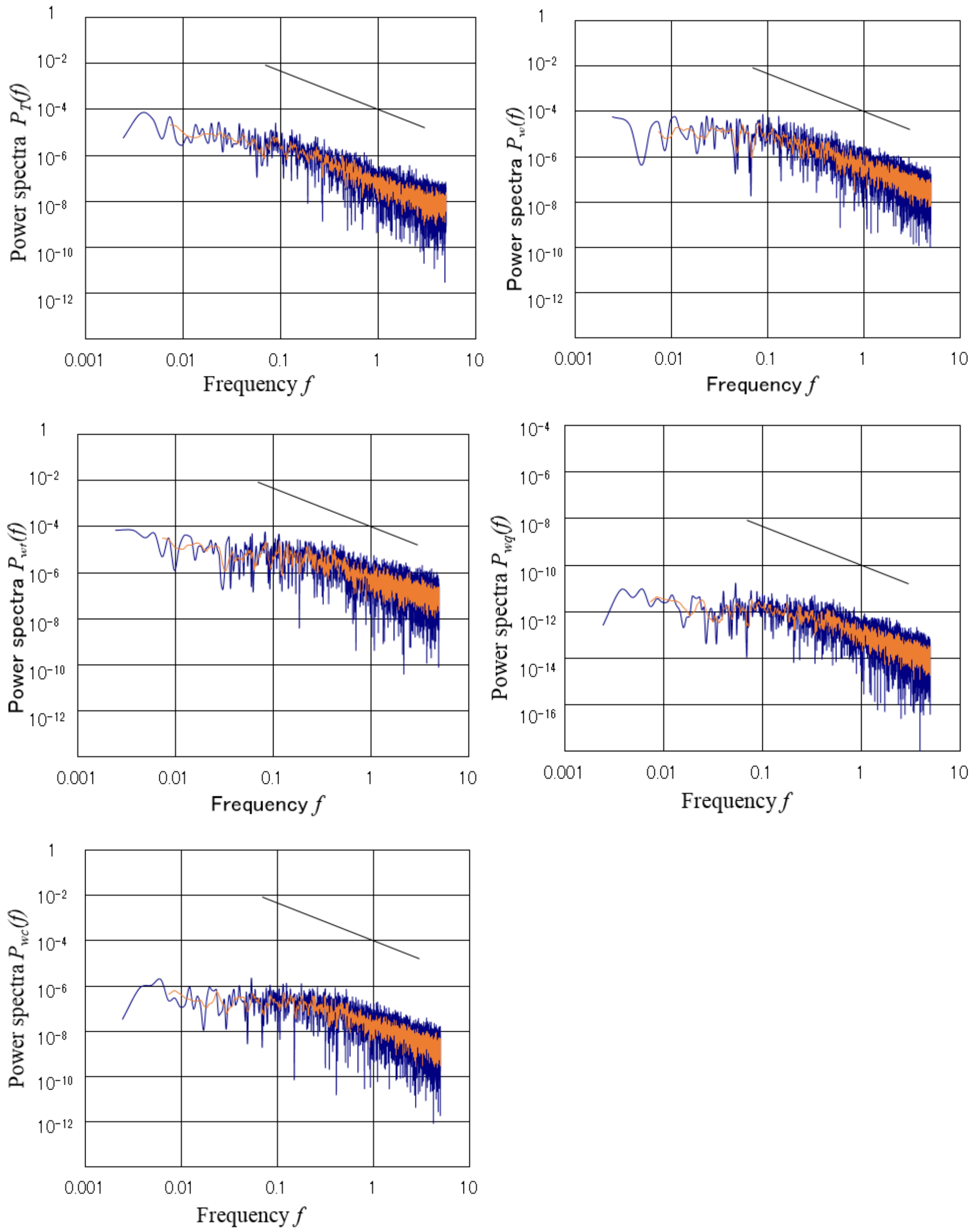

Fig. B- 9 Spectrum analysis of Run 4-1

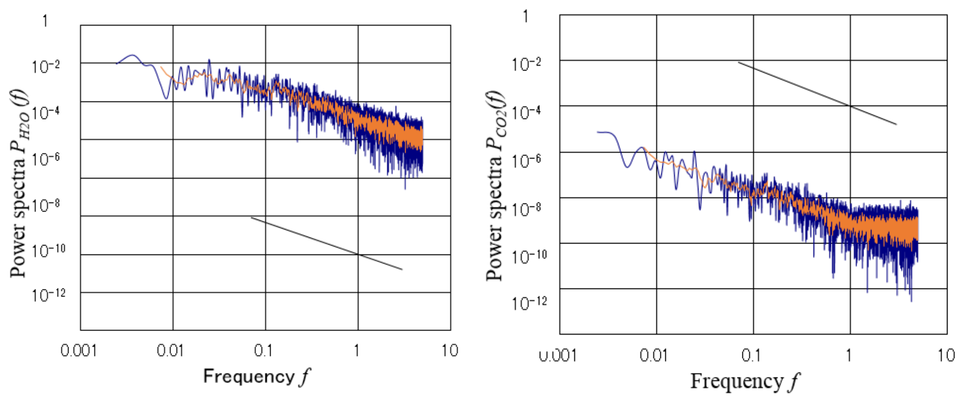

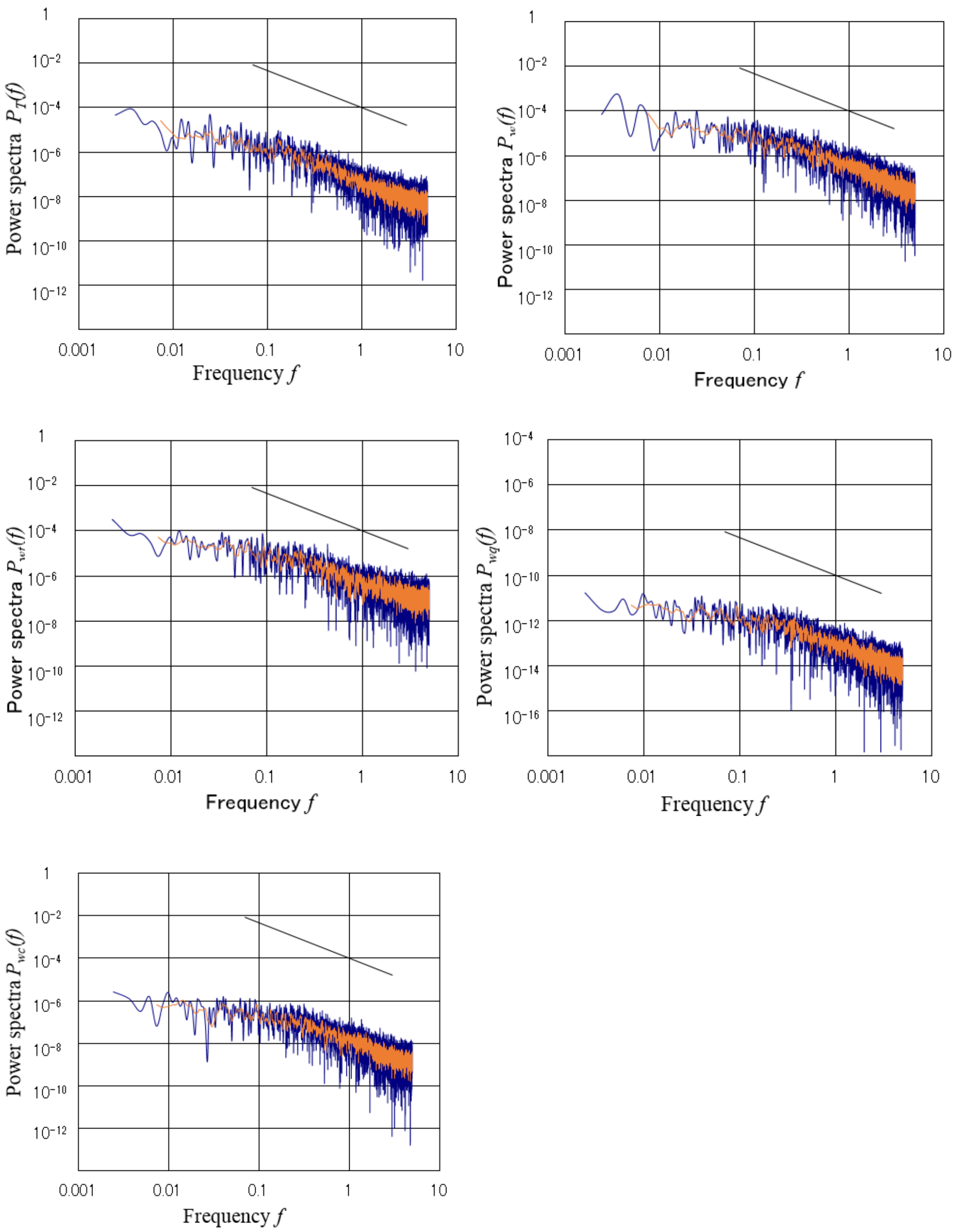

Fig. B-10 Spectrum analysis of Run 4-2

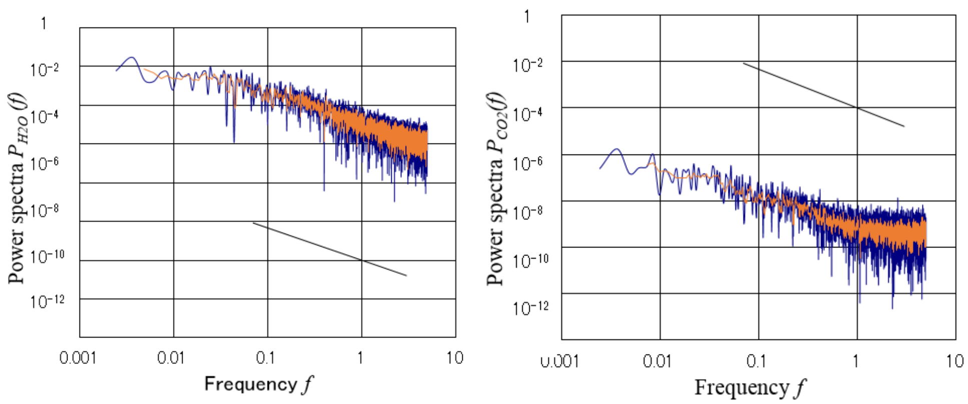

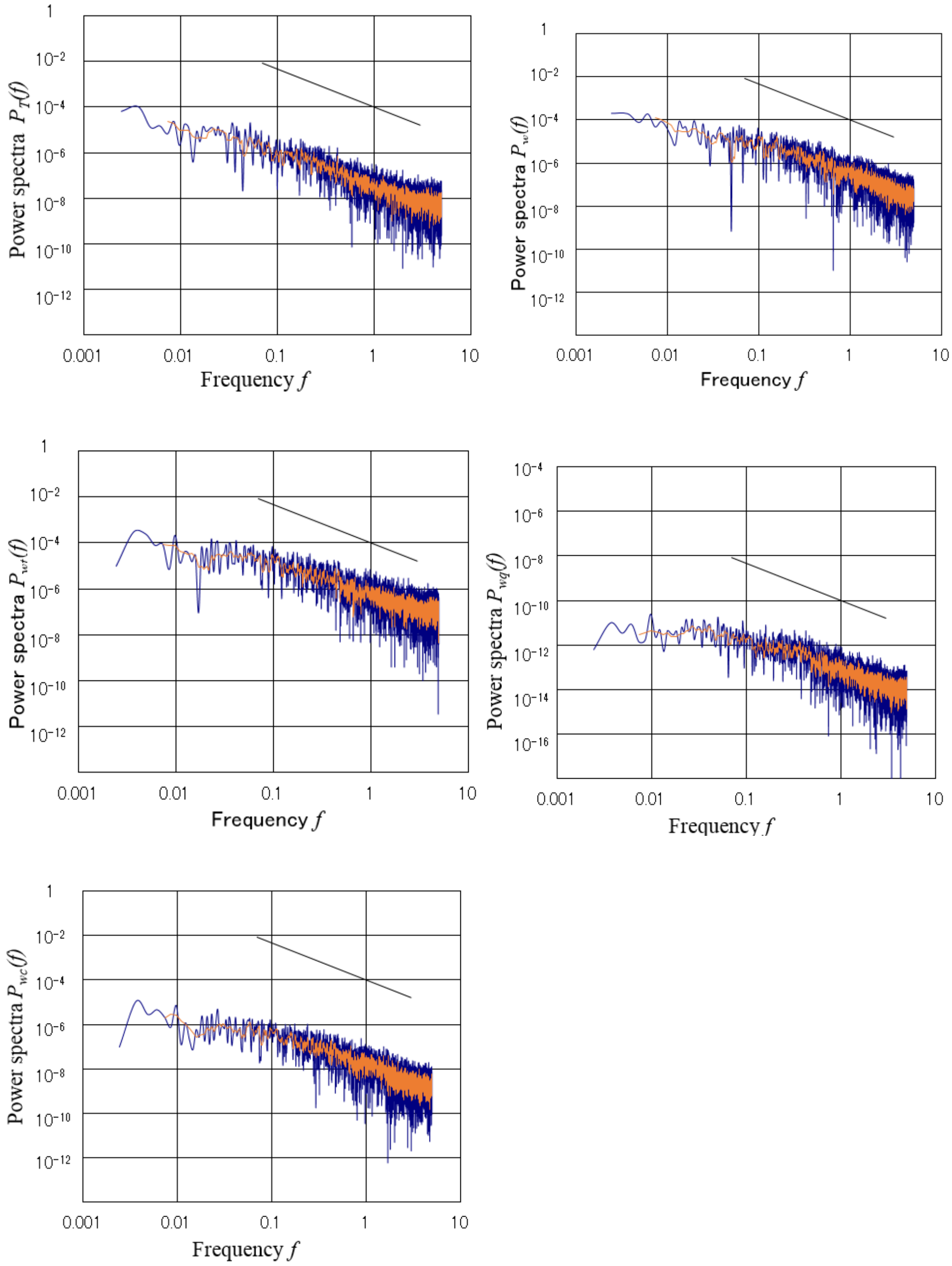

Fig. B-11 Spectrum analysis of Run 4-3

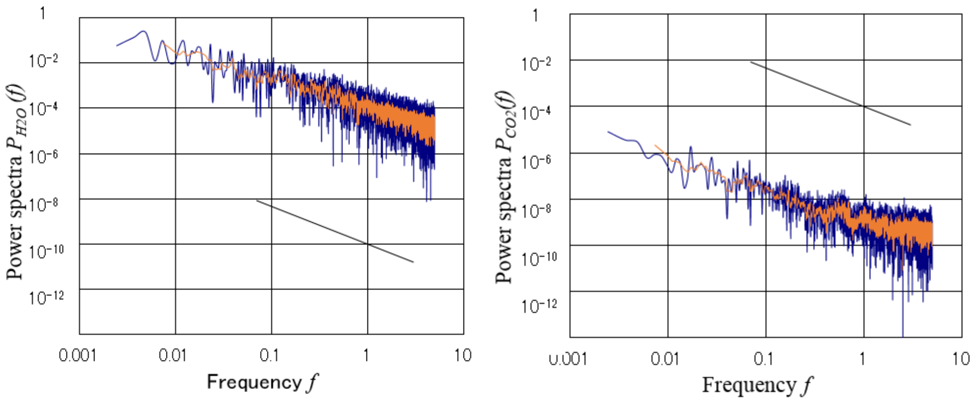

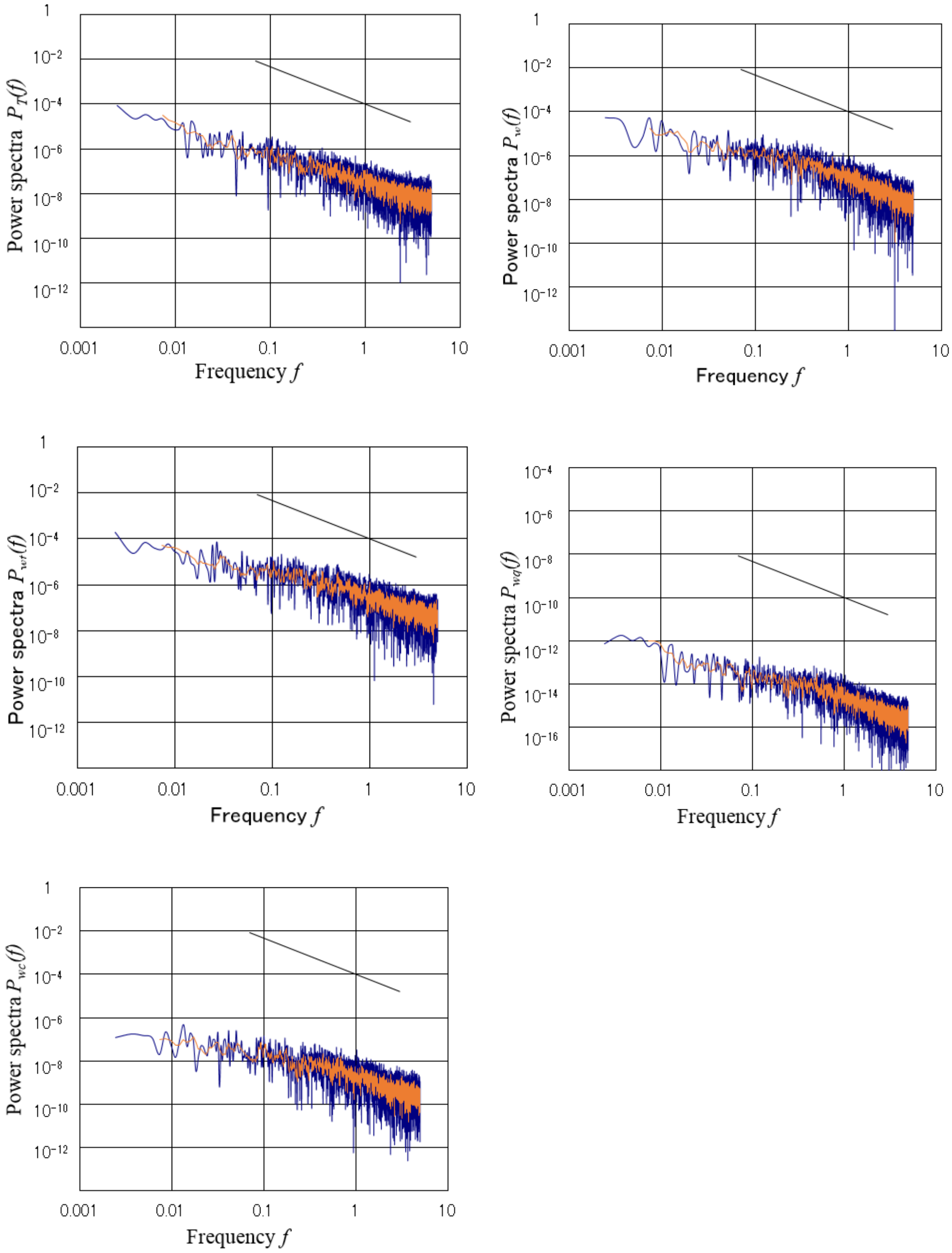

Fig. B-12 Spectrum analysis of Run 5-1

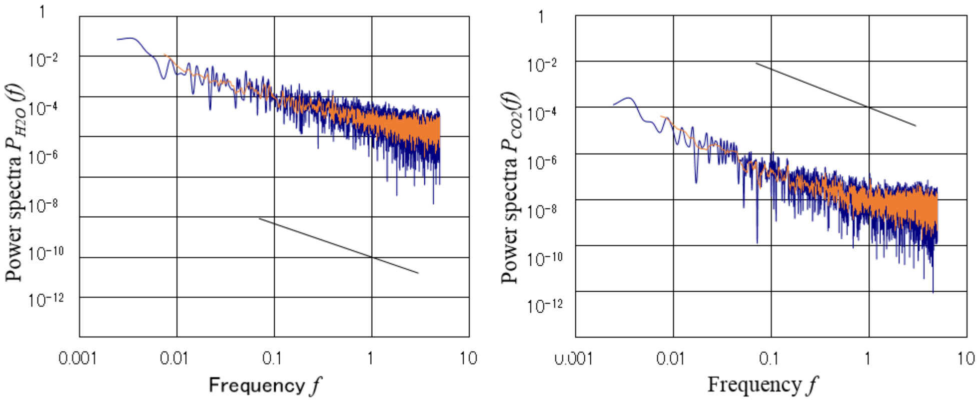

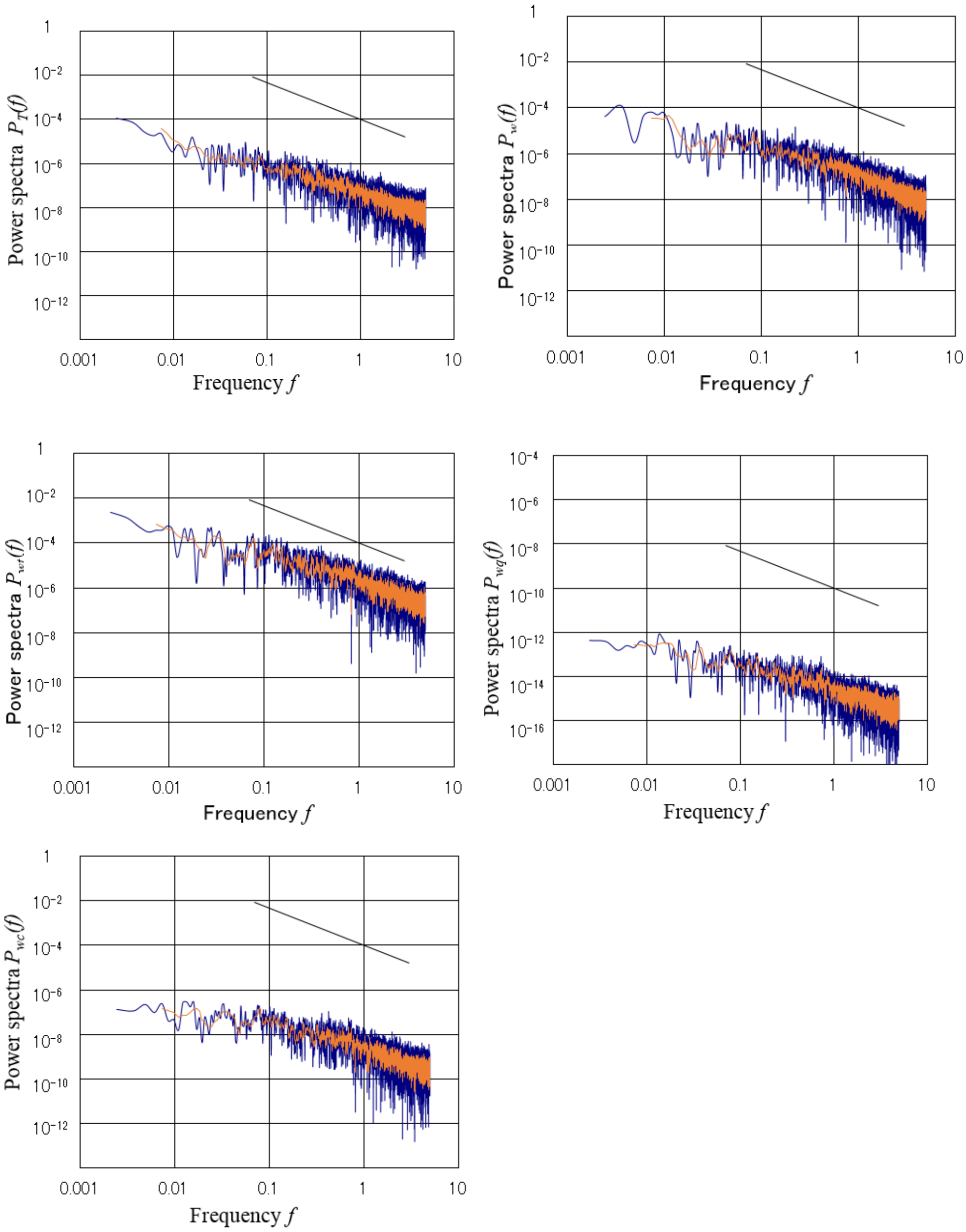

Fig. B-13 Spectrum analysis of Run 5-3

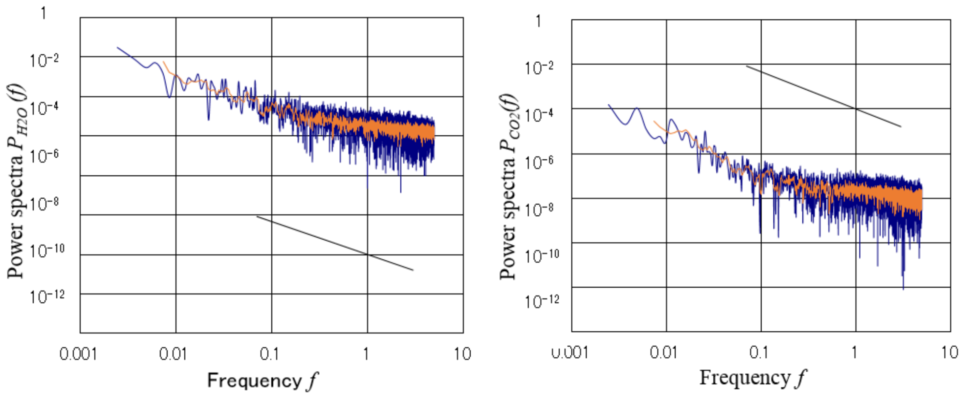

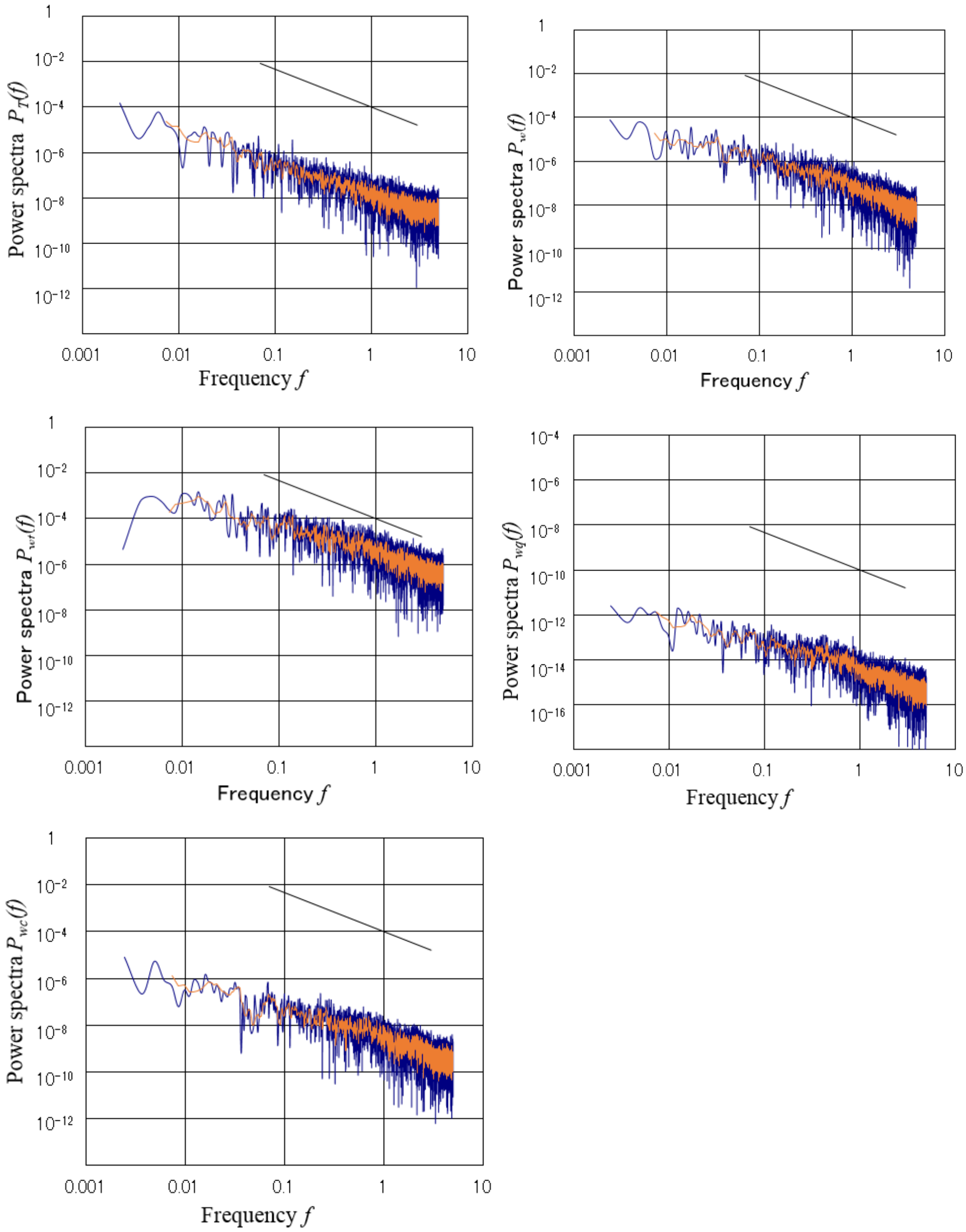

Fig. B-14 Spectrum analysis of Run 5-3

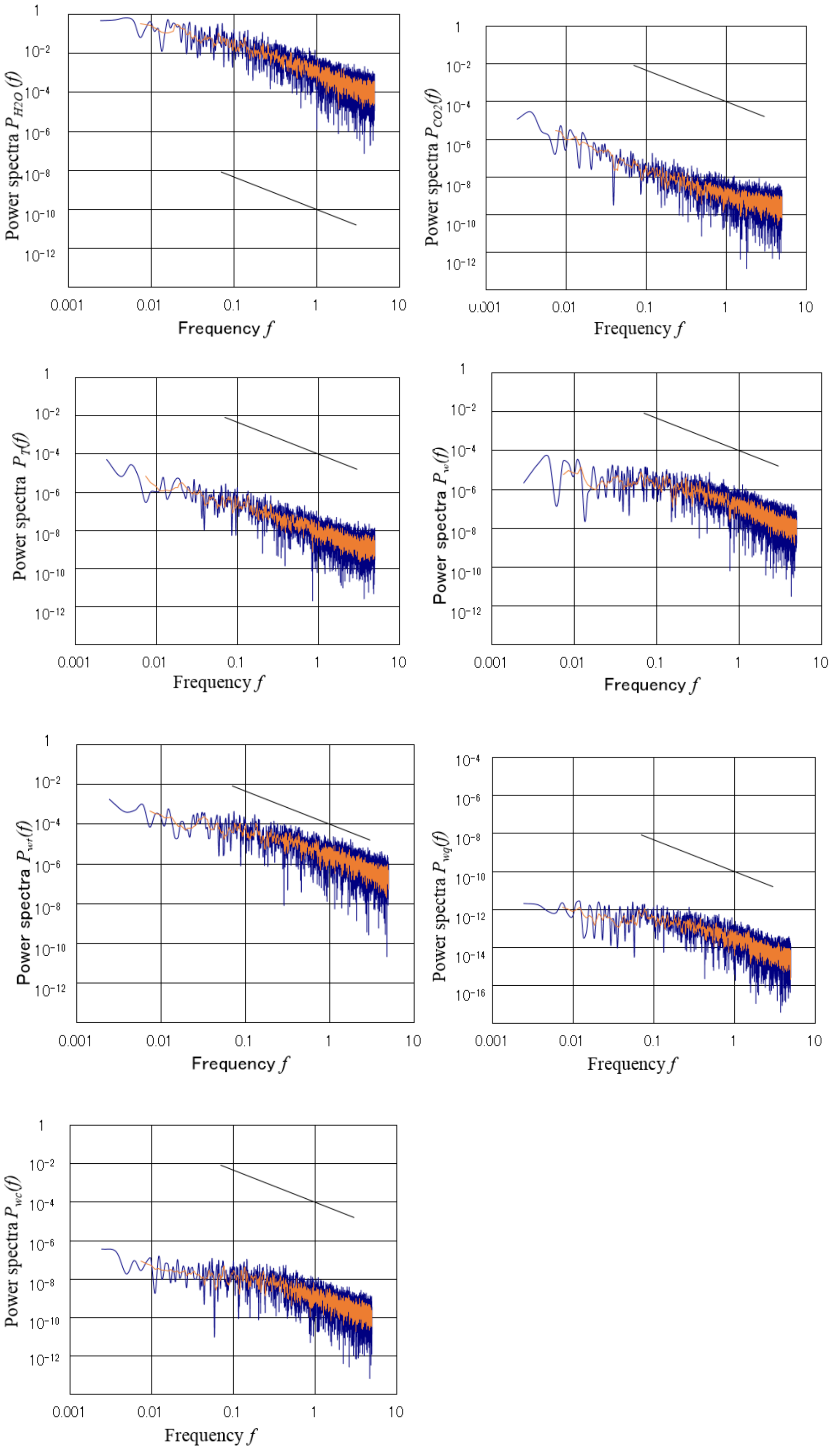

Fig. B-15 Spectrum analysis of Run 6-1

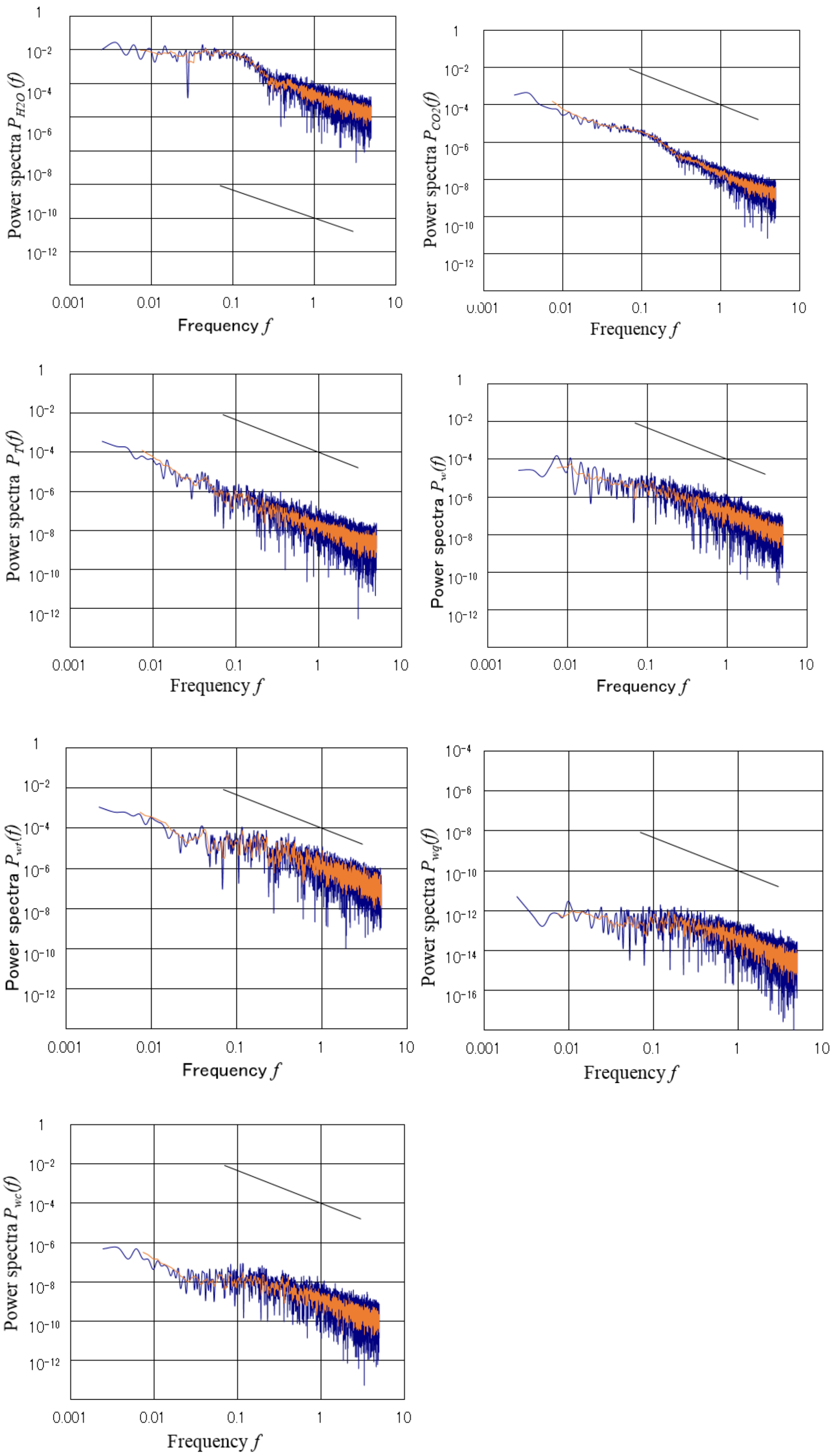

Fig. B-16 Spectrum analysis of Run 6-2

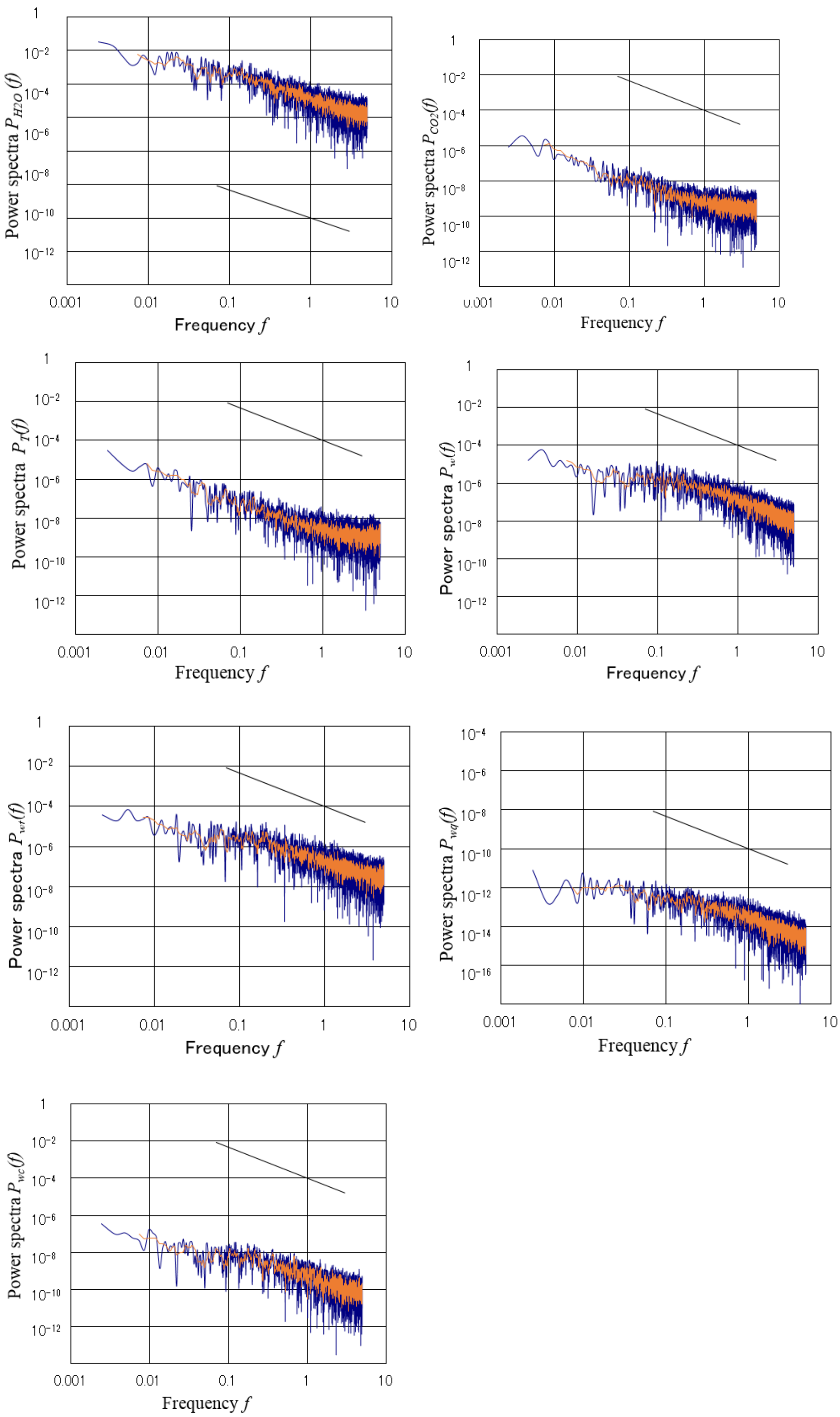

Fig. B-17 Spectrum analysis of Run 6-3

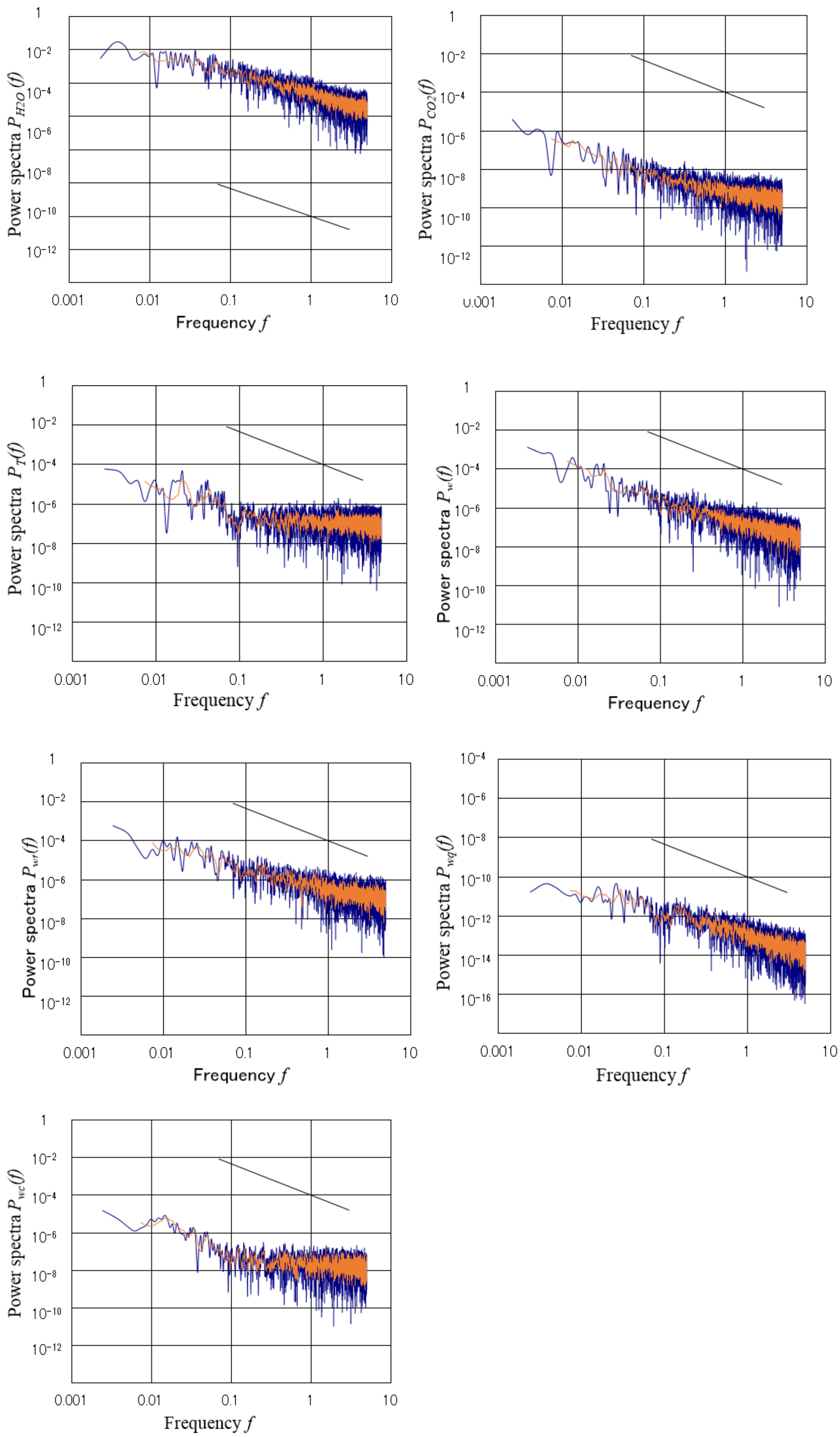

Fig. B-18 Spectrum analysis of Run 7-1